UNIVERSIDAD AUTÓNOMA DE MADRID

ESCUELA POLITÉCNICA SUPERIOR

TRABAJO DE FIN DE MÁSTER

Theoretical and experimental study of P300 ERP in the context of Brain-computer interfaces.

Part I:

Study and analysis of functional connectivity methods.

Máster Universitario en Ingeniería Informática

Autor: Vanessa Salazar Palacios

Tutor: Francisco de Borja Rodríguez Ortiz
Cotutor: Vinicio Changoluisa Panchi

Grupo de Neurocomputación Biológica (GNB)
Dpto. Ingeniería Informática

Febrero, 2021

THEORETICAL AND EXPERIMENTAL STUDY OF P300 ERP IN THE CONTEXT OF BRAIN-COMPUTER INTERFACES.
PART I:
STUDY AND ANALYSIS OF FUNCTIONAL CONNECTIVITY METHODS.

Autor: Vanessa Salazar Palacios
Tutor: Francisco de Borja Rodríguez Ortiz
Cotutor: Vinicio Changoluisa Panchi

Grupo de Neurocomputación Biológica (GNB)
Dpto. Ingeniería Informática
ESCUELA POLITÉCNICA SUPERIOR
UNIVERSIDAD AUTÓNOMA DE MADRID

Febrero, 2021

Acknowledgement

I would like to thank the National Secretariat for Higher Education, Science, and Technology (SENESCYT, *as its Spanish acronym*) for providing funding for the development of my graduate studies.

To my family, I thank them for believing in me, for inspiring me to achieve my goals, but most of all for lighting my path with their prayers. I hope life will continue to give me opportunities to share my accomplishments with all of you. Most of all, I thank my mother for being my friend and always supporting my decisions.

Paco and Vini, thank you for sharing your knowledge and experience with me during the development of this project, it would not have been possible without your constant support and patience. It has been an honor to learn under the guidance of great teachers and great people like you.

To my friends and colleagues, thank you for making this a wonderful experience and for making our friendship last.

Finally, I would like to thank the person who has accompanied me on this journey, who always trusted me, who had the courage to take the journey and face the unknown, who knew how to be strong and keep going despite the adversity, thank you for giving me the opportunity to grow and learn, thanks to me.

Agradecimiento

Quiero empezar agradeciendo a la Secretaría Nacional de Educación Superior, Ciencia, Tecnología e Innovación (SENESCYT) por brindar financiamiento para el desarrollo de mis estudios de posgrado.

A mi familia, les agradezco por creer en mí, por inspirarme a lograr mis metas, pero sobre todo por iluminar mi camino con sus oraciones. Espero que la vida continúe dándome la oportunidad de compartir mis logros con todos ustedes. Sobre todo, agradezco a mi madre por ser mi amiga y siempre apoyar mis decisiones.

Paco y Vini, gracias por compartir conmigo sus conocimientos y experiencia durante el desarrollo de este proyecto, no hubiera sido posible sin su constante apoyo y paciencia. Ha sido un honor aprender bajo la guía de grandes maestros y grandes personas como ustedes.

A mis amigos y compañeros, gracias por hacer de esta una experiencia maravillosa, que nuestra amistad perdure.

Finalmente, quisiera agradecer a la persona que me acompañó en este viaje, quien siempre confio en mi, quien tuvo el coraje de emprender el camino y enfrentar lo desconocido, quien supo ser fuerte y seguir adelante a pesar de la adversidad, gracias por darme la oportunidad de crecer y aprender tanto, gracias a mí.

Abstract

Abstract —

The analysis of connectivity in brain networks has been widely researched and it has been shown that certain cognitive processes require the integration of distributed brain areas. Functional connectivity attempts to statistically quantify the interdependencies between these brain areas. For this study, an analysis of functional connectivity in an ERP context, more specifically on the P300 component using the Granger Causality metric was proposed.

To this end, an analysis method is proposed which consists in quantifying the causality in the P300 signal and the non-P300 signal using the MVCG toolbox to determine if there are differences between the two results obtained. In this respect, a dataset from a Brain-Computer Interface (BCI) based on P300 is analyzed. Causality is determined in overlapping windows calculated from the signals under three aspects: i) Using standard electrodes, ii) Using electrodes selected by Bayesian Linear Discriminant Analysis and exhaustive search by forward selection (BLDA-FS), and iii) Using electrodes selected by the coefficient of determination (r2).

Based on this analysis, it is shown that the Granger Causality metric is valid to show the existence of a significant connectivity difference between the P300 signal and the non-P300 signal. This measure shows higher connectivity values for the P300 signal and lower connectivity values for the non-P300 signal. Among the three approaches considered, the standard electrodes and the electrodes selected with BLDA-FS were found to be more discriminative in showing differences between P300 and non-P300 connectivity.

Furthermore, through this study, it was possible to differentiate the level of functional connectivity between subjects with cognitive disabilities and nondisabled subjects, observing that the measured functional connectivity was higher in subjects without an underlying cognitive pathology.

Studying functional connectivity with Granger Causality may help to incorporate this information as new features that allow better detection of the P300 signal and consequently improve the performance of P300-based BCIs.

Key words — Connectivity, brain networks, Event-Related Potentials, P300, Granger Causality, Brain-Computer Interface, Standard Electrodes, Bayesian Linear Discriminant Analysis, exhaustive search by ”forward selection”, Coefficient of determination of P300.

Resumen

Resumen —

El análisis de la conectividad en redes cerebrales ha sido ampliamente estudiado habiéndose demostrado que ciertos procesos cognitivos requieren la integración de áreas cerebrales distribuidas. La conectividad funcional intenta cuantificar estadísticamente las interdependencias existentes entre estas áreas del cerebro. Para este estudio, se ha propuesto analizar la conectividad funcional en el contexto ERP, más específicamente sobre componente la P300 utilizando la métrica de Causalidad de Granger.

Para ello, se propone un método de análisis que consiste en cuantificar la causalidad en la señal P300 y la señal no P300 mediante el toolbox MVCG, para determinar si existen diferencias entre los dos resultados obtenidos. Para este propósito, se analiza un conjunto de datos de una Interfaz Cerebro-Computador (BCI) basada en P300. La causalidad es determinada en ventanas superpuestas calculadas a partir de las señales desde tres puntos de vista: i) usando electrodos estándar, ii) usando electrodos seleccionados por Análisis Discriminante Lineal Bayesiano y búsqueda exhaustiva mediante ”forward selection” (BLDA-FS), y iii) usando electrodos seleccionados mediante el coeficiente de determinación (r2).

Con base en este análisis, se demuestra que la medida de Causalidad de Granger es valida para evidenciar la existencia de una diferencia de conectividad significativa entre la señal P300 y la señal no P300. Esta medida muestra valores de conectividad más altos para la señal P300 y valores bajos de conectividad para la señal no P300. Entre los tres enfoques considerados, se encontró que los electrodos estándar y los electrodos seleccionados con BLDA-FS son más discriminantes para mostrar diferencias entre la conectividad de P300 y no P300.

Además, a traves de este estudio fue posible diferenciar el nivel de conectividad funcional entre sujetos con discapacidad cognitiva y sujetos no discapacitados, observando que la conectividad funcional medida fue mayor en sujetos sin una patología cognitiva subyacente.

El estudio de los niveles de conectividad funcional con Granger Causality puede ayudar a incorporar esta información como nuevas características que permitan un mejor reconocimiento de la señal P300 y, en consecuencia, mejorar el rendimiento de las BCI basadas en P300.

Palabras clave — Conectividad, redes cerebrales, Potenciales Relacionados con Eventos, P300, Causalidad de Granger, Interfaz Cerebro-Computador, Electrodos standard, Análisis Discriminante Lineal Bayesiano, búsqueda exhaustiva mediante ”forward selection”, Coeficiente de determinación de P300.

Contents

1 Introduction **1**

1.1 Motivation . . . 1
1.2 Aim of study . . . 2
1.3 Memory structure . . . 2

2 State of the Art **5**

2.1 Brain-computer interface . . . 5
2.1.1 Definition and characteristics . . . 5
2.1.2 BCIs Types . . . 6
2.1.2.1 Invasive acquisition techniques . . . 6
2.1.2.2 Partially Invasive acquisition techniques . . . 7
2.1.2.3 Non-Invasive acquisition techniques . . . 7
2.1.2.3.1 Electroencephalography . . . 7
2.1.2.3.2 Magnetoencephalography: . . . 8
2.1.2.3.3 Functional Magnetic Resonance Imaging . . . 8
2.1.2.3.4 Functional Near-Infrared Spectroscopy . . . 9
2.1.2.3.5 Positron Emission Tomography . . . 9
2.1.3 Brain Signals Patterns for BCIs . . . 10
2.1.3.1 Event Related Potentials . . . 10
2.1.3.2 Steady-State Evoked Potentials . . . 10
2.1.3.3 Sensory Motor Rhythms . . . 10
2.1.3.4 Slow Cortical Potentials . . . 11
2.2 The P300 ERP . . . 11
2.2.1 Oddball paradigm . . . 11
2.2.2 P300 detection . . . 12
2.2.2.1 Signal conditioning: . . . 12
2.2.2.2 Feature Extraction . . . 13
2.2.2.2.1 Time-domain features: . . . 14
2.2.2.2.2 Frequency-domain features: . . . 14
2.2.2.2.3 Time-Frecuency features: . . . 15
2.2.2.2.4 Similarity Features: . . . 15
2.2.2.3 Feature Conditioning . . . 16
2.2.2.3.1 Normalization: . . . 16
2.2.2.3.2 Feature Smoothing: . . . 16
2.3 Brain Connectivity . . . 16
2.3.1 Functional Connectivity . . . 17
2.3.1.1 Functional Connectivity metrics . . . 17

2.3.1.1.1 Model-based non-directed metrics . . . 17
2.3.1.1.2 Model-based directed metrics . . . 19
2.3.1.1.3 Model-free non-directed metrics . . . 21
2.3.1.1.4 Model-free directed metrics . . . 21
2.3.1.2 ERP and Functional Connectivity studies . . . 21

3 Methods and initial analysis of the problem 25
3.1 Dataset : characteristics and structure . . . 25
3.2 Preprocessing . . . 27
3.3 Connectivity Analysis . . . 28
3.3.1 Linear Granger Causality . . . 28
3.3.1.1 Vector Autoregressive Models . . . 28
3.3.1.2 Collinearity and non-stationarity . . . 30
3.3.2 GC calculation . . . 31
3.3.2.1 Electrode Selection Methods . . . 41
3.3.2.1.1 Electrode selection using BLDA and forward selection: . . . 41
3.3.2.1.2 Electrode selection using r2 selection: . . . 44
3.3.3 Statistical Analysis . . . 45

4 Results 47
4.1 GC calculation using standard electrodes . . . 47
4.2 GC calculation using BLDA-FS electrodes . . . 52
4.3 R2 selection . . . 55
4.4 Regions of Interest . . . 58
4.4.1 Electrode selection with BLDA and Forward Selection for ROIs . . . 58
4.4.2 Electrode selection with r2 for ROIs . . . 60
4.5 Granger Causality for abled and disabled subjects . . . 61
4.5.1 Summary of results . . . 63

5 Conclusions and Discussion 65

A Appendix: Results 81
A.1 Standard Electrodes . . . 81
A.1.1 Comparison of results after varying the number of standard electrodes. . . . 81
A.2 BLDA-FS Electrodes . . . 82
A.2.1 Comparison of results after varying the number of BLDA-FS electrodes. . . . 82
A.3 R2 Electrodes . . . 82
A.3.1 Comparison of results after varying the number of R2 electrodes. . . . 83

B Appendix: Electrode selection 85
B.1 Electrodes locations: BLDA-FS and R2 selection for all subjects and ROIs . . . 85

List of Figures

2.1 Sequential steps of a BCI system process. Modified from (J. Wolpaw and Wolpaw, 2012) . . . 6
2.2 Generation of an action based on a muscle movement. (A) Schematic of the process carried out by the CNS to generate an action controlled by muscle movement. (B) Schematic of the process of generating an action controlled by a BCI. (Modified from J. Wolpaw and Wolpaw, 2012). . . . 7
2.3 BCIs classification according to signal acquisition technique. . . . 8
2.4 International 10-20 system for electrode placement on the scalp (Navarro, 2014). . . . 9
2.5 Classification of common functional connectivity methods. (Modified from Bastos and Schoffelen, 2015) . . . 18

3.1 Set of images used to evoke the P300. Modified from (Hoffmann et al., 2008) . . . 26
3.2 Dataset structure for one subject . . . 27
3.3 Functions used to compute Granger Causality with the MVGC Toolbox (Barnett and Seth, 2014). . . . 30
3.4 P300 ERP characterization, Cz channel. The top graph corresponds to subjects with disabilities, and shows that the peak of the P300 signal occurs at approximately 400 ms. The lower graph corresponds to abled subjects and shows that the peak of the P300 signal occurs at approximately 350 ms. . . . 31
3.5 GC results for subject 6 using standard electrodes shown in Figure 3.6. Complete analysis with 1000 ms signal. The first line shows the results for the P300 signal, the second line shows the results for the non-P300 signal. . . . 33
3.6 Standard Electrodes location. . . . 35
3.7 C . . . 36
3.8 Area calculation results of overlapping windows curve for different and 'extreme' windows and overlap sizes, subject 6. W represents the window size, while O represents the overlap. . . . 37
3.9 Results of the area calculation for subject 6 with overlapping windows of 188 ms and an overlap of 31 ms. The first column shows the area curve obtained by addition of the significant GC values. The second column shows the area curve obtained by averaging the significant P-values. The third column shows the sum of the significant values. W represents the window size, while O represents the overlap. . . . 38
3.10 GC values, overlapping window from 217 ms to 404 ms. The first column corresponds to GC values, the second column corresponds to probability values calculated from GC, the third column corresponds to significant values, i.e. probability values ¡ 0.05, significant values are colored black. . . . 39
3.11 Area calculation results of the overlapping window curve for different windows and overlap sizes for subject 6. W represents window size, while O represents the overlap. 40

3.12 Comparison of area values calculated for different overlapping window sizes, subject 6. Color blue represents the P300 connectivity values, while color orange represents non-P300 connectivity values. 40
3.13 Results of area calculation for subject 1 with overlapping windows of 188 ms and an overlap of 31 ms. The first column shows the area curve obtained by adding the significant GC values. The second column shows the area curve obtained by averaging the significant P-values. The third column shows the sum of the significant values. W represents the window size, while O represents the overlap. 41
3.14 Comparison of area values calculated for different overlapping window sizes for subject 1, who is not one of the subjects giving good results. In this case, the window selection is not considered, leading to a poor GC result. The blue color represents the P300 connectivity values, while the orange color represents the non-P300 connectivity values. 42
3.15 Suggested Θ thresholds for selecting the right window size depending on Θ_{min} and Θ_{max}. 43
3.16 Results of area calculation for subject 1 after window selection tests. The irst column shows the P300 GC values for all Θ_{min} and Θ_{max} variations, the second column shows the non-P300 GC values for all Θ_{min} and $\Theta_{max}x$ variations and the third column shows the difference between P300 and non-P300 GC values for all Θ_{min} and Θ_{max} variations. 43
3.17 r2 results of general analysis. 45

4.1 Final area values for subjects 1-8 after window selection using standard electrodes. . 49
4.2 Mean GC area, considering all subjects and 8 standard electrodes. 49
4.3 GC results for all subjects varying the number of electrodes using standard electrodes. 50
4.4 Mean GC area, considering all subjects and 4 standard electrodes (Fz, Cz, Pz, Oz). . 51
4.5 Final area results, mean for subjects 1-8 after window selection using BLDA-FS electrodes. 53
4.6 GC results for all subjects varying the number of electrodes using BLDA-FS electrodes. 54
4.7 Mean value of GC area, considering all subjects and 8 selected electrodes with BLDA-FS. 54
4.8 Final area results for subjects 1-8 after window selection using r2 electrodes. 56
4.9 Mean value of GC area, considering all subjects and 8 selected electrodes with r2. . . 56
4.10 GC results for all subjects varying the number of electrodes using R2 electrodes. . . 57
4.11 Mean value of GC area, considering all subjects and 3 selected electrodes with r2 shown in Table 4.8 58
4.13 Mean value of GC area, considering all subjects and BLDA-FS electrodes with ROIs. 59
4.12 Final area results for subjects 1-8 after window selection using BLDA-FS electrodes with ROIs. 60
4.15 GC area considering all subjects and r2 selected electrodes with ROIs. 61
4.14 Final area results for subjects 1-8 after window selection using r2 electrodes with ROIs. 62
4.16 Comparison between abled and disabled subjects, data normalized as a function of the number of electrodes. 62

B.1 Electrode location using BLDA-FS for subjects 1-8 86
B.2 Electrode location using r2 selection for subjects 1-8 87
B.3 Electrode location using BLDA-FS for ROIs in subjects 1-8 88
B.4 Electrode location using r2 selection for ROIs in subjects 1-8 89

List of Tables

2.1 Neuroimaging methods comparison. Modified from (Ramadan and Vasilakos, 2017). 10
2.2 Brain Signal Patterns features summarized. Modified from (Ramadan and Vasilakos, 2017). 11

3.1 Standard electrode selection for the detection of P300 ERPs. Approaches by different authors. Modified from (Changoluisa et al., 2020). 34
3.2 Regions of Interest and their respective selected electrodes with BLDA. 44

4.1 Selected window and overlap size for subjects 1-8 with standard electrodes. 48
4.2 Selected window size for subjects 1-8. θ_{min} and θ_{max} values for window location with standard electrodes. 48
4.3 Final area values for subjects 1-8 after window selection using standard electrodes. . 48
4.4 Comparison of area results, considering a variable number of standard electrodes. . . 50
4.5 Electrodes selected with BLDA-FS for subjects 1-8. The location of the selected electrodes is shown in Appendix B, Figure B.1. 52
4.6 Final area values for subjects 1-8 after window selection using BLDA-FS electrodes. 52
4.7 Results of P value, GC area results for P300 signal and GC area results for non-P300 signal, where the number of BLDA-FS electrodes was varied from 2 to 6. 53
4.8 Electrodes selected with r2 for subjects 1-8. The location of the selected electrodes is shown in Appendix B, Figure B.2. 55
4.9 Final area values for subjects 1-8 after window selection using r2 electrodes. 55
4.10 Comparison of area results, considering a variable number of R2 electrodes. 56
4.11 Electrodes selected with BLDA-FS using ROIs for subjects 1-8.The location of the selected electrodes is shown in Appendix B, Figure B.3. 59
4.12 Selected window size for subjects 1-8. Description of the θ_{min} and θ_{max} values for window location using BLDA-FS with ROIs. 59
4.13 Final area values for subjects 1-8 after window selection using BLDA-FS electrodes with ROIs. 59
4.14 Electrodes selected with r2 using ROIs for subjects 1-8. The location of the selected electrodes is shown in Appendix B, Figure B.4. 60
4.15 Selected window size for subjects 1-8. Description of the θ_{min} and θ_{max} values for window location using r2 with ROIs. 61
4.16 Final area values for subjects 1-8 after window selection using r2 electrodes with ROIs. 61
4.17 Comparison of area results, between the analyzed approaches for electrode selection in general analysis and ROIs analysis. 63

A.1 Final area values for subjects 1-8 after window selection varying the number of standard electrodes shown in Table 4.4. e represents electrodes. 81

A.2 Final area values for subjects 1-8 after window selection varying the number of BLDA-FS electrodes shown in Table 4.5. e represents electrodes. 82
A.3 Final area values for subjects 1-8 after window selection varying the number of r2 electrodes shown in Table 4.8. e represents electrodes. 83

1

Introduction

1.1 Motivation

Due to the complexity of understanding brain activity, and despite significant advances in existing computational analysis and experimental techniques, how cognitive function is generated in the brain has not been fully understood. The paradigm commonly used for this purpose was based on the analysis of individual brain areas for cognitive constructs, but several studies suggest instead a common behavior of brain areas integrated into networks that require a coordinated flow of information (Sporns et al., 2005, Rubinov and Sporns, 2010, Bressler and Menon, 2010, Varela et al., 2001, Y. Li et al., 2009).

Event-Related Potential (ERP) allow to capture neural activity related to sensory and cognitive processes. It is manifested by electrical potentials generated by the brain in relation to a specific event, such as: Stimuli, responses, decisions, etc. (Luck, 2012). The P300 signal is a ERP component that has been studied to understand cognitive processes.

Several studies have shown that different brain areas are involved in the generation of a P300 signal (Polich, 2007, Tian et al., 2014, Y. Zhang et al., 2014). Networks within these areas correlate with cognitive processes such as attention, intelligence, response selection, working memory, etc.

Based on this paradigm, the need arises to use analytical methods with the aim of understanding the relationships between the structure and dynamics of networks in the context of ERP generation, and more concretely the P300 ERP, in order to identify measures of connectivity between neural regions. There are some definitions of connectivity and different criteria about the appropriate way to measure it, however, some authors agree that there is a clear distinction between two types of connectivity: functional and effective (Horwitz, 2003, Friston, 1994).

For this project, we will consider functional connectivity, which is defined in (Friston, 1994) as the temporal correlations between spatially distant neurophysiological events, and as such can be quantified by measures of statistical dependencies such as correlations, coherence, transfer entropy, and so on.

Studies have shown that individuals with cognitive deficits exhibit variations in P300 behavior,

such as variations in the latency and amplitude of the signal (Honig et al., 1992, Fusar-Poli et al., 2011). In the context of functional connectivity, these behavioral differences found between the P300 and non-P300 signals can also be evidenced, it was observed that there is greater synchronization between specific brain regions during target trials, i.e., where a cognitive process occurs. On the other hand, low values of functional connectivity are observed when brain activity is at rest. To obtain these results, some connectivity measures were used, such as: Phase Locking Value (Kabbara et al., 2016), coherence (Thee, Nisar, and Soh, 2018), Pearson correlation (Thee, Nisar, Yeap, et al., 2018), Cross correlation (Nisar et al., 2018,Guo et al., 2016), Wavelet coherence (J.-F. Gao et al., 2016), etc.

The concept of Granger causality (GC) was originally introduced by Nobel Prize in economics (Granger, 1969) and was later introduced into the field of neuroscience in (Ding et al., 2006), it has been used in various analyzes of functional connectivity on electroencephalography (EEG) data (Protopapa et al., 2014, Coben and Mohammad-Rezazadeh, 2015, Barrett et al., 2012, Fahimi Hnazaee et al., 2020), but as far as we know, Granger Causality method has not yet been applied to the study of P300 in the current state-of-the-art.

1.2 Aim of study

The present project, proposed as a master's thesis, consists of a theoretical and experimental investigation of P300 Event-Related Potentials (ERPs) in the context of Brain Computer Interfaces (BCIs) through the analysis of data acquired with EEG . This project is divided into two parts, this document corresponds to the first part and focuses on a study and analysis of functional connectivity on P300 ERPs.

The aim of this study is to determine if there are connectivity differences between a P300 signal (when a cognitive process is underlying) and a non-P300 signal (when the subject waits for the target image), using the statistical concept of Granger Causality to characterize connectivity. To conduct the proposed study, it is essential to consider the following secondary objectives:

- Understand the underlying statistical concepts of the chosen metric to adequately interpret the neural interactions resulting from the analyzed ERPs.
- Study the available estimation tools for Granger Causality, to select the one that best fits the conditions of the study to be conducted. Also understand the Granger Causality toolbox selected and handle it appropriately to avoid misinterpretations of connectivity that can lead to incorrect values.
- Analyze and appropriately pre-process the dataset selected for the study so that it can be used for the connectivity analysis.
- Perform a connectivity analysis by calculating GC between electrodes of different brain regions.

1.3 Memory structure

This study includes five chapters distributed as follows:

- Chapter 1 describes the introduction, which includes the motivation for the study in addition to the aim of the study.
- As a summary of the state of the art, Chapter 2 details some concepts, theoretical underpinnings, and developed research that are considered essential to the understanding of the present project.
- Next, Chapter 3 describes the methods used to develop this project, considering the entire process used to prepare and analyze the selected dataset. In addition, the description and application of the tool used for causality analysis is detailed and exemplified with preliminary results for the study.
- The results and partial conclusions found after the analysis are included in Chapter 4.
- In Chapter 5, the discussion and conclusions arising from the proposed project is described and the future work to be carried out from this analysis is also addressed.
- Finally, appendices with more detailed information on specific sections of the document are included.

2

State of the Art

The state of the art includes important concepts necessary to understand the development of this project. A description of BCI systems is provided, as the data analyzed in the project belongs to a P300-based BCI system. Furthermore, the connectivity analysis performed is intended to contribute to the development of BCI systems in terms of connectivity in the future. Next, a description of the P300 signal in the context of BCI is given, this component is analyzed to evaluate connectivity. Finally, certain aspects and metrics of functional connectivity are presented in detail, focusing on Granger Causality.

2.1 Brain-computer interface

This section focuses on the Brain-Computer interfaces and briefly explains their definition, the types of BCIs that exist, and the brain signals used in the context of BCIs.

2.1.1 Definition and characteristics

Research in the field of neuroscience in recent years has allowed us to better understand the nervous system at several levels. For this study, a greater focus will be placed on the central nervous system (CNS). CNS activity includes a range of metabolic, electrophysiological, and neurochemical phenomena that can be detected by monitoring electrical activity or magnetic field using sensors on the scalp, on the surface of the brain, or within the brain (J. Wolpaw and Wolpaw, 2012).

A BCI is a system based on these neural activity registers, from which specific features are extracted. These are translated into outputs capable of interacting with the outside world or the human body, replacing the brain's normal output pathways. This means that the operation of the BCI depends on the interaction of two controllers: the user's brain, which generates the signal that is measured by the BCI and the BCI itself, which extracts features from these signals and translates them into specific commands (J. R. Wolpaw et al., 2002).

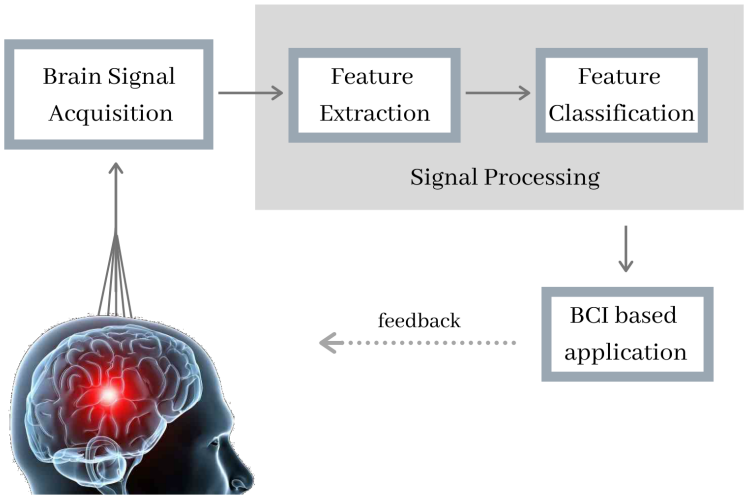

Figure 2.1: Sequential steps of a BCI system process. Modified from (J. Wolpaw and Wolpaw, 2012)

According to (Nam et al., 2018), the development of a BCI system consists of a series of sequential steps, which are divided into four categories: Generation of brain activity patterns for an external stimulus (visual, auditory) or by neuromodulation, signal acquisition, feature extraction and classification; after this process, control commands are generated that are finally used in BCI-based applications, this is illustrated in Figure 2.1.

The process of executing a muscle movement generated by the CNS is illustrated in Figure 2.2A, where specific areas of the CNS work together to control the motor neurons that activate the muscle movement to generate an action. On the other hand, Figure 2.2B shows how BCIs are used to extract the output signal that controls the action from the cerebral cortex and take over the role that motor neurons normally do.

A BCI system aims to be a helpful tool for people with physical disabilities who are unable to perform movements by themselves. It is an artificial channel between the brain and the final actuator, with the ability to understand the intention of the individual to perform an action.

2.1.2 BCIs Types

According to (Hassanien, 2015), BCIs can be classified by the way the electrical signal is measured in neurons, Figure 2.3, shows this classification. Each method is described in detail, providing a deeper analysis of the non-invasive techniques used in the development of this project.

2.1.2.1 Invasive acquisition techniques

In invasive signal acquisition, electrodes are implanted directly into the brain through a surgical procedure called a craniotomy, and signal recording occurs from within the gray matter, with the electrodes placed within the brain (Niedermeyer and Silva, 2005).

Signal acquisition by invasive methods offers not only a very good temporal spatial resolution but

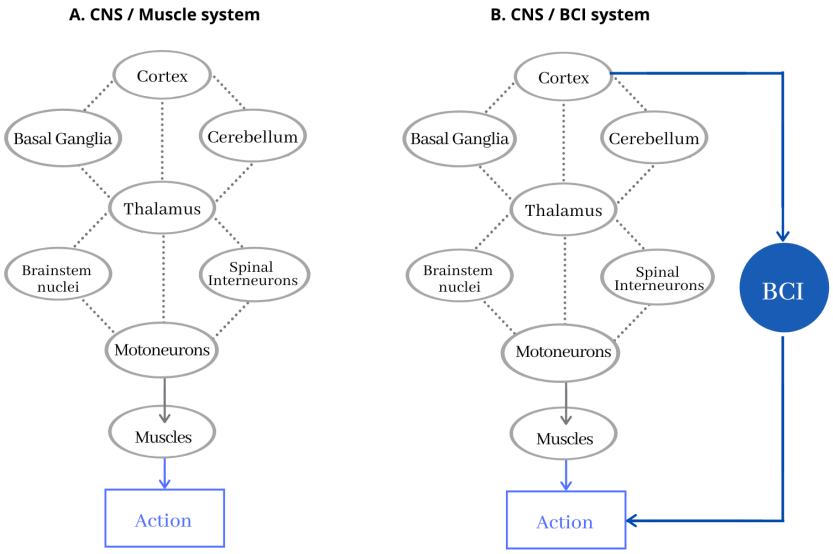

Figure 2.2: Generation of an action based on a muscle movement. (A) Schematic of the process carried out by the CNS to generate an action controlled by muscle movement. (B) Schematic of the process of generating an action controlled by a BCI. (Modified from J. Wolpaw and Wolpaw, 2012).

also the best data quality.

2.1.2.2 Partially Invasive acquisition techniques

In this case, the electrodes are located outside the gray matter of the brain, this recording technique is called electrocorticogram (ECoG), the signal quality is lower than the invasive method but there is a lower risk of brain damage (Tiwari et al., 2018).

2.1.2.3 Non-Invasive acquisition techniques

This data acquisition technique uses sensors that are located on the skin, e.g., on the scalp. According to (Nam et al., 2018), two methods of acquiring non-invasive signals can be distinguished: 1. Direct measurements, these record the electrical (EEG) or magnetic activity of the brain (MEG), and 2. Indirect measurements, these reflect the metabolism or hemodynamics of the brain, e.g., fMRI, fNIRS, and PET, which does not directly characterize neuronal activity.

2.1.2.3.1 Electroencephalography EEG is a technique for monitoring electrical brain activity and can be analyzed in the time domain or in the frequency domain. In the time domain, EEG is measured as variations in voltage values at specific times in response to a stimulus. If the voltage changes after a certain amount of time after an event or stimulus has occurred, it is referred to as event-related potentials (ERPs). On the other hand, EEGs in the frequency domain are measured as voltage fluctuations at certain frequencies (Graimann et al., 2010).

As explained in (Peng et al., 2015), to record EEG signals, it is necessary to use a helmet with at

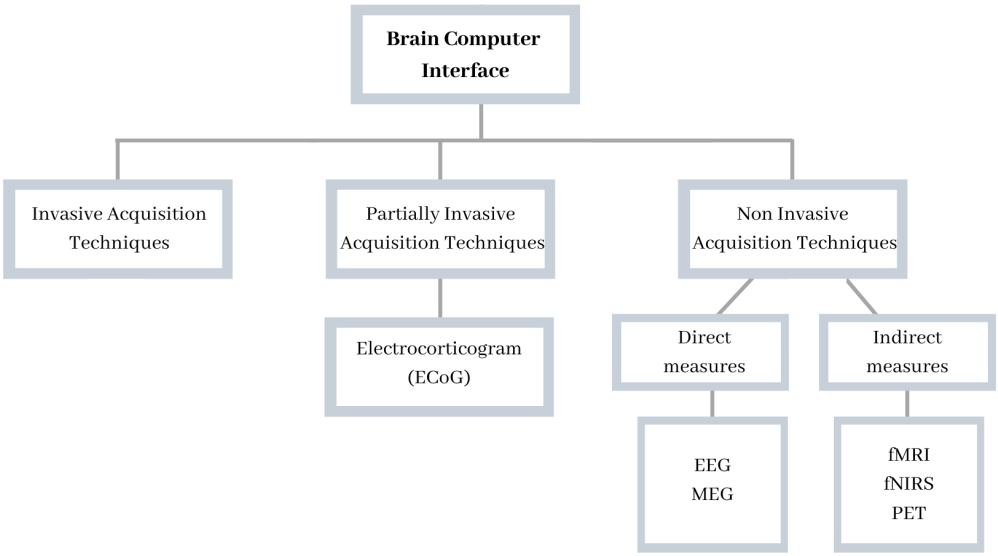

Figure 2.3: BCIs classification according to signal acquisition technique.

least three electrodes corresponding to the ground, reference, and recording electrodes. The electrodes can be made of different materials such as silver, silver chloride or gold and these can be wet or dry. In the first case, a conductive gel can be placed between the electrode and the scalp and the second is directly over the skin.

The location of the electrodes in relation to the cortical areas is critical to obtain an accurate and reliable recording. Therefore, the international 10/20 system describes the location of scalp electrodes in the context of EEG (Homan et al., 1987). This method was developed to obtain standardized test methods to ensure that the results of a subject's study can be reproduced and compared. The system is based on the relationship between the location of an electrode and the underlying area of the brain (Klem et al., 1999). Electrode distribution of the 10/20 system is shown in Figure 2.4, which divides the skull into six lobes or areas: frontopolar (Fp), frontal (F), temporal (T), parietal (P), occipital (O), and central (C). From the Nz=Nasion to the Iz=Inion, the Z-electrodes are located along the midline, at intervals of 10% (Fp), 20% (F), 20% (C), 20% (P), and 10% (O).

According to the analysis conducted in (Hwang et al., 2013), EEG is the most popular technique used in BCI-related research between 2007 and 2011. EEG will be the technique used for the development of this project.

2.1.2.3.2 Magnetoencephalography: Magnetoencephalography (MEG) technique, on the other hand, measures the magnetic fields generated by the neuronal activity of the brain. This is due to the small currents that occur when groups of neurons are activated due to a stimulus or spontaneous activity (Hämäläinen et al., 1993).

2.1.2.3.3 Functional Magnetic Resonance Imaging Functional magnetic resonance imaging (fMRI), records brain activity by measuring the hemodynamic response of the brain. When a neuron fires, there

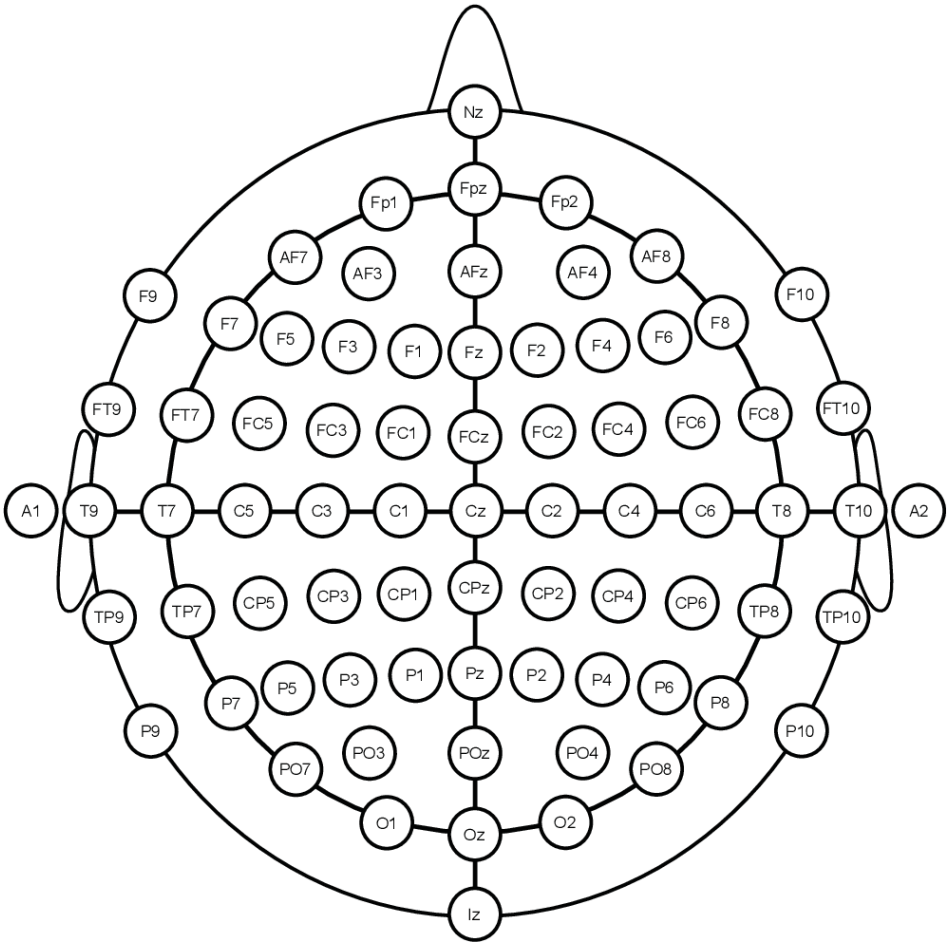

Figure 2.4: International 10-20 system for electrode placement on the scalp (Navarro, 2014).

is a decrease in blood oxygenation and an increase in the cerebral blood flow (CBF) (Kayser and Logothetis, 2013). Although this technique does not directly measure neuronal activity, it allows us to infer this activity by varying the blood volume and its flow in specific areas.

2.1.2.3.4 Functional Near-Infrared Spectroscopy Since neuronal activity is driven by glucose metabolism, this activity leads to an increase in oxygen consumption in the capillary region, which, in turn, stimulates arterial vasodilation in the brain, which consequently increases CBF. The fNIRS measures the changes between oxygenated and deoxygenated blood in the cerebral cortex, these are distinguished by the amount of light they can absorb, in this way the ratios of absorbed light are related to the detected brain activity (Irani, 2011).

2.1.2.3.5 Positron Emission Tomography Positron emission tomography (PET) technique is used to show detailed images of structures in one plane by attenuating other images in the remaining planes and to mesure the functional processes of the human body, including neuronal activity.

This method measures positrons produced by fludeoxyglucose, which is concentrated in areas of greater metabolic needs. With these measures, it is feasible to build a 3D image of areas of the brain with higher metabolic demand, which generally respond to the most active areas (Townsend, 2008).

Table 2.1 shows a summary of the techniques described above, considering important features for BCI analysis, such as temporal resolution, spatial resolution, and so on.

Method	Activity Measured	Risk	Spatial Resol.	Temporal Resol.	Portability
ECoG	Electrical	Semi-invasive	1 mm	0.003 s	Portable
EEG	Electrical	Non-invasive	10 mm	0.001 s	Portable
MEG	Magnetic	Non-invasive	5 mm	0.05 s	Non-portable
fMRI	Metabolic	Non-invasive	1 mm	1 s	Non-portable
fNIRS	Metabolic	Non-invasive	2 cm	1 s.	Non-portable
PET	Metabolic	Non-invasive	1 mm	0.2 s	Non-portable

Table 2.1: Neuroimaging methods comparison. Modified from (Ramadan and Vasilakos, 2017).

2.1.3 Brain Signals Patterns for BCIs

BCIs respond to the type of signal for which they are designed. There are several types of signals used to drive BCIs. The most common signals are briefly described below, with the P300 signal discussed in detail later, which will be the signal to be analyzed for the development of this project.

2.1.3.1 Event Related Potentials

An ERP is an electrophysiological response to a stimulus reflected as a fluctuation in the EEG, elicited by a sensory, motor, or cognitive event. The P300 wave is the largest ERP component; it is a positive parieto-central wave that occurs when the subject perceives a relevant stimulus. It owes its name to the fact that its peak latency occurs approximately 300 ms after a sensory discrimination has been performed (Picton, 1992), i.e., after a relevant stimulus has been detected by other non-relevant ones. In general, the P300 wave is generated by the oddball paradigm. The P300 wave is discussed in more detail in the next section, as it is the object of study in this project.

2.1.3.2 Steady-State Evoked Potentials

Following the presentation of steady-state stimuli that can be visual, auditory, or tactile, rhythmic activity occurs in the cortical area of the brain which mimics the frequencies it picks up from the stimulus. Deppending on the nature of the stimulus, we can identify: SSSEPs that occur after a vibrotactile stimulus (Müller-Putz et al., 2006), SSAEPs that are produced by an auditory stimulus (Kim et al., 2011), and the SSVEPs most commonly used in BCI, which are generated following a visual stimulus, usually light from light-emitting diodes (LEDs) at different frequencies (Müller-Putz et al., 2005).

2.1.3.3 Sensory Motor Rhythms

Sensorimotor rhythms (SMRs) are patterns of brain waves that occur in the motor and somatosensory cortex. Two relevant rhythms are distinguished between these waves: the Mu band, with a frequency between 8 - 14 Hz, and the beta band, with frequencies between 14-30 Hz.

The amplitude of the SMRs decrease (event-related de-synchronization) or increase (event-related synchronization) when a real movement occurs in the first case or when the individual imagines a different movement (Lu et al., 2012).

2.1.3.4 Slow Cortical Potentials

Slow cortical potentials (SCPs) are changes in the degree of polarization of neurons on the cortical surface and provide a measure of the excitability of these cortical neural networks. (Birbaumer et al., 1990) explains that the electrical sources of these potentials lie in the dendritic trees of pyramidal cortical neurons, it is also known that negative potentials represent an increase in activity in the underlying neural tissue, and positive potentials, on the other hand, represent the general absence of activity. The main characteristics of the different brain signals described are shown in Table 2.2.

Signal	Characteristics	Transfer rate(bits/min)	Training	Stimuli Needed
P300	Positive peaks by an infrequent stimulus.	20-25	No	Yes
SSVEP	Based on signal modulations in the cortex.	60–100	No	Yes
SMR	Modulations synchronized with motor activities.	3-35	Yes	No
SCP	Slow voltages shift in the brain signals.	5-12	Yes	No

Table 2.2: Brain Signal Patterns features summarized. Modified from (Ramadan and Vasilakos, 2017).

2.2 The P300 ERP

As briefly mentioned before, the P300 signal is a positive deflection that can be detected in EEG recordings. It occurs with a latency of about 300 ms after a stimulus has occurred under certain experimental circumstances, this latency value can vary in a range from 250-750 ms, and depends on the age of the subject, the stimulus modality, the characteristics of the task, and so on. (McCarthy and Donchin, 1981, Comerchero and Polich, 1999, van Dinteren et al., 2014). It was first reported over 50 years ago (Sutton et al., 1965), and since then this signal has been used to study cognitive functions in humans, such as attention (Gray et al., 2004, Brandeis et al., 2002, Becker and Shapiro, 1980, Riccio et al., 2013, Dux and Marois, 2009), memory (Fabiani et al., 1986, Karis et al., 1984, Johnson et al., 1985, Verschuere et al., 2009), learning (Peters et al., 1977, Amin et al., 2015, Pfueller et al., 2011), etc.

2.2.1 Oddball paradigm

Despite the existence of other paradigms for eliciting a P300 signal (Polich and Margala, 1997), the oddball paradigm is commonly used by researchers for experimental tasks because good amplitude and latency values can be obtained with the P300 signal (Alexander et al., 1995, Furdea et al., 2009, Hoffmann et al., 2008).

The specific experimental conditions necessary to obtain a P300 signal from the odd ball paradigm are described in detail below (Donchin and Coles, 1988):

- A person is confronted with a series of events or stimuli corresponding to two categories: ”target” and ”non-target”.
- Events belonging to the ”target” category are presented at a lower frequency than the ”non-target” events.
- The subject's task is to classify each event into one of the two classes: the events that belong to the ”target” category and generate a P300 signal, and the events that belong to the ”non-target” category.

As long as you have these attributes within the experimental design, its properties are free to vary.

2.2.2 P300 detection

The purpose of a BCI is to identify characteristics in the brain signals that allow to distinguish the user's intention to translate them into commands later. These characteristics are called features, therefore, for a correct detection of P300 it is necessary to perform an adequate feature extraction.

The process of feature extraction is to isolate the important features of the signal from noise and artifacts. Artifacts are considered as interference from sources unrelated to neurological activity, while noise is due to background neural activity. A high signal-to-noise ratio (SNR) value indicates minimal interference from background noise relative to the signal of interest. Unfortunately, the SNR of EEG signals is very low and usually contains muscle and ocular artifacts (Rivet et al., 2008). The feature extraction process generally involves three steps:

- Signal conditioning, noise reduction, and enhancement of relevant aspects of the signal.
- Feature extraction from the conditioned signals.
- Feature conditioning and preparation of the feature vector for classification.

2.2.2.1 Signal conditioning:

This step is also called preprocessing stage and it is necessary to improve the signal by removing the maximum possible interference or improving the relevant properties of the signal (Bashashati et al., 2007). Signal conditioning may include various techniques such as:

- **Frequency-range prefiltering:** The signals are filtered to remove frequencies that are outside the frequency range of brain activity. For P300 signals, a band-pass filter is often used to isolate the relevant brain activity. In (Manyakov et al., 2010), the frequency interval $[f_1, f_2]$ suitable for processing a P300 signal is analyzed, it was found that f_1 should be a small value of about 0.1 Hz, also a frequency value of 10 Hz is recommended for f_2, it was verified that this pre-filtering range improves the classification results.

- **Normalization or data decimation:** Decimation is the periodic removal of samples, reducing the signal to the minimum effective sampling rate for more efficient processing and storage. In this step, it is important to avoid aliasing, for this purpose the signal must be low-pass filtered before decimation, with a cut-off frequency equal to half the decimated sampling frequency. Typically, a signal is normalized by subtracting the mean from each signal and then dividing the resulting signals by their variance. However, in (Naumann et al., 1992) three normalization methods are proposed, which are adapted to the data depending on the type of stimulus that elicited the P300 signal.

- **Space filtering:** A channel reflects the voltage fields generated by several nearby brain sources and even non-brain sources. It depends on the source of each channel to be more sensitive to some sources and less sensitive to others. If all recorded channels have an electrode in common, it is possible to reconstruct an alternative set of channels by combining the channels after digitization. This procedure is called spatial filtering. The common electrode or reference electrode is generally placed at a relatively inactive or insensitive location with respect to brain activity.

  Spatial filters are generally designed to improve sensitivity to specific brain sources, to improve source localization, or to suppress specific artifacts. In (Jian et al., 2017, Wu et al., 2018) it is shown how their use improves the quality of the signal. Moreover, in (Rivet et al., 2012) spatial filtering is highly dependent on the location of the most relevant sensors for the detection of P300 signals.

- **Environmental interference or biological artifacts removal:** The interference of environmental factors includes electrical sources in the environment, on the other hand, biological artifacts arise from biological sources such as muscle activity or electromyographic (EMG), eye movement, or electrooculographic (EOG), heart or electrocardiographic (ECG) activity, respiratory activity, etc.

  Environmental artifacts can be removed with a filter because their frequency does not match the desired signals. Biological artifacts are more difficult to filter because they require special algorithms depending on their type (Jiang et al., 2019).

  One of the main sources of artifacts in event-related potentials (ERP) and P300 is eye activity, which is mostly unavoidable during the experiment, especially in visual paradigms, making the elimination of these artifacts an essential step in signal processing. In (Ghaderi et al., 2014, Semlitsch et al., 1986), certain techniques for filtering ocular artifacts are proposed, with satisfactory results.

2.2.2.2 Feature Extraction

Features are characteristics of brain signals used to distinguish user intent. The process of defining the relevant features to represent the user's efficiently and meaningfully is called feature extraction.

In the field of BCIs, features such as linear or non-linear combinations, statistical measures, etc., are used which, if properly selected, can more accurately reflect the user's intention. Most of these features are based on spatial, temporal, or spectral analysis of brain signals, defined within a vector of features. After conditioning the signal, as explained previously, the selected features are extracted using different methods, the most commonly used methods of feature extraction for P300 signals are:

- Time-domain feature
- Frequency-domain features
- Time-Frequency features
- Similarity features

2.2.2.2.1 Time-domain features: Some time domain feature extraction techniques used in BCI contact are explained in more detail below.

Peak Picking: This technique finds the maximum or minimum value of the signal in a time block and uses that value as the feature for that time block. In (Farwell and Donchin, 1988), peak picking is used; calculated as the difference between the lowest negative point before the P300 window and the highest positive point in the P300 window.

Correlation: The similarity of signal behavior to the expected behavior can be used as a feature, yielding higher correlation values when the analyzed segments behave according to the expected behavior and vice versa.

2.2.2.2.2 Frequency-domain features: To transform signals from the time domain to the frequency domain, the Fourier transform is commonly used, but there are other methods depending on the objective, including:

Band Power: To track the amplitude modulations at a given frequency, the frequency of interest must first be isolated by filtering the signal with a bandpass filter and obtaining the absolute value of it to attain pure positive values. Then the adjacent peaks are smoothed by integration.

Fast Fourier Transform (FFT): The FFT is an efficient implementation of the discrete Fourier transform and represents the frequency spectrum of a digital signal with a frequency resolution of the sample-rate/FFT-point, where the FFT point is a scalar greater than or equal to the length of the digital signal (J. Wolpaw and Wolpaw, 2012, Takahashi, 2019).

Autoregressive Modeling (AR): It is a representation of a stochastic process in which the variable of interest depends on its past observations, i.e., there is a linear dependence on its previous values. An AR model assumes that the signal to be modeled is generated by passing white noise through an infinite impulse response (IIR) filter. The weights of the IIR filter shape the input of the white noise to match the characteristics of the signal being modeled. White noise is random noise (scholastic process) that is not correlated with any delayed version of itself.

In (Zetterberg, 1969) it is suggested that filtering a white noise process with an AR filter is a suitable model for generating EEGs, due to the properties of EEGs, i.e., an EEG is a mixture of sources firing spontaneously, and measured at different locations (synapses, electrode positions).

The main problem with AR modeling is that the precision of spectral estimation depends to a large extent on the choice of model order (p). An insufficient model order tends to blur the spectrum, while too high order can create artificial peaks in the spectrum. Model order can be calculated using standard techniques such as the Akaike (AIC) or Bayesian information criterion (BIC) (McQuarrie and Tsai, 1998).

AR modeling is appropriate for EEG because of its non-stationary properties, so it must be evaluated in short time periods where the data are assumed to be stationary. The spectral resolution of an AR model is not limited by the duration of the input process and can therefore provide better resolution for short segments of data. In (C. W. Anderson et al., 1998), an autoregressive model was used to extract features and was found to have better accuracy in classification.

2.2.2.2.3 Time-Frecuency features: There are several different techniques to formulate a time-frequency distribution function used in EEG, such as: short-time Fourier transform (Bashar and Bhuiyan, 2016), Hilbert-Huang transform (Yuyi1, 2017), etc. However, it is considered that the wavelet transform for feature extraction gives favorable results for P300 signals.

Wavelet Transform: Wavelet analysis produces a representation of the signal in time and frequency that allows to determine, in a sampling block, when a pulse occurs at a particular frequency.

Feature extraction for P300 ERPs based on the Wavelet transform has been used by some researchers (Demiralp, Ademoglu, et al., 1999, Saavedra and Bougrain, 2010, Markazi et al., 2006), furthermore, it has been considered to carry out the feature extraction process using the Discrete Wavelet Transform (Demiralp, Yordanova, et al., 1999) , and the Continuous Wavelet Transform (Bostanov, 2004).

2.2.2.2.4 Similarity Features: Similarity measures used for feature extraction are described; among these measures is the phase-locking value, which is discussed in more detail in the next sections.

Determination Coefficient: This statistical measure is computed on a pair of sampling distributions and yields a measure of how much the means of the two distributions differ relative to the variance.

In the context of BCI, specifically applied to P300 signals, the coefficient of determination r^2 is calculated on the signals measured in two different task conditions (target and non-target), and represents the fraction of the total variance of the signal attributable to the condition J. R. Wolpaw et al., 2002, Blankertz et al., 2011, BCI2000 Wiki, 2013). The coefficient of determination is defined by the equation 2.1:

$$r^2 = \frac{cov(x,y)^2}{var(x)var(y)}, \tag{2.1}$$

where "x", are the values measured under two conditions (for example: target and non-target), and "y" is the value of the condition to which the data belong (1 for target images and -1 for non-target images).

Another similar alternative commonly used with P300 signals is the signed r^2 (M. Li et al., 2013, Riccio et al., 2018 , Changoluisa et al., 2020, Brunner et al., 2010), which is a useful tool or distinguishing between target and non-target responses.

2.2.2.3 Feature Conditioning

The performance of the algorithm depends largely on the distribution and relationships of the features, so proper feature translation is important. Proper feature conditioning improves the performance of translation algorithms, and some methods used for this purpose are described below.

2.2.2.3.1 Normalization: It is usually achieved by subtracting the mean of the signal and scaling the amplitude of the signal to have a variance equal to 1. It improves the translation algorithm if the features that make up the feature vector have similar dynamic ranges, if not, it maximizes the features with larger size even if they are not useful, so it should be used with caution. In (Liu et al., 2018), Batch Normalization is proposed for features, its use improves the character recognition performance in P300 speller systems.

2.2.2.3.2 Feature Smoothing: There are several feature smoothing techniques, but we will refer to the ones most commonly used for P300 ERPs:

PCA and ICA: When highly correlated features are present, it is appropriate to perform Principal Component Analysis (PCA) or Independent Component Analysis (ICA), to decorrelate the features or reduce the dimensionality of the feature vector, which can simplify the training and effectiveness of the translation algorithm. These techniques have been widely applied to P300 signals (Dien et al., 2003, Tahirovic et al., 2015, Friedman, 1984) and improve classification accuracy by increasing the discriminative features between target and non-target stimuli.

2.3 Brain Connectivity

The analysis of connectivity between brain networks is widely used to assess the interactions between different areas of the brain. In the neuroscience context, it can be divided into two main types, functional connectivity, and effective connectivity (Kabbara et al., 2016).

Effective connectivity refers to the effects or causal influences that one neural system exerts on another (Friston, 1994), and for this reason considers itself superior to functional connectivity, (Aertsen and Preißl, 1991) suggests that ”the notion of effective connectivity should be understood as the experimental and time-dependent simplest possible circuit diagram that would replicate the observed temporal relationships between the recorded neurons”.

Functional connectivity (FC) focuses on temporal correlations or activities between neurons compared to effective connectivity. Functional connectivity is said to exist when there is a statistical dependence between the two sets of brain activity being compared.

Functional and effective connectivity refers to a coupled or joint activity of two areas or brain regions during the performance of a task or cognitive process. An important limitation of both connectivity types is that they operate at the level of measured signals (Stephan and Friston, 2009). In the case of EEG signals, there is an important difference between the measured signals and the underlying neuronal activity; consequently, the variation of neuronal activity in different brain areas causes a change in the electrical potentials, which are linearly superimpose. Therefore, the electrodes register activity mixed with the influence of potentials generated by several different sources.

2.3.1 Functional Connectivity

Functional connectivity is defined as statistical dependencies that exist between remote neurophysiological events as output when cognitive activity occurs. The main metrics used to measure functional connectivity in ERPs are detailed below.

2.3.1.1 Functional Connectivity metrics

Quantifying neural interactions is challenging due due to the complex nature of the signals analyzed, moreover there are several metrics used and each has a some complexity of understanding, use and interpretation as shown in (H. E. Wang et al., 2014), most of them are based on a rigorous statistical theory and it is not easy to give a valid interpretation of the results. In (Bastos and Schoffelen, 2015) a possible taxonomy of FC metrics is proposed.

The first classification considered refers to the ability of the metric to provide information about the direction of the interaction generated between two signals, which can be undirected and directed. The first tries to capture a type of interdependence between signals without considering the direction of influence, while the second tries to establish a statistical causality describing what causes certain effects. In both classifications, model-based and model-free metrics can be distinguished. Model-based metrics assume linearity in the interactions that occur between time series, while model-free metrics do not assume this linear relationship.

Correlation, coherence, and phase looking value are considered within the model-based non-directed metrics, these measures provide information about the directionality of interactions between two signals in the time or frequency domain, but do not provide information about causal interactions. Regarding model-free non-directed metrics, mutual information is considered.

On the other hand, within model-based directed metrics, cross-correlation and Granger Causality are used to observe the relationship between electrodes in different time windows, the latter is also used in phase analysis. Within model-free directed metrics, transfer entropy is used. The summary of this classification is shown in detail in Figure 2.5. Some metrics considered for the analysis to be performed in this project are described in detail.

2.3.1.1.1 Model-based non-directed metrics

In this section, within model-based non-directed metrics, there is Phase Locking Value, which is described in more detail below.

Phase Locking Value: The Phase Locking Value (PLV) method was first proposed by (Lachaux et al., 1999) and aims to study functional areas of the brain that oscillate within a defined frequency range, in which precise phase-locking occurs during a limited period of time, referred to as]phase synchronization.

This method uses the response signals to a stimulus and looks for latencies where the phase difference has a minimal deviation, i.e., where there is a phase block. Given two signals x and y, and a frequency f, a phase locking measure between these components is calculated for each latency, the

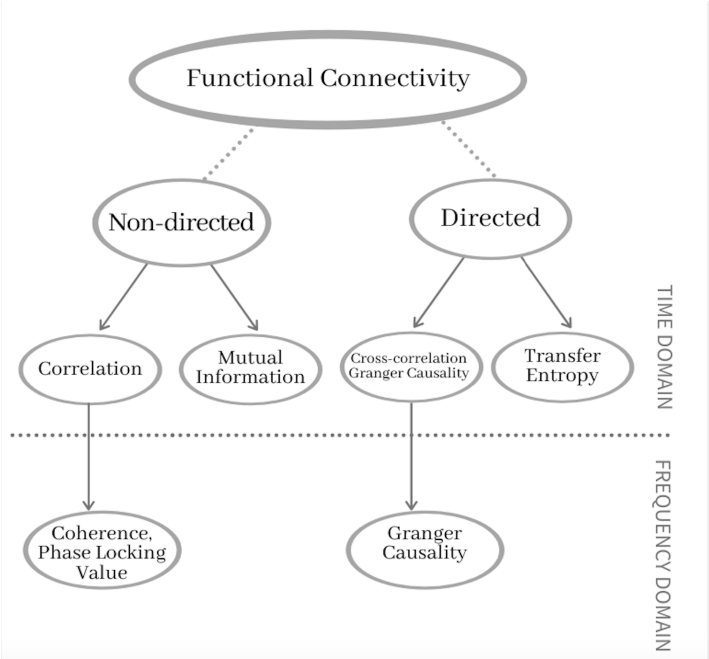

Figure 2.5: Classification of common functional connectivity methods. (Modified from Bastos and Schoffelen, 2015)

.

resulting value is the PLV, defined by Equation 2.2:

$$plv_{xy}(\omega) = |\frac{1}{n}\sum_{k=1}^{n} e^{i(\varphi_x(\omega,k)-\varphi_y(\omega,k))}|, \tag{2.2}$$

where each pair of electrodes is represented by x and y in time ω, with trial k = 1,..,n trials, and $(\varphi_x(\omega,k) - \varphi_y(\omega,k)$ is the phase difference.

The assumption is that if two brain areas are connected, then the difference between the instantaneous phases of the signals should remain constant. PLV = 0 means that there is no phase synchrony and PLV = 1 means that the phase between the analyzed signal is identical. As explained above, one of the limitations of EEG measurements of brain activity, since the acquired signals may not only be the result of mixing multiple sources, but multiple electrodes may acquire signals from the same source, giving a false result of connectivity between the acquired time series.

In EEG signals, the reference electrode contributes components that are similar to the other signals, which can influence false connectivity results. Several studies have shown that the estimation of coherence or phase synchronization values is influenced by the reference electrode (Nunez et al., 1997, Nunez et al., 2006, Guevara et al., 2005). To face and solve this problem, two approaches have been proposed. The first consists of an inverse procedure that aims to create a source space, to be used as a basis for the subsequent determination of synchronization patterns(Amor et al., 2005) but since there is no single possibility of a source model, the results may be compromised.

The other approach attempts to identify information or features in the correlation structure between the two time series being compared that cannot be explained by possible common sources. In (Stam

et al., 2007), the phase lag index is proposed as a measure of statistical interdependence that aims to be less sensitive to the problem of common source or also called volume conduction.

The phase-lag-index, which is a measure of the asymmetry of the distribution of phase differences between two signals, which aims to exclude phase differences centered around zero phase, under the assumption that the phase shift of the volume conduction signals is zero phase. The observed non-zero phase relationships between two interdependent signals cannot be attributed to the volume conduction, so they are attributed to a relationship between these time series. Mathematically,the PLI can be expressed as follows in Equation 2.3:

$$PLI = |\langle sign[\Delta\Phi(t_k)]\rangle|, \tag{2.3}$$

where $\Delta\Phi(t_k), k = 1,...,N$ is the phase difference time series, and sign is the sign function responsible for discarding a phase difference of zero.

2.3.1.1.2 Model-based directed metrics

In this section, within model-based directed metrics are: Cross-correlation and Granger causality. Both are described in more detail below.

Cross-correlation: Usually used to observe the relationship between electrodes at different time points. This technique is linear in nature and measures the similarity between two series of variables and the lag between these variables. This value varies between -1 and 1. The higher the correlation value, the greater the similarity between the signals. The normalized cross correlation (NCOR) for a time interval between electrodes, can be calculated as in Equation 2.4 (Beckenbach, 2013):

$$NCOR[n] = \sum_{m=0}^{T} \frac{(f_m - \bar{f})(\bar{t}_{m+n})(\bar{t}_{m+n} - \bar{t})}{\sigma_f \sigma_t}, \tag{2.4}$$

where n represents the time delay, T represents the total number of samples, m represents the number of samples, and σ_f and σ_t represent the deviations of f and t.

Granger Causality: The concepts of causality are generally related to the idea of cause and effect, a variable X_1 is causal for a variable X_2, if X_1 is the cause of X_2 or vice versa. Granger causality (GC), on the other hand, is a statistical concept of causality based on prediction. It does not test for a true cause-effect relationship, but attempts to infer whether the past behavior of a time series X_1 can predict the behavior of a time series X_2.

GC was proposed by Clive Granger (Granger, 1969) in 1969, and was planned as part of a bottom-up strategy that assumes that the data generation processes in each time series are independent, so the datasets are then analyzed to see if they are correlated (Kirchgässner and Wolters, 2008). GC analysis is an adaptation of the definition of causality proposed by Norbert Wiener, which stated that if the prediction of one time series can be improved by incorporating knowledge about a second, then the second series has a causal influence on the first (Ding et al., 2006, Beckenbach, 2013).

Given two time series $X_1(t)$, $X_2(t)$, we intend to predict $X_1(t+1)$ based on the past terms of

$X_1(t)$. Then, we try to predict $X_1(t+1)$ using past terms of $X_1(t)$ and $X_2(t)$. If the second prediction proves to be more successful, then the past of $X_2(t)$ seems to contain information that is useful in predicting $X_1(t+1)$, that is not in the past $X_1(t)$. Therefore, $X_2(t)$ "G-causes" (has information flow with) $X_1(t+1)$ if:

- $X_2(t)$ precedes $X_1(t+1)$.
- $X_2(t)$ contains useful information for predicting $X_1(t+1)$ that is not contained in other variables.

The roles of the two time-series can be reversed to analyze causality in the opposite direction. Time flow plays an important role in determining the direction of causal influence between the time series (Ding et al., 2006). GC is a directed version of Shannon's mutual information.

Mathematical Formulation of Granger Causality: GC is usually tested in the context of linear regression models. For the formulation, a linear vector autoregressive model (VAR) bivariate of two variables X1 and X2 is assumed:

$$X_1(t) = \sum_{j=1}^{p} A_{11j} X_1(tj) + \sum_{j=1}^{p} A_{12j} X_2(tj) + E_1(t), \tag{2.5}$$

$$X_2(t) = \sum_{j=1}^{p} A_{21j} X_1(tj) + \sum_{j=1}^{p} A_{22j} X_2(tj) + E_2(t). \tag{2.6}$$

Where:

- p: maximum number of lagged observations (defines the order of the model).
- Matrix A: contains the coefficients of the model (weights or contribution of past observations to the prediction > 0).
- E1 and E2: prediction errors.

If the variance of E_1 (or E_2) is reduced by including the terms X_2 (or X_1) in the first (or second) equation, then X_2(or X_1) is said to be "G causes" X_1 (or X_2).

Granger causality was originally proposed for linear systems, but it was intended to extend this concept to nonlinear problems (Ancona et al., 2004), but as with other approaches, there is the problem of detecting false causalities. To address this problem, a method for performing connectivity analysis using Granger Causality has been proposed, assuming an arbitrary degree of nonlinearity by exploiting kernel properties (Marinazzo et al., 2008b).

The method reformulates Granger Causality for linear problems and introduces a statistical procedure to reduce the over fitting problem. In the formulation, it was generalized to nonlinear cases using the kernel trick, which achieved control over the nonlinearity of the regression model using the kernel function, in addition to reducing the spurious causality problem using a Gram matrix (Marinazzo et al., 2008a).

2.3.1.1.3 Model-free non-directed metrics

In this section, within model-based non-directed metrics, there is Mutual Information, which is described in more detail below.

Mutual Information: Mutual information (MI), is a measure of the amount of information that one random variable contains about another random variable, i.e., it is the reduction in uncertainty of one random variable due to the knowledge of the other.

Let us have two random variables X and Y with a joint probability mass function $p(x,y)$ and marginal probability mass functions $p(x)$ and $p(y)$. The mutual information $I(X;Y)$ is the relative entropy between the joint distribution and the product of the distributions $p(x)p(y)$. MI can be calculated using the probability density function (PDF), with two time series, $X(t)$ and $Y(t)$, with t = 1,2, ..., T, at T discrete points and $p(X(t),Y(t))$, being the joint PDF between $X(t)$ and $Y(t)$ (Thomas M. Cover and Joy A. Thomas, 2006), this is shown in Equation 2.7:

$$MI = MI(X(t),Y(t)) = -\sum_{X(t),Y(t)} p(X(t),Y(t)) log \frac{p(X(t),Y(t))}{p(X(t))p(Y(t))}. \tag{2.7}$$

2.3.1.1.4 Model-free directed metrics

In this section, within model-based non-directed metrics, there is Transfer Entropy, which is described in more detail below.

Transfer Entropy: Based on information theory of Wiener and Granger, in (Schreiber, 2000) a measure of effective connectivity was introduced, Transfer Entropy (TE). This measure allows the estimation of linear and non-linear connections between channels and quantifies the amount of information transmitted between two random processes X and Y. Mathematically, TE can be expressed as in Equation 2.8:

$$TE(X \rightarrow Y) = TE_{XY} = \sum_{(Y(t+1),Y_t^n,X_t^m)} log \frac{p(Y(t+1))|Y_t^n,X_t^m)}{p(Y(t+1))|Y_t^n)}. \tag{2.8}$$

2.3.1.2 ERP and Functional Connectivity studies

In this section, we illustrate some examples of functional connectivity analysis in the context of ERP and briefly present the techniques and metrics used for it.

The cognitive functions of humans have become a widely studied topic in an attempt to understand their behavior. To this end, individual brain areas have been analyzed, but recent studies suggest instead a shared behavior of integrated brain areas that have a coordinated flow of information and are additionally connected by reciprocal and dynamic connections (Bressler and Menon, 2010, Varela et al., 2001). This complex network structure is often referred to as the "connectome" (Sporns et al.,

2005).

To evaluate this behavior, functional connectivity analysis (FC) is used to understand the relationship between these areas as they perform different activities. Temporal correlations between brain areas provide an estimate of the FC, and this is quantifiable by statistical measures, such as correlation, transfer entropy, coherence, etc., to explain the observed dependencies between time series (Friston, 2011).

In neuroscience, FC, as mentioned above, can be estimated by bivariate and multivariate analysis. The bivariate method only provides information about the directionality of interactions between two signals, whereas multivariate analysis can provide information about the flow of direct or indirect causality between neural systems (Kuś et al., 2004). It is important to note that several studies have shown that nonlinear analysis of EEG signals provides important information about the dynamics of the underlying neural networks (Lehnertz, 1999, Hosseinifard et al., 2013, Quian Quiroga et al., 2002).

In the literature, there are several metrics and techniques that have been used for connectivity studies. Some of these studies are listed below, grouped where possible in terms of the methodology used.

Non-Directed metrics

In (Kabbara et al., 2016) PLV was used to characterize the ERPs. The results showed that phase synchrony provides relevant information for classification, with high synchrony observed between brain regions during target trials. On the other hand, 9 features are extracted in (Z.-K. Gao et al., 2016) from which correlation analysis is performed. Measures such as small-world, global efficiency and local efficiency are used to characterize and define the topological structure of brain networks.

On the other hand, less common metrics have been used for the same purpose, such as Wavelet Coherence in (J.-F. Gao et al., 2016), to assess FC between different brain regions, subjects had to either tell the truth or lie when confronted with certain stimuli. This study showed that deceptive responses elicited greater connectivity strength than truthful responses, these results indicate that both groups can be effectively discriminated.

Directed metrics

In (Nisar et al., 2018) and (Guo et al., 2016), FC analysis was used to characterize the ERPs, obtained by the oddball paradigm in the case of visual stimuli, cross-correlation was used for FC analysis, examining connectivity across different brain lobes, in both of which the target stimuli were found to have high connectivity.

In (Thee, Nisar, Yeap, et al., 2018) Pearson Correlation was used and it is clearly observed that there is a difference between the results of FC, when the target and non-target stimuli are presented, the resulting network density value is higher in the first case than the second. Similar behavior is observed in (Thee, Nisar, and Soh, 2018), where coherence was used to analyze FC. This analysis was able to identify the differences in FC patterns caused by the different oddball tasks and found a denser brain network when the target stimulus occurs. In addition to coherence, graph theory was also used for connectivity analysis in this study.

In (Chang et al., 2020), a concealed information test is proposed that uses functional connectivity analysis to obtain information about the interdependence of different brain areas. For this study, Phase Lag Index (PLI) was used, and also, as in previous cases, graph theory was used to represent topological connectivity. PLI is also used in (Padilla-Buritica et al., 2020), but in this case a weighted

PLI, to validate the proposed rule. Through this study, it was found that functional connectivity scores increase significantly once the stimulus is presented. Similarly, in (F. Li et al., 2016), a Adaptive Directed Transfer Function (ADTF), it was found that two cerebral hemispheres show asymmetric functions in information processing for different phases of the P300 signal.

Metrics based on graph theory

In (Bola and Sabel, 2015) an event-related network analysis (ERNA) was performed to analyze the topology of neural networks during cognitive processes using graph theory. Through this study, the concept of the ”network fingerprint” of cognition has been defined. Furthermore, in (H. Wang et al., 2016), a connectivity study is conducted for lie detection. In this study, a nonlinear interdependence analysis was performed in addition to a graph analysis constructed from the nonlinear correlation values computed between pairs of electrodes.

Also using graph theory, in F. Li et al., 2019 a connectivity analysis is used to quantitatively describe the effect of the stimulus sequence in the P300 network through the properties of the brain network. Following the evidence shown by the studies described above, the present research project intends to use the GC metric to assess the functional connectivity between electrodes and seeks to find differences in the results of time series analysis when the target and non-target stimuli were shown.

3

Methods and initial analysis of the problem

In this chapter, the methods used for the development of the proposed project are described in detail. However, to illustrate the explanation of the methodology through examples, preliminary results of the project are also presented.

3.1 Dataset : characteristics and structure

A dataset of a P300-based BCI system from (Hoffmann et al., 2008) was used to develop this project, a six-choice P300 paradigm was used to collect data. The experiment was conducted on a population of 8 subjects, 4 of whom were disabled.

The images shown to the participants in the experiment are shown in Figure 3.1, consisting of a television, a telephone, a lamp, a door, a window, and a radio. These images were shown in random order during a period of 100 ms, with a 300 ms period in which nothing was shown until the next image was presented. Considering the display time of the image and the time when no image is shown in an Inter-Stimulus Interval (ISI) of 400 ms can be defined.

As mentioned above, the set of subjects considered in the experiment consists of 4 participants with disabilities, all of whom use wheelchairs and suffer from various communication disorders and limb muscle control. For subjects 1 and 2, spoken communication was not possible and could only make slight movements with their upper limbs. Subject 3 responded with ”yes/no” answers, by blinking. It was not possible to establish spoken communication, this subject was only able to perform movements with one of his hands without being able to control the other limbs. In subject 4. spoken communication was possible, but there was mild dysarthria. The other subjects (subject 5 to subject 8) had no known neurological pathology.

The experiment consisted of 4 sessions, two per day, with an interval of less than two weeks between each day. Each of the sessions had six runs, one run for each of the six selected images. During the development of the experiment, the subject was asked to count how many times the target

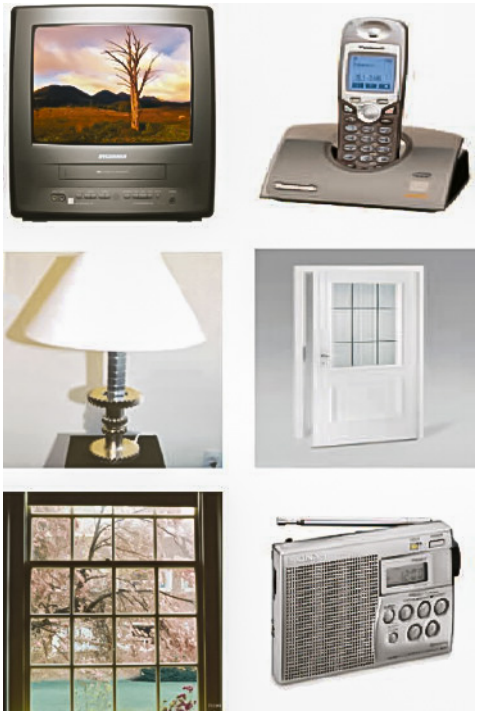

Figure 3.1: Set of images used to evoke the P300. Modified from (Hoffmann et al., 2008)

.

image was shown after hearing a warning tone.

During the development of the experiment, the following protocol that was used:

- The subject was asked to silently count the number of times the ”target” image appeared.
- The six pictures considered for the experiment were shown at the beginning.
- After 4 seconds, an alarm tone sounded and the sequence of random images was shown.

The sequence of flashes was block-randomized, and the number of blocks was randomly set between 20 and 25. On average, 22.5 target images and 22.5 x 5 = 112.5 non-target images were shown. A session consists of approximately 810 trials and the dataset for each subject consists of an average of 3,240 trials. The duration of a run was approximately one minute, and the duration of a session was approximately 30 minutes.

For this analysis, it was decided to limit the blocks to 20 in all cases, i.e., a total of 20 target trials and 100 non-target trials, 120 target trials and 600 target trials per session and, 480 target trials and 2400 non-target trials considering all sessions. The Figure 3.2 shows the structure of the dataset. As mentioned earlier, a trial consists of six images, 5 of which correspond to a non-target image and 1 to a target image; a run consists of 20 trials; a session consists of 6 runs; and finally, a day consists of 2 sessions. EEG signals were recorded at a sampling frequency of 2048 Hz from 32 electrodes positioned according to the international 10-20 system shown in Figure 2.4.

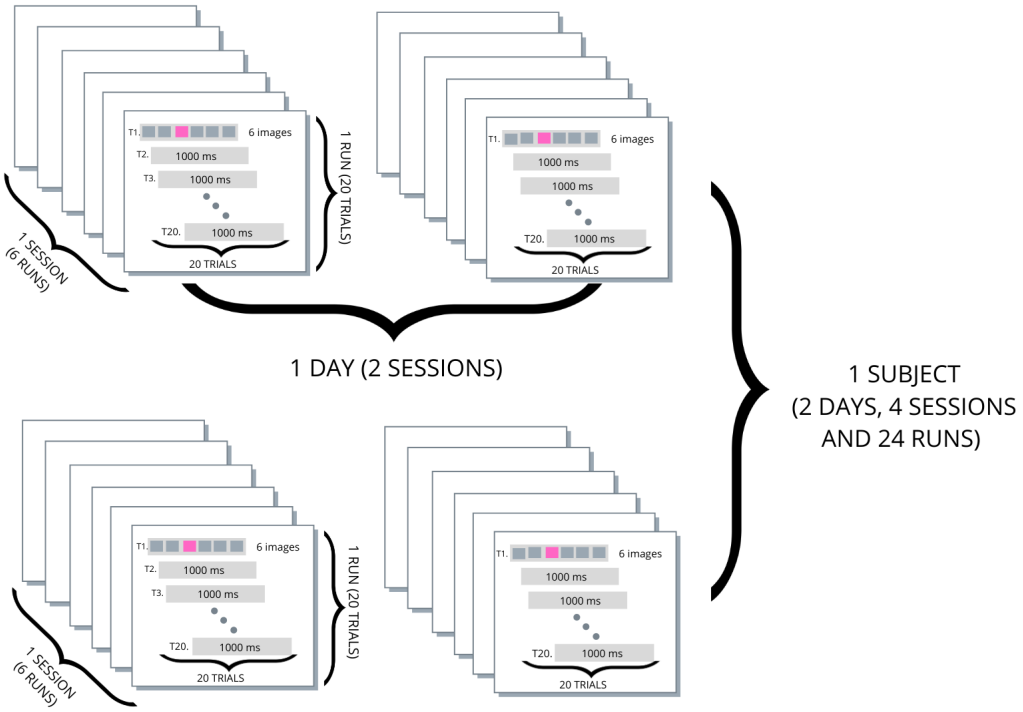

Figure 3.2: Dataset structure for one subject

.

3.2 Preprocessing

Data processing was performed in MATLAB, it was necessary to apply several preprocessing operations to the signals before performing the proposed functional connectivity analysis.

The mean value of the two electrodes corresponding to the mastoids was used as a reference. Then, a sixth-order forward-backward Butterworth bandpass filter was applied based on the data processing performed in (Hoffmann et al., 2008), which is preferred because it eliminates the side effect of phase distortion (Y.-T. Zhang, 2013). The MATLAB functions BUTTER [1] was used to calculate the filter coefficients and FILTFILT [2] for filtering. Cutoff frequencies of 1.0 Hz and 12.0 Hz were set. For scaling the data, it was normalized considering the mean and standard deviation. Once filtered, the data were downsampled to 32 Hz with every 64th sample selected from the filtered data.

Single trials of 1000 ms duration were extracted, a single trial started at stimulus onset and ended 1000 ms thereafter. Considering the ISI of 400 ms, as mentioned, the last 600 ms of each trial overlapped with the first 600 ms of the next trial. To reduce the effects of biological artifacts such as blinks, eye movements, subject muscle activity, which may affect EEG data, data from each electrode were windsorized, with values below the 10th percentile being replaced by the 10th percentile, and similarly values above the 90th percentile replaced by the 90th percentile.

[1] BUTTER: https://www.mathworks.com/help/signal/ref/butter.html
[2] FILTFILT: https://www.mathworks.com/help/signal/ref/filtfilt.html

3.3 Connectivity Analysis

As discussed in Chapter 2, connectivity analysis has been increasingly studied because of the information it provides about network dynamics. Several studies have shown that connectivity can help in detecting a P300 (F. Li et al., 2020). For this purpose, several metrics have been used, such as PLV (Kabbara et al., 2016), PLI (Chang et al., 2020), Pearson Correlation (Thee, Nisar, Yeap, et al., 2018), etc. For this reason, it was decided to explore the use of Granger causality to analyze the dynamics of the network in the P300 signals.

3.3.1 Linear Granger Causality

Based on an approach that focuses on neural networks describing the flow of information, the behavior of these networks can be described by non-deterministic processes that evolve over time, i.e., given an input stimulus, a different outcome may occur at the output. The dynamics of the networks are governed by probabilities, which is why they are treated as stochastic processes (Terrell, 2019).

In the present analysis, Granger Causality was used for linear systems in the time domain to quantify information flow, it has been shown to solve some of the limitations that other metrics create (Bressler and Seth, 2011). However, GC for nonlinear systems (Marinazzo et al., 2008b, Marinazzo et al., 2008a) is an approach that should be considered in future analyzes.

The computational calculation of GC analysis requires the estimation of AR models of stochastic processes, it is necessary that these stochastic processes must be stationary for the model to be estimated, if the data are initially non-stationary, several pre-processing steps may be considered. For the GC analysis on the data described above, the MVGC toolbox proposed in (Barnett and Seth, 2014) is used, which is based on the Vector Autoregressive (VAR) model theory.

3.3.1.1 Vector Autoregressive Models

A Vector Autoregressive (VAR) model allows the analysis of the relationship between k variables in a given period t = 1, ..., T. Each variable has an associated equation that models its evolution over time, this equation contains information about the past values of the variables and other variables in the model, as well as an error term.

The k variables are modeled as a linear function of their past values and are collected into a vector U_t of length k. The components of the vector are denoted as u_{nt} which means the observation at time t of the nth variable. VAR models are characterized by order p, the model order is the number of previous time periods used by the model. A $p-th$ order model VAR refers to a VAR model that contains lags for the last p time period:

$$U_t = A_1 U_{t-1} + A_2 U_{t-2} + ... + A_p U_{t-p} + \varepsilon_t, \tag{3.1}$$

$$U_t = \sum_{k=1}^{p} A_k U_{t-k} + \varepsilon_t, \tag{3.2}$$

where A_k is the nxn matrix of regression coefficients, ε_t the residuals, representing a white noise

process.

First, it is necessary to determine an appropriate model order for the regression, this is done using standard procedures such as Akaike Information Criteria (AIC) (Akaike, 1974) or Bayesian Information Criteria (BIC) (Stone, 1979), as explained earlier for AR models, in this case both calculations are performed.

AIC is a measure of the relative quality of a statistical model, it balances the goodness of fit of the model and its complexity. Models with the lowest AIC are considered "the best" and models where the difference in AIC relative to AICmin < 2 can be considered to have substantial support (Burnham and Anderson, 2003). BIC, on the other hand, is a criterion for selecting models from a finite set of models, closely related to AIC. As in the previous case, the model with the lowest BIC is selected. Unlike AIC, BIC penalizes the model more for its complexity, i.e., more complex models have a higher score; since the lower scores are selected, they are less likely to be selected in this case (Bishop, 2006). The following equations are used to estimate both the AIC and BIC of a model:

$$AIC = 2k - 2 * ln(L), \tag{3.3}$$

$$BIC = -2 * ln(L) * ln(N) * k, \tag{3.4}$$

where L is the likelihood, N is the number of recorded measurements, and k is the number of parameters in the model, in this case, the model order (Mohammed et al., 2015).

After defining the model order, the next step is to define the model parameters that maximize the likelihood function for VAR models and minimize the model error. To this end, several techniques are used, including the Ordinary Least Square (OLS) regression algorithm (Hamilton, 1994), which computes least squares estimation as a standard method, and the Levinson, Wiggins, Robinson (LWR) algorithm (Levinson, 1946), which is based on the idea of maximum entropy. OLS computes a least-squares estimate for the sample estimators $\hat{A}_k$. Given a time series $u_1, ..., u_m$ matrices of regression coefficients $\hat{A}_1, ..., \hat{A}_p$ are the residual errors of the regression:

$$\varepsilon_t = U_t - \sum_{k=1}^{p} \hat{A}_k \mathbf{u}_{t-k}, \tag{3.5}$$

where t = p+1,...,m. The values of $\hat{A}_k$ are chosen to minimize the squared error $E^2 = \frac{1}{m-p} \sum_{t=p+1}^{m} ||\varepsilon_t||$.

LWR algorithm is an extension of the Morf variant to Durbin recursion (Morf et al., 1978, Durbin, 1960). The Morf variant estimates the regression coefficient matrices $\hat{A}_k$ recursively for k = 1,2,... from the time series data u_t (Barnett and Seth, 2014). It is very stable, and the covariance matrix of the residuals is computed recursively, this is an advantage in OLS that need to be recomputed for each model order. The calculation of Granger Causality is done in the order of the functions defined in Figure 3.3, these functions are part of the MVGC Toolbox (Barnett and Seth, 2014).

The function TSDATA_TO_INFOCRIT [3] computes Akaike and Bayesian information criteria for VAR models from time series data, which may be single- or multi-trial. The result is later used to determine the model order. For the definition of VAR models, the function TSDATA_TO_VAR [4] is used, the tool uses BIC by default to estimate the model order, as it works better with long time series as

[3] TSDATA_TO_INFOCRIT: https://users.sussex.ac.uk/∼lionelb/MVGC/html/tsdata_to_infocrit.html

[4] TSDATA_TO_VAR: https://users.sussex.ac.uk/∼lionelb/MVGC/html/tsdata_to_var.html

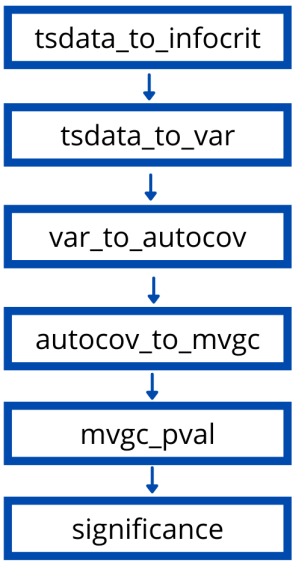

Figure 3.3: Functions used to compute Granger Causality with the MVGC Toolbox (Barnett and Seth, 2014).

.

found in neural applications (Ding et al., 2006) and LWR to determine the coefficients.

After all relevant parameters of the model are computed, the function VAR_TO_AUTOCOV [5] is used to calculate the autocovariance sequence Γ_k according to the previously defined VAR model, for which the study of the "reverse solution" of the Yule-Walker equations is necessary (Anderson, 1971). Finally, the function AUTOCOV_TO_MVGC [6] computes the conditional causalities in the time domain, using the autocovariance sequence G.

With this result, a statistical significance test is performed using the functions MVGC_PVAL [7] and SIGNIFICANCE [8]. A Fisher test (F-test) is used, for which a null hypothesis is defined, in this case: "X_2 no G-causes $X_1(t+1)$" and an alternative hypothesis, in this case: "X_2 G-causes $X_1(t+1)$ ". A value of $\alpha = 0.05$ was set, if the probability values defined for the compared channels exceed this value, the null hypothesis is rejected.

3.3.1.2 Collinearity and non-stationarity

Collinearity occurs when there are linear relationships between the individual time series, the presence of collinearity is detected at the VAR model estimation stage, using the MVGC toolbox Barnett and Seth, 2014, displaying this error as "deficient range" regression. To eliminate linear dependencies, different techniques can be used, such as a PCA analysis, a factorial modeling approach, or a signal separation technique using ICA, as explained above.

[5] VAR_TO_AUTOCOV: https://users.sussex.ac.uk/∼lionelb/MVGC/html/var_to_autocov.html
[6] AUTOCOV_TO_MVGC: https://users.sussex.ac.uk/∼lionelb/MVGC/html/autocov_to_mvgc.html
[7] MVGC_PVAL: https://users.sussex.ac.uk/ lionelb/MVGC/html/mvgc_pval.html
[8] SIGNIFICANCE: https://users.sussex.ac.uk/∼lionelb/MVGC/html/significance.html

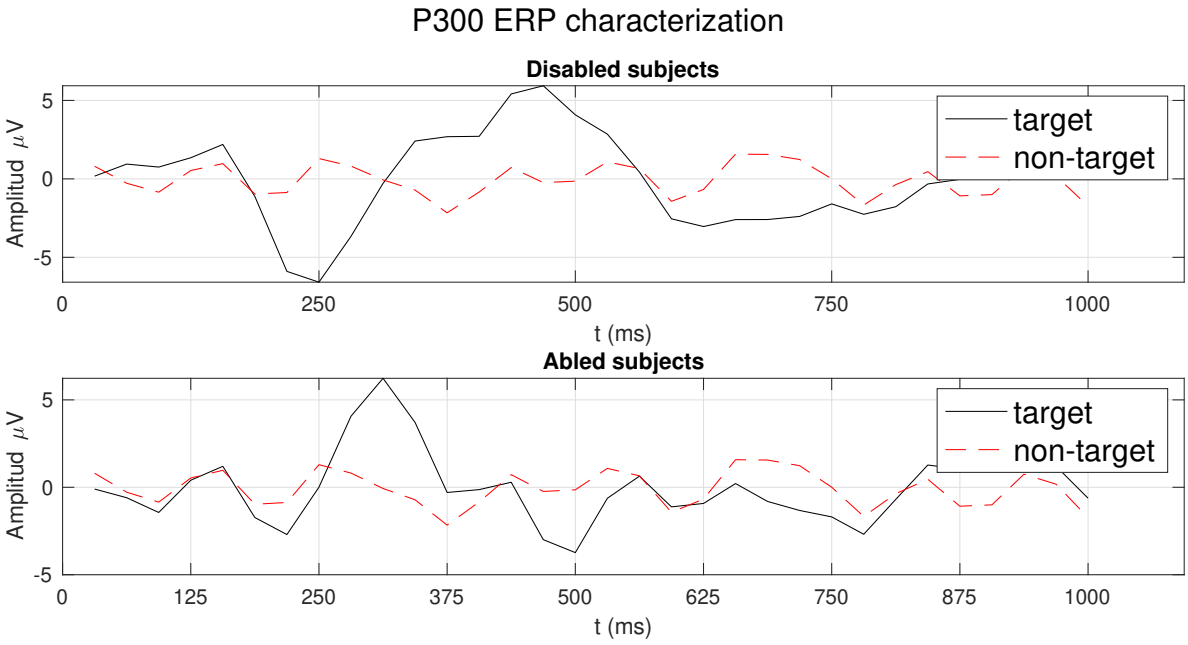

Figure 3.4: P300 ERP characterization, Cz channel. The top graph corresponds to subjects with disabilities, and shows that the peak of the P300 signal occurs at approximately 400 ms. The lower graph corresponds to abled subjects and shows that the peak of the P300 signal occurs at approximately 350 ms.

In this case, there are 32 time series corresponding to each of the electrodes where the EEG signals were measured, with high collinearity verified. In order to reduce the computational complexity and limit the existing collinearity between the analyzed time series, it was decided to limit the set of analyzed variables which, after selection, was verified that there was no collinearity. The number of variables chosen depends on the analysis performed, but in most cases a maximum number of 8 electrodes was used.

Stationarity, on the other hand, can be achieved by techniques such as detrending, or notch filtering techniques. For the present analysis, stationarity was achieved by splitting the data into overlapping windows and using shorter periods that provide stationarity to the data. This analysis also allows us to analyze how the GC changes over time, as it is shown in (Ding et al., 2000).

3.3.2 GC calculation

After preprocessing, and due to the pursued goal of differentiating the existing causality between the P300 signal and the non-P300 signal, the dataset was divided into two groups, the first group that includes the trials containing the P300 signal, i.e., those generated by the target stimulus, and the second group containing the trials of the non-P300 signal, i.e., the non-target stimulus.

To visually distinguish the two signals, the data corresponding to the Cz channel were averaged. The data from all subjects were divided into two groups, the first group corresponding to the disabled subjects (subject 1 to subject 4) and the second group corresponding to abled subjects (subject 5 to subject 8). The signals corresponding to P300 and non-P300 were recorded as shown in Figure 3.4.

Both groups can clearly distinguish the peak of the P300 signal, but both groups show different behaviors in terms of the latency and amplitude of the P300 signal. In the disabled subjects, it can be

that the peak of the P300 signal occurs at about 450 ms, while in the abled subjects, the difference in the signals is noticeable after 250 ms. As for the amplitude, the difference is small, but it exists and is greater in the case of the abled subjects.

After splitting the data into both groups, P300 and non-P300, the first GC calculation is performed. Three considerations were made for the analysis, in the first instance, the data is analyzed using all subject sessions, this approach is called ”full analysis”. In the full analysis, after averaging the trials corresponding to the 6 runs of each session and considering the 4 sessions, the structure is 32 x 32 x 480 for the P300 signal and 32 x 32 x 2400 for the non-P300 signal, which corresponds to electrodes x samples x trials.

To explain the functional connectivity methodology used in this project, Subject 6 and Subject 1 are used as examples, in the first case due to the remarkable difference between the connectivity estimates found between P300 and non-P300, and in the second case due to the similarity between the measurements of both connectivity values.

In a first test, without prior processing, as expected, the tool shows collinearity and non-stationarity errors. The Figure 3.5, shows the obtained result, using subject 8 as an example. The electrodes that are compared are on the X and Y axes. The first column corresponds to the calculated GC values for each pair of electrodes, the second column corresponds to the calculated p-values and the third column shows the values considered significant. A p-value less than 0.05 is statistically significant showing strong evidence against the null hypothesis. As explained in the previous sections, the null hypothesis yields a causality value of zero, i.e., there is no causality between the compared pair of electrodes. The alternative hypothesis, on the other hand, states that there is a significant causality value between these electrodes.

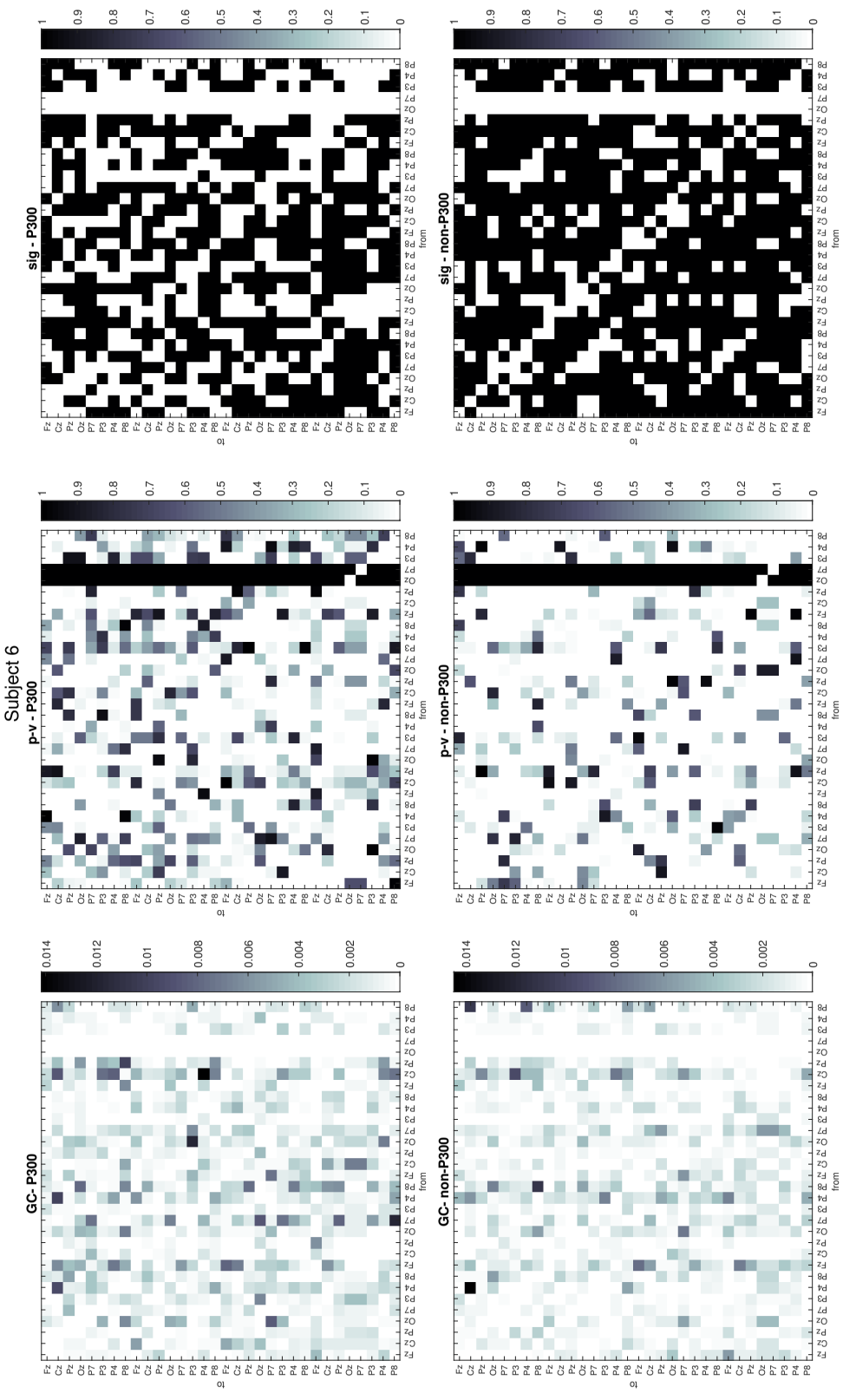

Figure 3.5: GC results for subject 6 using standard electrodes shown in Figure 3.6. Complete analysis with 1000 ms signal. The first line shows the results for the P300 signal, the second line shows the results for the non-P300 signal.

After considering the results, due to the existing collinearity and the non-stationary nature of the analyzed signals, the connectivity values are difficult to study, the calculated model order is 20, which is the maximum, it is a high model order and GC does not work. It is also important to consider that the evaluated nodes are not sources, the analysis of all electrodes can produce false values of causality, as explained above, for this process PLI can be used (Stam et al., 2007), since this study is limited to Granger Causality analysis to study the dynamics of brain network, its application is suggested in future studies; for the above, to exhibit this problem, a reduction of the number of electrodes to a smaller set is suggested.

For ERP, it is assumed that the electrodes located in the occipital and parietal lobes, considering the international 10/20 system, are the ones that provide more information about recognition according to several studies conducted (Vidal, 1977, Blankertz et al., 2011, Krusienski et al., 2006, Qin et al., 2016 Hoffmann et al., 2008), where very high precision was achieved in identifying the signals produced by the target stimuli.

For this analysis, the first approach considered was to apply the combination of 8 standard electrodes used in (Hoffmann et al., 2008), these electrodes are: Fz, Cz, Pz, Oz, P7, P3, P4, P8; their location on the scalp can be seen in Figure 3.6.

The electrodes, which are referred to as the standard, are the result of extensive research and analysis by several authors, as shown in Table 3.1. These have used various techniques, such as forward selection and backward elimination, to determine which electrodes are more suitable for different subjects and different experimental conditions. depending on the accuracy of the classification obtained with these electrodes. In Table 3.1, authors propose different electrodes, but it can be observed that many of them are repetitive and it is precisely this consistency of results, despite the differences in the analyzes, that has led to the definition of standardization in the use of the above electrodes.

Reference	Electrodes
Vidal, 1977	Pz, Oz, O1, O2, Fz
Farwell and Donchin, 1988	Pz
Polikoff et al., 1995	Pz, Cz, Fz
Donchin and Coles, 1988	Pz, Cz, Fz, O1, O2
Kaper et al., 2004	Pz, Cz, Fz, Oz, P3, P4, PO7, PO8, C3, C4
Serby et al., 2005	Pz, Cz, Fz, Oz
Sellers and Donchin, 2006	Pz, Cz, Fz
Piccione et al., 2006	Pz, Cz, Fz, Oz
Krusienski et al., 2006	Pz, Cz, Fz, Oz, P3, P4, PO7, PO8
Hoffmann et al., 2008	Pz, Cz, Fz, Oz, P3, P4, P7, P8
Cecotti et al., 2011	Pz, Oz, P3, P7, P8
Ryan et al., 2017	Pz, Cz, Fz, Oz, P3, P4, PO7, PO8
Sheng et al., 2018	Pz, Cz, Fz, Oz, O1, O2

Table 3.1: Standard electrode selection for the detection of P300 ERPs. Approaches by different authors. Modified from (Changoluisa et al., 2020).

Another observation made from the results is that the number of GC values considered significant is larger for the non-P300 signals than for the P300 signals. This is partly attributed to the existing asymmetry in the dataset. For this reason, to balance the available dataset, the trials corresponding

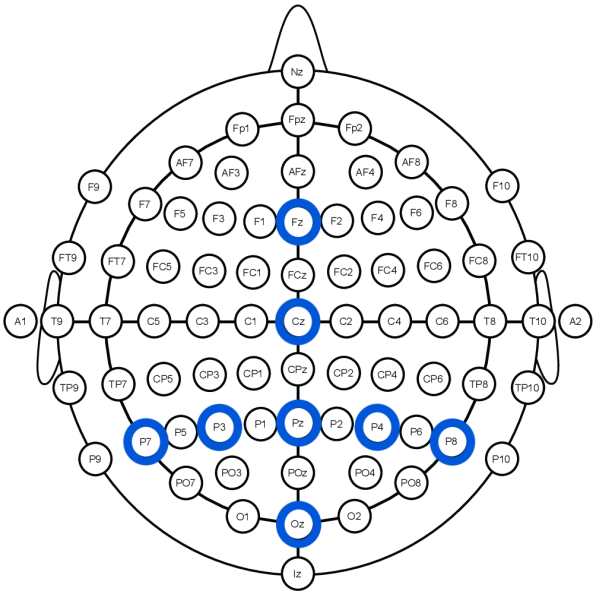

Figure 3.6: Standard Electrodes location.

to the non-target stimulus cases were limited to the same number of trials as in the target stimulus case. Bootstrapping is used to select the trials that provide some randomness for the selection of the non-target set. The bootstrapping method was proposed in (Efron, 1979). The idea of this method is that inference to a population can be modeled from sample data by performing a new sampling on the sample data, and being able to make an inference to a sample from the re-sampled data.

For this step, the MATLAB function BOOTSTRP [9] is used, it is performed once at the beginning of the analysis, the selected items are kept throughout the process. To remove the problem of non-stationarity, the entire signal is no longer analyzed i.e., 1000 ms. Now the signal is divided into 4 windows of 250 ms each, where a priori stationarity can be assumed. The results can be seen in Figure 3.7. Reducing the number of electrodes used for the analysis helped with the collinearity problem, plus performing an analysis with shorter windows eliminated the non-stationarity problem.

[9] BOOTSTRP: https://www.mathworks.com/help/stats/bootstrp.html

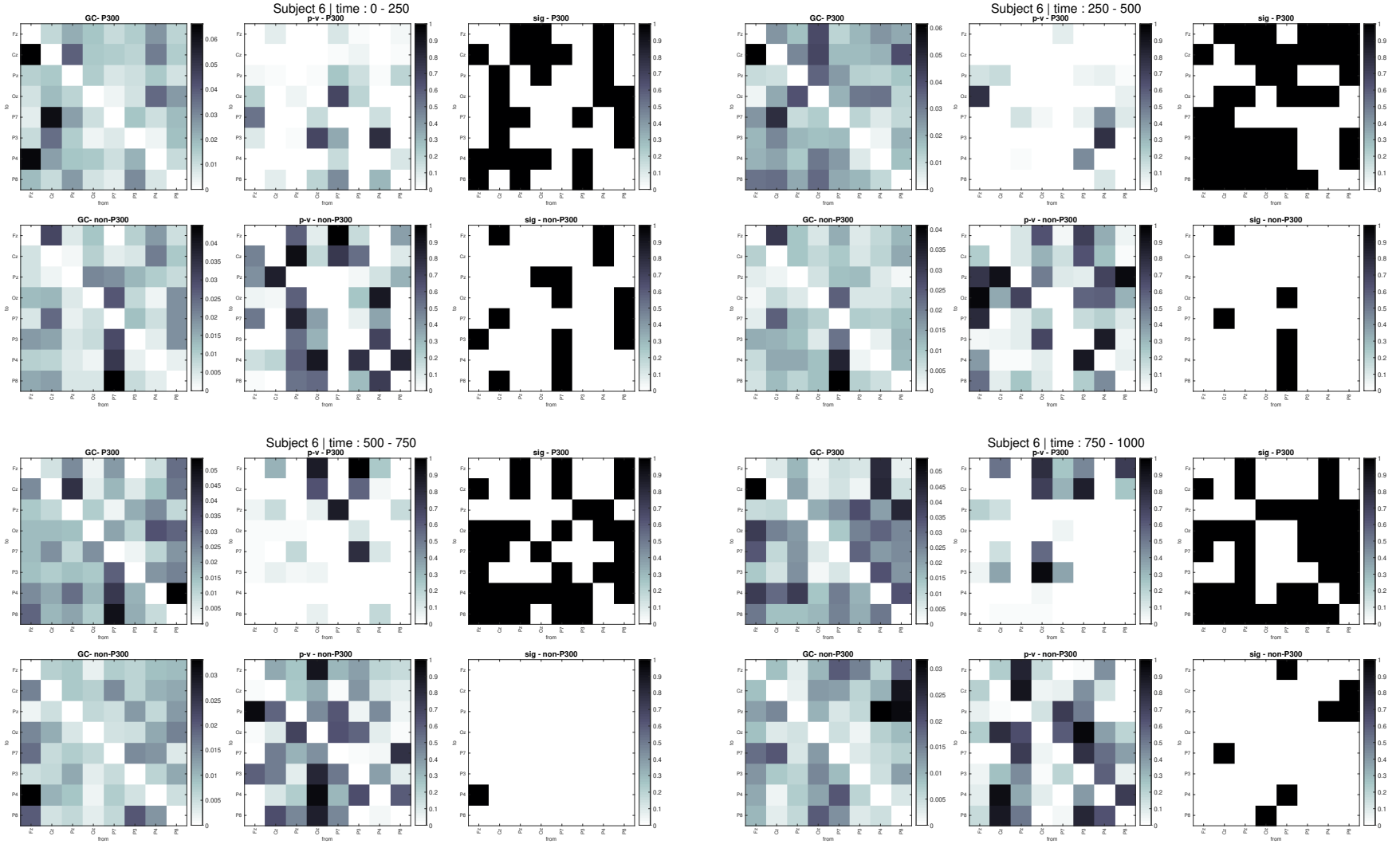

Figure 3.7: GC results for subject 6 using standard electrodes shown in Figure 3.6. 250 ms window analysis. The first column of each window corresponds to GC values, the second column corresponds to probability values calculated from GC, the third column corresponds to significant values, i.e., probability values < 0.05, significant values are colored black.

As can be seen in Figure 3.7, the window corresponding to the interval from 0 to 250 ms, similar to the behavior of the characterization of the P300 signal for abled subjects shows greater connectivity in the non-P300 signal. On the other hand, in the window between 250 and 500 ms, where a greater connectivity of the P300 signal would be expected compared to the non-P300 signal, the difference is clearly seen, and noticeable compared to the first window, where both signals behave similarly.In the window corresponding to the interval from 500 to 750 ms, as in the previous window, the non-P300 values are still lower than in the P300 case. Finally, in the window from 750 to 1000 ms, the significant values decrease in both cases. It can be seen that the connectivity increases in the non-P300 signal, but the significant values of the P300 signal remain larger.

To analyze this behavior in depth, an analysis with overlapping windows is proposed in order not to lose features of the signal that would otherwise be omitted. Since the goal is to eliminate the non-stationarity without affecting the accuracy of the model fitting, the selection of the appropriate window size is an important step, for this purpose, different window and overlap sizes have been tested.

3 An analysis of the results is proposed using overlapping windows of variable size, from 62 to 469 ms as a first approximation, attempting to analyze the behavior in extreme cases. It is also proposed to analyze the differences that occur when varying the size of the overlap, i.e., the signal segment on which the windows overlap; overlap sizes from 0 ms to 156 ms are initiallyproposed. When analyzing extreme cases, as mentioned, it is found that in all cases the best window size is close to the 250 ms window, as can be seen in Figure 3.8, for this reason, for a more realistic analysis in a second approximation, values close to 250 ms are proposed for the analysis, i.e., 118 ms, 219 ms, 250 ms, 281 ms. The sizes proposed for the overlap are kept.

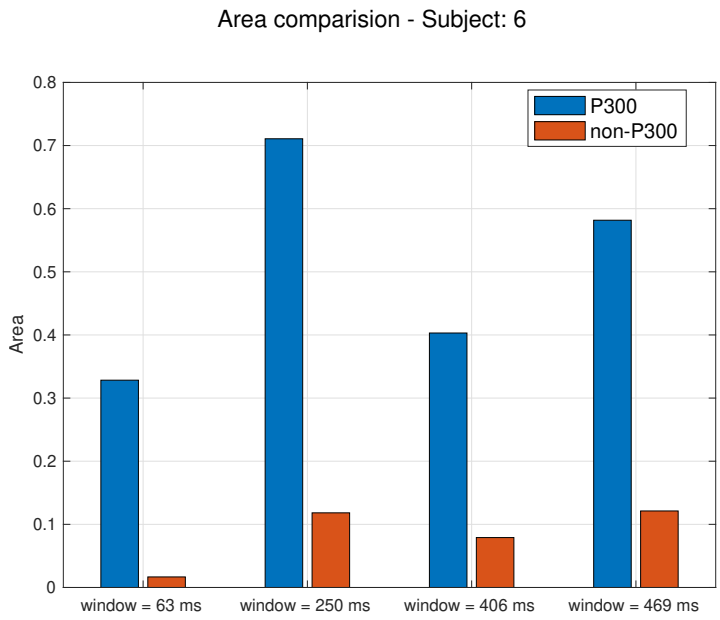

Figure 3.8: Area calculation results of overlapping windows curve for different and 'extreme' windows and overlap sizes, subject 6. W represents the window size, while O represents the overlap.

To quantify the causality value calculated in each window, 3 measures were proposed:

- The sum of GC values, considered significant per window.
- The mean of the p-values considered significant per window.

- The sum of the significant values per window.

To illustrate this calculation, we again analyze the second case of an overlapping window of 188 ms, with an overlap of 31 ms, using subject 6 as an example. In this case, there are 26 windows along the signal, so 26 values are generated per window. Figure 3.9 shows this result for the three measures considered.

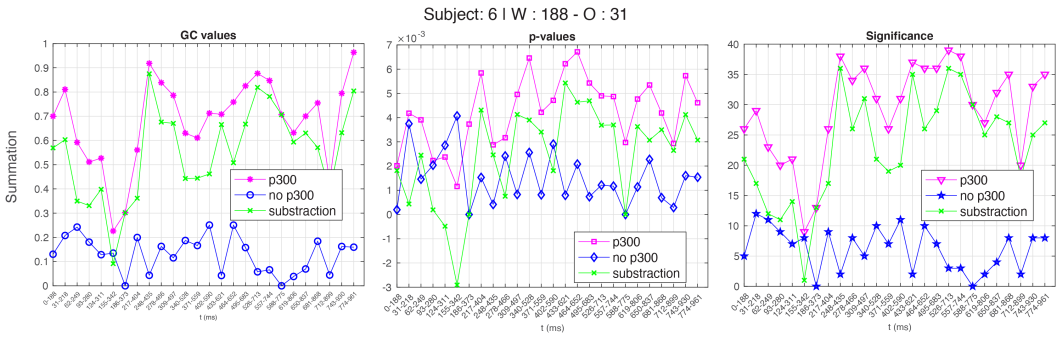

Figure 3.9: Results of the area calculation for subject 6 with overlapping windows of 188 ms and an overlap of 31 ms. The first column shows the area curve obtained by addition of the significant GC values. The second column shows the area curve obtained by averaging the significant P-values. The third column shows the sum of the significant values. W represents the window size, while O represents the overlap.

The calculation of each point is performed as follows: the point corresponding to the window from 217 ms to 404 ms is taken as reference, the GC probability and significant values corresponding to this window are shown in Figure 3.10. As can be seen in the third column of Figures 3.9 and 3.10, there are 26 significant causality values in the case of P300 and 9 in the case of non-P300. The three metrics considered are explained below:

- In the first column, a summation of GC values is performed, a GC value is considered if the significance for this value is 1, i.e., 26 values for P300 and 9 values for non-P300. The result of the sum is equal to 0.5609 for P300 and in case of non-P300 the sum is equal to 0.1994.
- The 26 and 9 significant values of p-values corresponding to P300 and non-P300 respectively are averaged, the result of this calculation is 0.0058 for P300 and 0.00015 for non-P300.
- Finally, in the case of significance, the significant values are added, obtaining 26 significant values for P300 and 9 significant values for non-P300, as mentioned.

After obtaining the results of the proposed metrics for each overlapping window, a curve is obtained to parameterize the P300 signal, the non-P300 signal and the difference between them, in the case of the analyzed example with 26 points per curve. The calculation of the area under the curve was proposed to quantify the causality in each case.

For this calculation, only the first proposed measure is considered, i.e., the sum of the significant GC values, since it is the measure that best captures the characteristics of the connectivity of the signal, considering not only whether the connectivity is present or no, but also at what level it is present. From

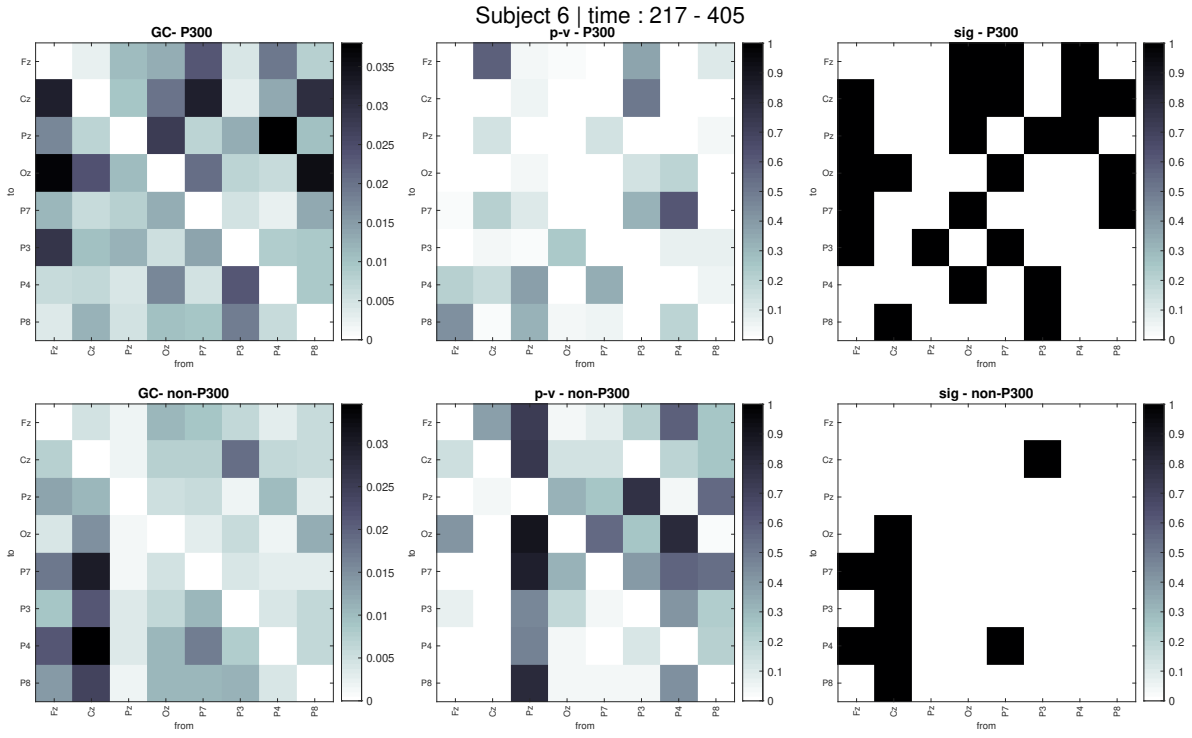

Figure 3.10: GC values, overlapping window from 217 ms to 404 ms. The first column corresponds to GC values, the second column corresponds to probability values calculated from GC, the third column corresponds to significant values, i.e. probability values ¡ 0.05, significant values are colored black.

the area calculation, a single value corresponding to each overlapping window and the overlap used is obtained. The Figure 3.11, shows the area results obtained for both signals in all the cases considered.

From Figure 3.12, we can see that in the case of the example subject (subject 6), the window that provides a larger P300 signal area value corresponds to the 219 ms window, and the best overlap corresponds to 31 ms overlap in all cases. However, the same behavior is not observed for all subjects, this is discussed in (Salazar, 2020).

Although the behavior observed in subject 6 is ”ideal”, this does not occur in all subjects due to the variability present between and within subjects, this analysis is explained in detail in (Salazar, 2020), Figure 3.13, shows one of the cases of the curves generated from the overlapping windows in subject 1. The difference between the P300 signal and the non-P300 signal is not clearly distinguishable in subject 1, although an increase in the values for causality, p-values, and significance can be seen in the standard P300 range. It is important to emphasize that the behavior observed in the first values of each analyzed curve, where the non-P300 signal is larger than the P300 signal, was also observed in other subjects. This behavior can be attributed to influence from other components of the ERP.

In the case studied, when evaluating the total signal without considering the window selection technique, the area calculation with different overlapping windows shows that in most cases the non-P300 signal is larger, as shown in Figure 3.14.

Due to the small difference between the analyzed curves, the initial behavior may strongly influence the result, and it may be found that in certain cases the expected behavior, i.e., there is a greater connectivity in the P300 signal, is not fulfilled. For this reason, it is important to define the exact

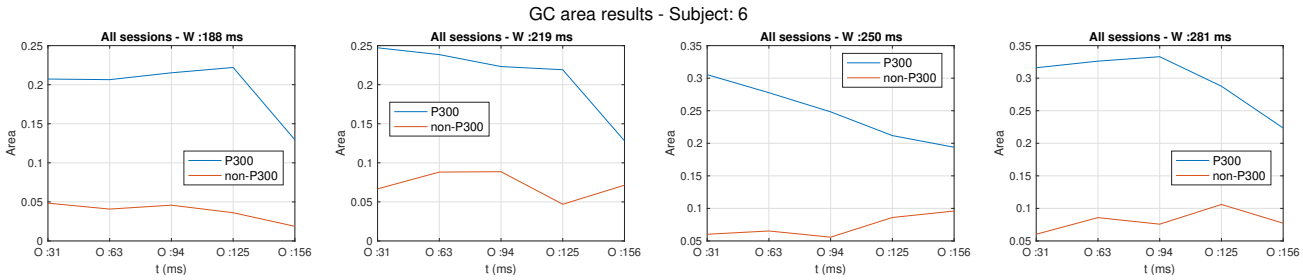

Figure 3.11: Area calculation results of the overlapping window curve for different windows and overlap sizes for subject 6. W represents window size, while O represents the overlap.

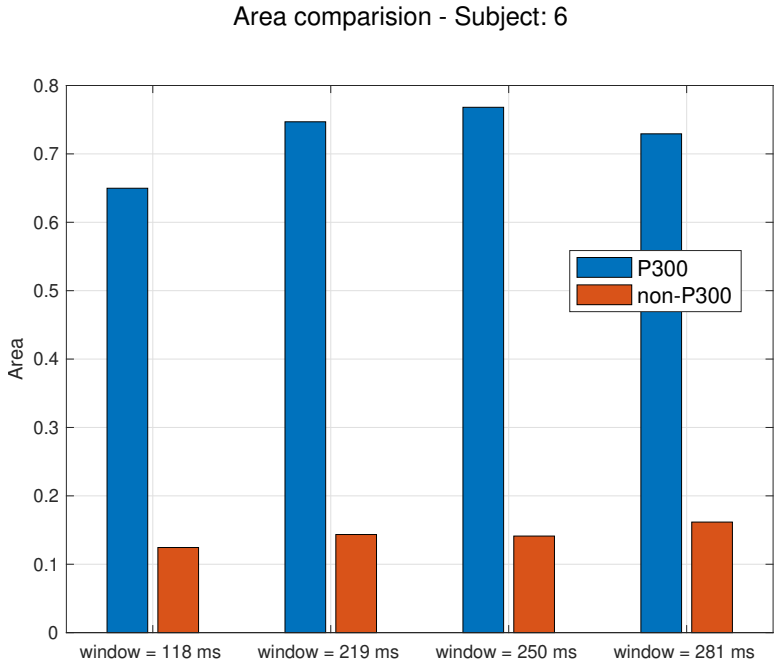

Figure 3.12: Comparison of area values calculated for different overlapping window sizes, subject 6. Color blue represents the P300 connectivity values, while color orange represents non-P300 connectivity values.

window in which the P300 activity occurs, from which the functional connectivity can be roughly evaluated.

To define the proper size of the window, an interval of 250 ms and 750 ms is taken as a reference, since this is the approximate range in which the latency variation of the P300 signal is detected, as explained in the previous sections. From the established range, the lower threshold of the signal is varied as a function of the minimum Θ values, which is defined by: $\Theta_{min} = [220ms, 255ms, 290ms]$. In the same way, the higher threshold of the signal varies as a function of the maximum theta value, which is defined by: $\Theta_{max} = [590ms, 630ms, 670ms]$. Figure 3.15, illustrates in a better way what has been explained, being observed in a representation of the signal, and how it is proposed to vary the thresholds.

After calculating the area values corresponding to each window size variation as shown in Figure 3.16, it was found that the window providing the largest area of the P300 signal is the one in the range from 210 ms to 710 ms. However, this area does not provide the greatest difference between the P300 and non-P300 signals. On the other hand, the window in the range from 290 ms to 670 ms provides

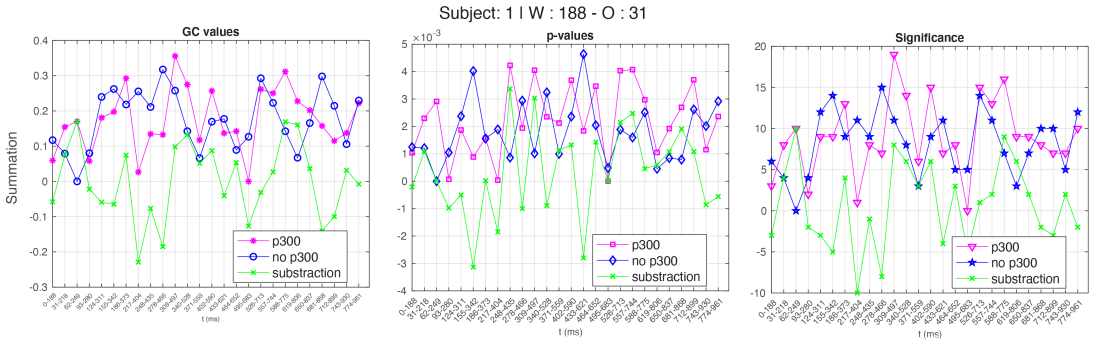

Figure 3.13: Results of area calculation for subject 1 with overlapping windows of 188 ms and an overlap of 31 ms. The first column shows the area curve obtained by adding the significant GC values. The second column shows the area curve obtained by averaging the significant P-values. The third column shows the sum of the significant values. W represents the window size, while O represents the overlap.

the largest difference between the P300 and non-P300 signals.

Although what we are trying to demonstrate is the difference between the existing connectivity levels between P300 and non-P300, we assume that this behavior is ignored. We will not select the window that shows the largest difference between P300 and non-P300, but the one that provides the largest value of area. In the case of subject 1, the window between 210 ms to 710 ms is chosen.

After selecting the appropriate window size in which the P300 signal is maximum, we will to analyze what influence the number of electrodes has on this result, for this purpose tests will be performed by varying the number of electrodes selected, the observations from this analysis will be discussed in the next section. As it is obvious and has already been discussed, the connectivity levels between P300 and non-P300 signals are highly dependent on the electrodes used for the analysis, for this reason other electrode selection methods are also proposed to analyze the differences found in functional connectivity.

3.3.2.1 Electrode Selection Methods

Two approaches are proposed for electrodes selection, the first is selection using the Bayesian Linear Discriminant Algorithm (BLDA) with forward selection, and the second using values of the coefficient of determination analysis, also called r2 analysis, both approaches are described in detail below.

3.3.2.1.1 Electrode selection using BLDA and forward selection:

Implementing an algorithm that can adapt to the possible differences in the data for each subject or session allows for a more robust system and higher precision in event detection. (Speier et al., 2015, Lotte et al., 2018, Changoluisa et al., 2020).

BLDA is a variation of Fisher's Linear Discriminant Analysis (LDA), it is based on a probabilistic regression network in which the targets t_i depend linearly on the observed features X with an additive Gaussian noise term n, as observed in the equation 3.6:

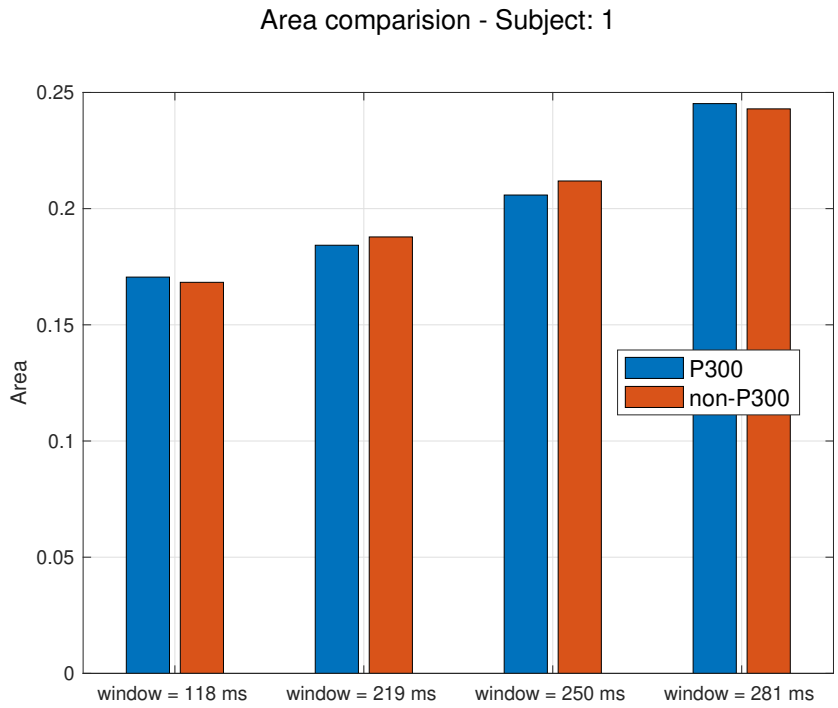

Figure 3.14: Comparison of area values calculated for different overlapping window sizes for subject 1, who is not one of the subjects giving good results. In this case, the window selection is not considered, leading to a poor GC result. The blue color represents the P300 connectivity values, while the orange color represents the non-P300 connectivity values.

$$t = w^T X + n, \tag{3.6}$$

where w represents the weight vector. BLDA regularization is used to avoid overfitting in large and noisy datasets, as is often the case with EEG signals. The degree of regularization can be estimated automatically and quickly by Bayesian analysis based on training data. A more detailed explanation of this algorithm can be found in Hoffmann et al., 2008, where the high classification accuracy that can be achieved by its use was shown, results similar to those in (Cecotti and Ries, 2017, Ludwig and Kong, 2017, Momennezhad et al., 2014).

For the selection of electrodes with BLDA-FS, we first propose a selection on all electrodes and then a selection by ROIs. Electrode selection with BLDA was done by testing the electrode combinations and finding the highest values of accuracy in classification, finally the electrodes that showed the best results were selected, for this the forward selection method was used. Forward selection(FS) is a straightforward variable selection strategy (Herrera et al., 2009), for this study electrode selection was performed using BLDA and forward selection (BLDA-FS) as follows:

- To select the first electrode, it is necessary to calculate the accuracy values resulting from BLDA classification, from these results the electrode that showed the best performance is selected.
- The first selected electrode is combined with another electrode between the unselected electrodes. The results obtained after classifying each pair of electrodes are compared to select the pair of electrodes that provides the highest accuracy.

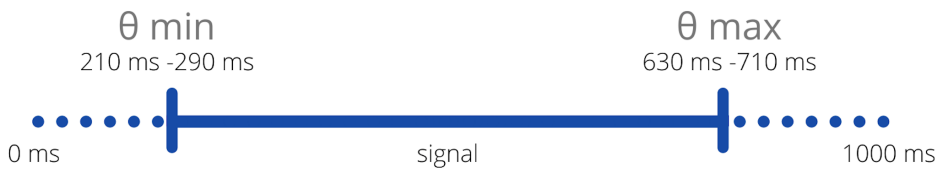

Figure 3.15: Suggested Θ thresholds for selecting the right window size depending on Θ_{min} and Θ_{max}.

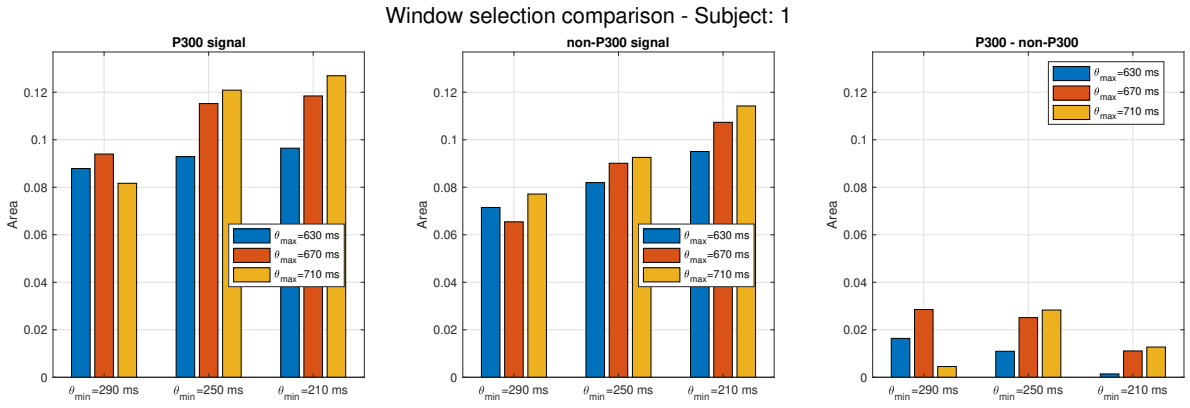

Figure 3.16: Results of area calculation for subject 1 after window selection tests. The irst column shows the P300 GC values for all Θ_{min} and Θ_{max} variations, the second column shows the non-P300 GC values for all Θ_{min} and $\Theta_{max}x$ variations and the third column shows the difference between P300 and non-P300 GC values for all Θ_{min} and Θ_{max} variations.

- After the electrode pair with the best accuracy is selected, it is combined with another electrode from the group of unselected electrodes to evaluate their performance in the classification and select the 3 electrodes that provide the best performance.

- This process is repeated iteratively until the desired number of selected electrodes is reached.

This process was performed from two points of view, in the first the electrodes are selected considering the window selected for each subject with the process described previously, this window varies around 250 ms to 750 ms as explained, being the interval in which the P300 activity is detected as mentioned in the previous literature.

The second consideration provides for the division of the scalp into 4 regions of interest (ROIs), this refers to partial volumes of the totality of the electrodes, these samples are used to analyze the behavior of functional connectivity between the 4 defined quadrants. The electrodes assigned to each ROI can be seen in Table 3.2. For the selection, a rule was established that adjacent electrodes cannot be selected with a parameter n that defines the distance that must exist between the selected electrodes, in this case being been set equal to 1. Furthermore, the selection was performed according to the following procedure:

- From the total set of electrodes, the one that achieves the best accuracy in classification is selected.
- The ROI, to which this electrode belongs, is identified and the electrodes belonging to this ROI are excluded.
- The first electrode selected is combined with the others, accuracy values are calculated from each combination. The electrode pair with the highest accuracy is selected.
- The electrodes belonging to the second ROI are also excluded, and the process is repeated to find a third electrode considering the maximum accuracy.
- The last electrode is selected from the last ROI. One electrode is selected for each ROI.

ROIs	Location	Electrodes
1	Left Frontal - Parietal	Fp1, AF3, F7, F3, FC5, FC1
2	Right Frontal - Parietal	Fp2, AF4, F4, F8, FC2, FC6, Fz
3	Left Occipital - Parietal	T7, C3, CP5, CP1, P7, P3, PO3, O1
4	Right Occipital - Parietal	Cz, C4, T8, CP2, CP6, Pz, P4, P8, PO4, Oz, O2

Table 3.2: Regions of Interest and their respective selected electrodes with BLDA.

A cross-validation scheme of type K-folds was used to validate the classification, with the value of K varying depending on the case analyzed. For the full analysis, 3 of the 4 sessions are used for training and the remaining session is used for testing.

3.3.2.1.2 Electrode selection using r2 selection:

As an alternative method for electrode selection, the calculation of r2 was implemented. As observed, the behavior of r2 values varies by subject and shows discriminant information in different regions. This study is similar to the one presented in (Changoluisa et al., 2020). The r2 results can be seen in Figure 3.17. Darker colors represent high values of r2, while lighter colors indicate low values.

To select electrodes based on r2, the values of r2 for each electrode are added, in this case 32 values are considered. After the sum for each electrode is determined, the electrodes with the highest values are selected. For electrode selection based on r2 values, non-adjacent electrodes are selected, i.e., channels that are not distributed adjacent to each other according to the international 10/20 system, where the maximum values of r2 are determined. The window used for this selection was defined by the procedure described previously.

For the selection of electrodes based on r2 for analysis by ROIs, a procedure is performed as previously explained for the case of BLDA, where a single electrode is selected for each ROI. In this case, after adding the r2 values of the electrodes that are part of each ROI, the one that gives the largest value after the sum is selected.

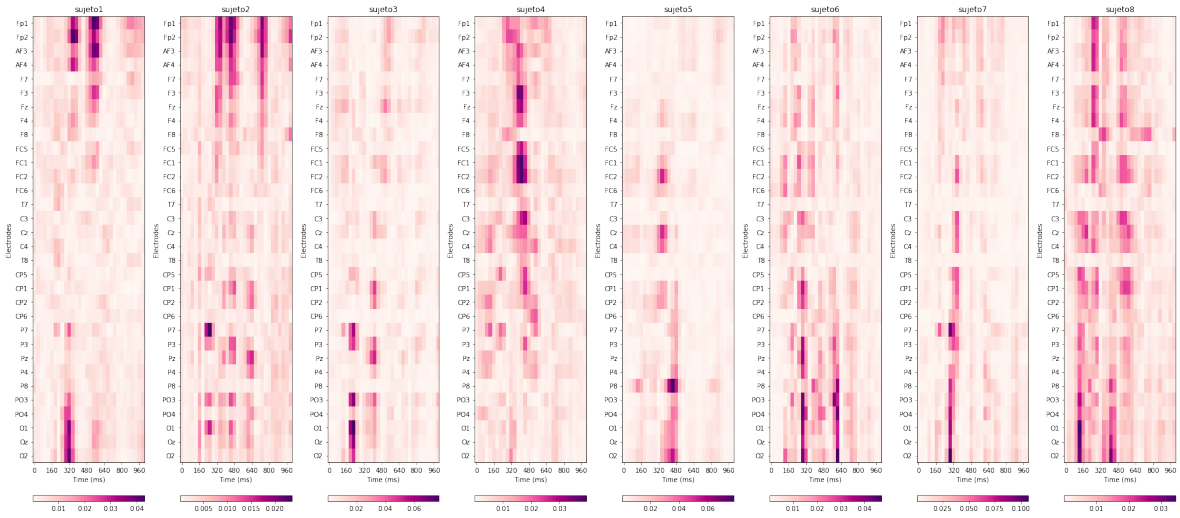

Figure 3.17: r2 results of general analysis.

3.3.3 Statistical Analysis

In order to analyze the differences found in functional connectivity between the P300 and non-P300 signals and to determine whether they are significantly different, the use of the t-test is proposed due to the characteristics of the sample to be analyzed and the required discriminant analysis to be performed. The hypotheses established for this analysis are:

- **Null hypothesis:** There is no difference between the means of the P300 ($\bar{x}P300$) and non-P300 ($\bar{x}non-P300$) signals, i.e., $\bar{x}P300\bar{x}non-P300=0$.
- **Alternative Hypothesis:** There is a difference between the mean values the P300 ($\bar{x}P300$) and non-P300 ($\bar{x}non-P300$) signals, i.e. $\bar{x}$P300 - $\bar{x}$non-P300 0.

The significance level set for the study is 5%, however the resulting p-values for the analysis are shown.

4

Results

For the present analysis of the results, a study considering the 4 sessions of each subject as a single dataset is proposed. The standard electrodes described earlier in the methodology are used as a first approximation, and later two approaches of electrode selection are proposed, BLDA-FS and R2.

In Chapter 2, when explaining the GC calculation, how the GC was calculated in the dataset was defined. This calculation starts with the preparation of the data, which consists in limiting the dataset to the selected electrodes, then limiting the set of non-target trials to the total number of target trials by selecting through bootstrapping, for the subsequent partitioning into sliding windows of the dataset.

For the causality calculation, the different pairs of selected electrodes are compared, from the resulting values, those considered significant are selected and with these results the causality value of each sliding window is determined. After these values are determined, a curve formed by the point from each sliding window is obtained. The area of this curve is the one that defines the total value of causality. The size of the final window is determined by this value, considering the thresholds that maximize causality. Finally, the last causality value will be the amount calculated within the general window defined as explained.

4.1 GC calculation using standard electrodes

For this analysis, the electrodes shown in Figure 3.6 are used. As explained in the previous section, after proper data processing, a connectivity analysis can be started, for which the MVGC toolbox (Barnett and Seth, 2014) is used. First, it is necessary to divide the dataset into P300 and non-P300 signals, limiting both sets to the same dimensions.

Then, the selection of overlap and overlapping window size for each subject is done as explained in Chapter 2 3.15. Table 4.1, shows the resulting values of window size and ideal overlaps for each subject, Appendix A, Table A.1 shows the area calculation performed for this selection. As mentioned earlier, the ideal window is considered the one that provides the largest area of the P300 signal, although it does not necessarily indicate the largest connectivity difference between the P300 and non-P300 signals.

Subject	1	2	3	4	5	6	7	8
Window (ms)	281	281	281	281	250	250	281	250
Overlap (ms)	156	31	156	31	125	31	31	125

Table 4.1: Selected window and overlap size for subjects 1-8 with standard electrodes.

After selecting the overlap and overlap windows, the GC values for each one are estimated, producing a curve on which the area can be calculated. Before calculating the area, the process of window selection is performed, selecting the appropriate one for each subject. The results of this analysis are shown in Table 4.2, where the maximum area value is used to determine the correct θ_{min} and θ_{max}.

Subject	1	2	3	4	5	6	7	8
θ_{min}	220	220	220	220	220	255	220	220
θ_{max}	670	670	670	670	670	670	670	670

Table 4.2: Selected window size for subjects 1-8. θ_{min} and θ_{max} values for window location with standard electrodes.

Once the window size is determined, the area values are calculated for each subject within the bounds of the selected window. Table 4.3, shows the calculated area values for the different subjects. Figure 4.1, illustrates these results. The area values represent the value of causality calculated based on the sum of causality in each overlapping window. The larger the area, the greater the causality found and therefore the greater the information flow and functional connectivity. The calculation of the area is described in detail in Session 3.2 of Chapter 3.

Subject	1	2	3	4	5	6	7	8
P300	0.2362	0.2949	0.2373	0.4268	0.3367	0.8393	0.3853	0.2298
no-P300	0.1683	0.3051	0.1036	0.4927	0.1054	0.1315	0.2030	0.1157

Table 4.3: Final area values for subjects 1-8 after window selection using standard electrodes.

As can be seen, in the case of the standard electrodes, all subjects except 2 and 4 satisfy the premise that the functional connectivity found in the P300 signal is greater than that found in the non-P300 signal. In Figure 4.2, the average area values for connectivity calculated for the P300 signal are higher than the average area values estimated for the non-P300 signal, as expected. The difference between the two areas is greater than zero in all cases.

For statistical analysis, the t-test was used for samples composed of the area values calculated for the P300 and non-P300 signals. The resulting p-value is equal to 0.067, this result is considered not quite statistically significant, but close to the established significance. The null hypothesis is not rejected, i.e., there is no significant difference between the P300 GC area and the non-P300 GC area as shown in Figure 4.1. This means that using standard electrodes, no difference can be identified between the causality results of the P300 signal and the non-P300 signal. Statistically, the difference found is not significant.

Another factor to be analyzed is how the number of electrodes used in the analysis affects the connectivity results. Several tests were performed to evaluate this behavior. The previous analysis was repeated, varying the number of electrodes. Tests were performed with 2 to 8 electrodes. The

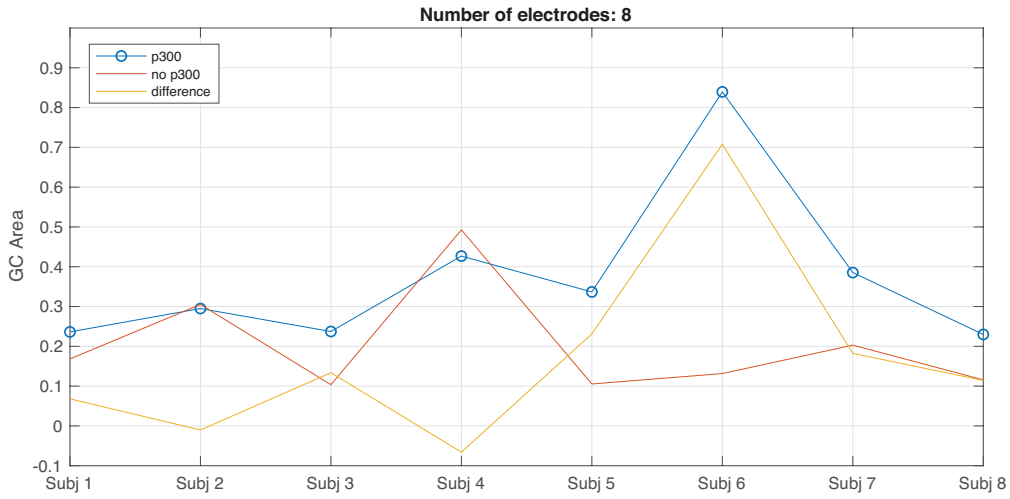

Figure 4.1: Final area values for subjects 1-8 after window selection using standard electrodes.

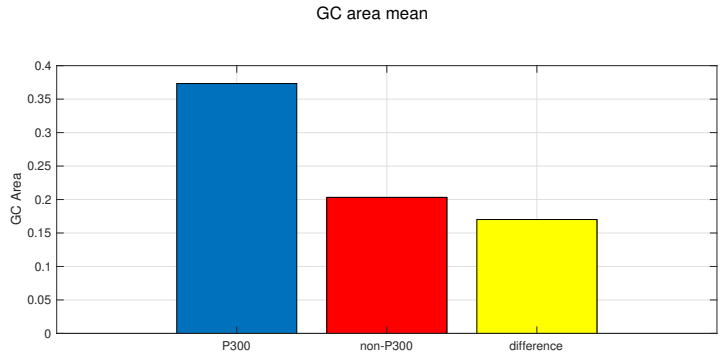

Figure 4.2: Mean GC area, considering all subjects and 8 standard electrodes.

electrodes and results of this analysis are shown in Figure 4.3. On the other hand, Table 4.4 shows the statistical and average results for all subjects. It is important to emphasize that this electrode configuration was performed as a first approximation, based on the known results observed in (Serby et al., 2005), where the electrodes Fz, Cz, Pz and Oz were proposed for P300 detection, and in (Polikoff et al., 1995) where the electrodes Fz, Cz and Pz were selected, however it is necessary to perform a more exhaustive search for future work to determine which are the electrodes that together produce a greater flow of information related to Granger Causality.

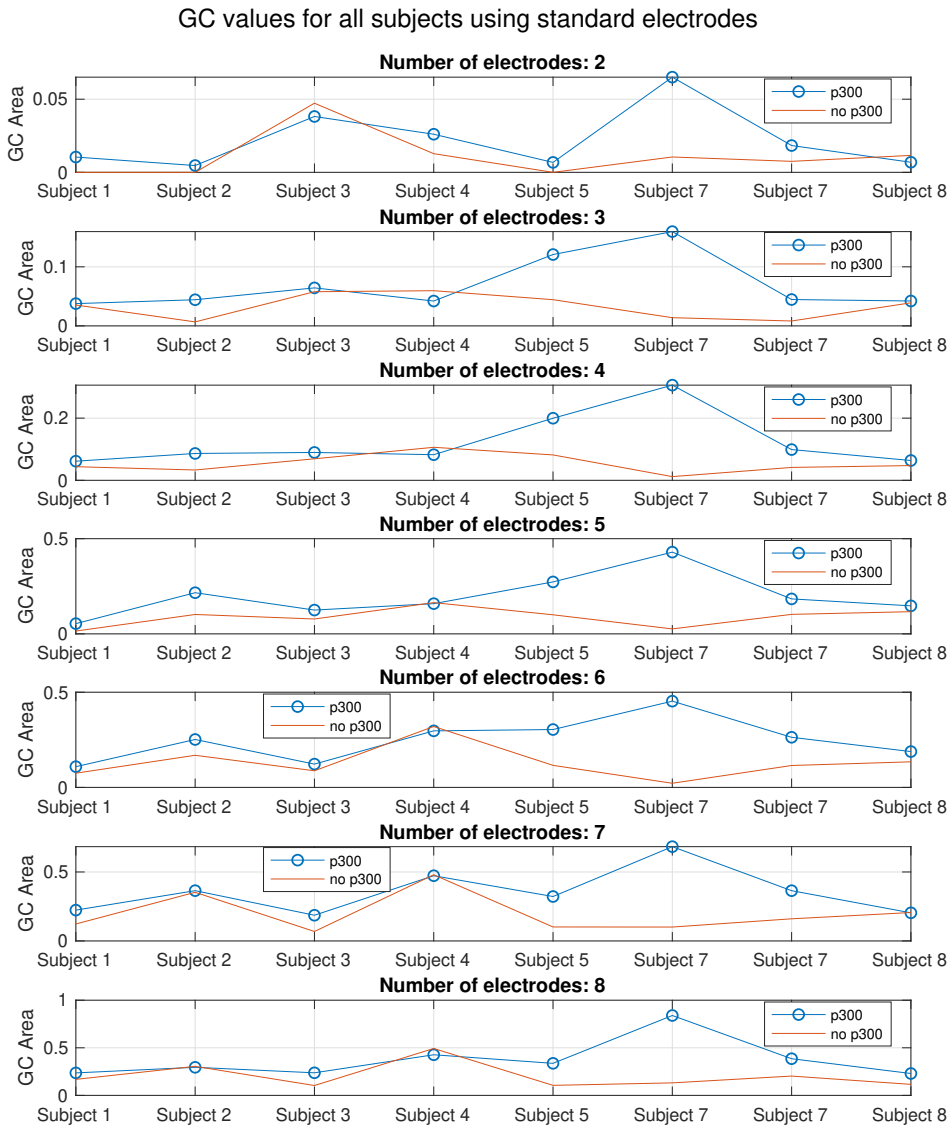

Figure 4.3: GC results for all subjects varying the number of electrodes using standard electrodes.

N. Elec.	Electrodes	t-test p-value	P300 GC	non-P300 GC
8	Fz, Cz, Pz, Oz, P7, P3, P4, P8	0.0676	0.3733	0.2032
7	Fz, Cz, Pz, Oz, P7, P3, P4	0.0680	0.3526	0.1991
6	Fz, Cz, Pz, Oz, P7, P3	0.0329	0.2486	0.1297
5	Fz, Cz, Pz, Oz, P7	0.0240	0.1983	0.088
4	Fz, Cz, Pz, Oz	0.0489	0.1236	0.0544
3	Fz, Cz, Pz	0.0605	0.0694	0.0331
2	Fz, Cz	0.2577	0.0221	0.0112

Table 4.4: Comparison of area results, considering a variable number of standard electrodes.

As can be seen in Table 4.4, varying the number of electrodes reduces the size of the functional connectivity measurements recorded in the analysis. It was found that by using a smaller number of

electrodes, a significant difference between the two signals can be obtained, as is the case when using 4, 5, and 6 electrodes. It is important to note that for the selected configuration of electrodes, the lower the number of electrodes, the higher the calculated p-value.

Figure 4.4 shows that when 4 electrodes are used, This case was chosen because it represents the smallest number of electrodes necessary to measure connectivity. The average connectivity area values for the P300 signal are higher than the average area values estimated for the non-P300 signal. The difference between these two areas is larger when using a smaller number of electrodes than when using 8 electrodes.

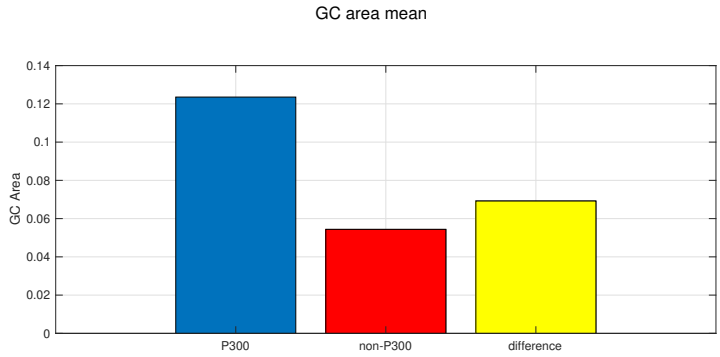

Figure 4.4: Mean GC area, considering all subjects and 4 standard electrodes (Fz, Cz, Pz, Oz).

4.2 GC calculation using BLDA-FS electrodes

To analyze the behavior of connectivity in other brain regions adapted to the characteristics of each subject's ERPs, a selection of electrodes is proposed using the BLDA algorithm and forward selection, explained in the previous chapters.

As already indicated, the selection consists in choosing the electrode combinations that had the highest accuracy after classification. The electrodes selected for each subject are shown in Table 4.5. It should be noted that one of the conditions for selection was that the selected electrodes were not adjacent, with a jump of n = 1 between electrodes. The location of the selected electrodes within the scalp is shown in Appendix B in Figures B.1 and B.2. For this analysis, it was decided to select 6 electrodes because the collinearity error was repeatedly presented with a larger number of electrodes.

Subject	Electrodes
1	AF3, T7, Fp2, C4, F7, OZ
2	FP2, FC2, AF3, OZ, CP6, P7
3	T7, F8, CP6, PO3, Fz, F4
4	FP1, P3, CP2, Fz, P8, O1
5	P3, FP1, Fz, CP6, F7, P7
6	F8, Cz O2, O1, F4, Fp1
7	Fp1, T7 AF4, FC6, Fz, P4
8	FC5, Fz, F8, Fp2, C4, Cz

Table 4.5: Electrodes selected with BLDA-FS for subjects 1-8. The location of the selected electrodes is shown in Appendix B, Figure B.1.

The process carried out in the previous case is repeated, we first proceed to the selection of the size of the overlapping window and the overlap, then the causality values per window are quantified. From here it is possible to choose the window size after varying the value of θ both at the beginning and at the end of the signal. The results of this calculation for all subjects are summarized in Table 4.6. In turn, Figure 4.5 illustrates these results. The window chosen for all cases was the 220 to 670 ms window.

Subject	1	2	3	4	5	6	7	8
P300	0.0478	0.1763	0.1255	0.0917	0.2429	0.2799	0.2237	0.0373
no-P300	0.0286	0.1062	0.0380	0.1379	0.0303	0.1065	0.1278	0.0141

Table 4.6: Final area values for subjects 1-8 after window selection using BLDA-FS electrodes.

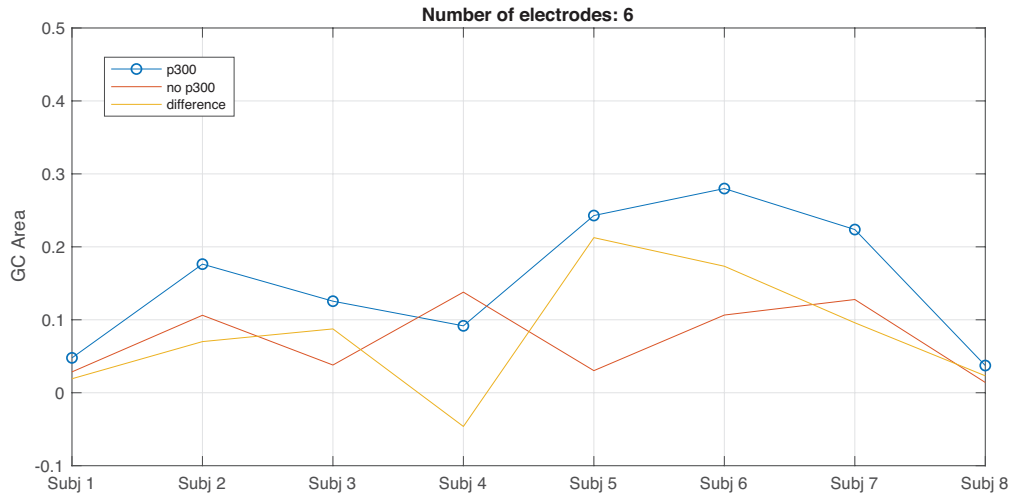

Figure 4.5: Final area results, mean for subjects 1-8 after window selection using BLDA-FS electrodes.

The t-test was applied obtaining a p-value of 0.0497, rejecting the null hypothesis, i.e., there is a significant difference in connectivity results between the P300 and non-P300 signals using the electrodes selected by BLDA-FS.

As in the previous case, it is also proposed to analyze how the connectivity results change by varying the number of electrodes. For this purpose, the results obtained for all subjects by varying the number of electrodes from 2 to 8 are shown in Figure 4.6 and in Table A.2 from Appendix A. In addition, Table 4.7 shows the results of the statistical analysis and the average values for all subjects of the connectivity found in both the P300 signal and the non-P300 signal.

N. Elec.	t-test p-value	P300 GC	non-P300 GC
6	0.0497	0.1531	0.0737
5	0.1322	0.1203	0.0733
4	0.1197	0.895	0.0566
3	0.3234	0.0458	0.0303
2	0.2762	0.0272	0.0189

Table 4.7: Results of P value, GC area results for P300 signal and GC area results for non-P300 signal, where the number of BLDA-FS electrodes was varied from 2 to 6.

As can be seen in the connectivity results calculated from the selected electrodes in Figure 4.7, the calculated area in the case of causality measured in the P300 signals is larger than that in the non-P300 case. The difference between the two results is greater than zero.

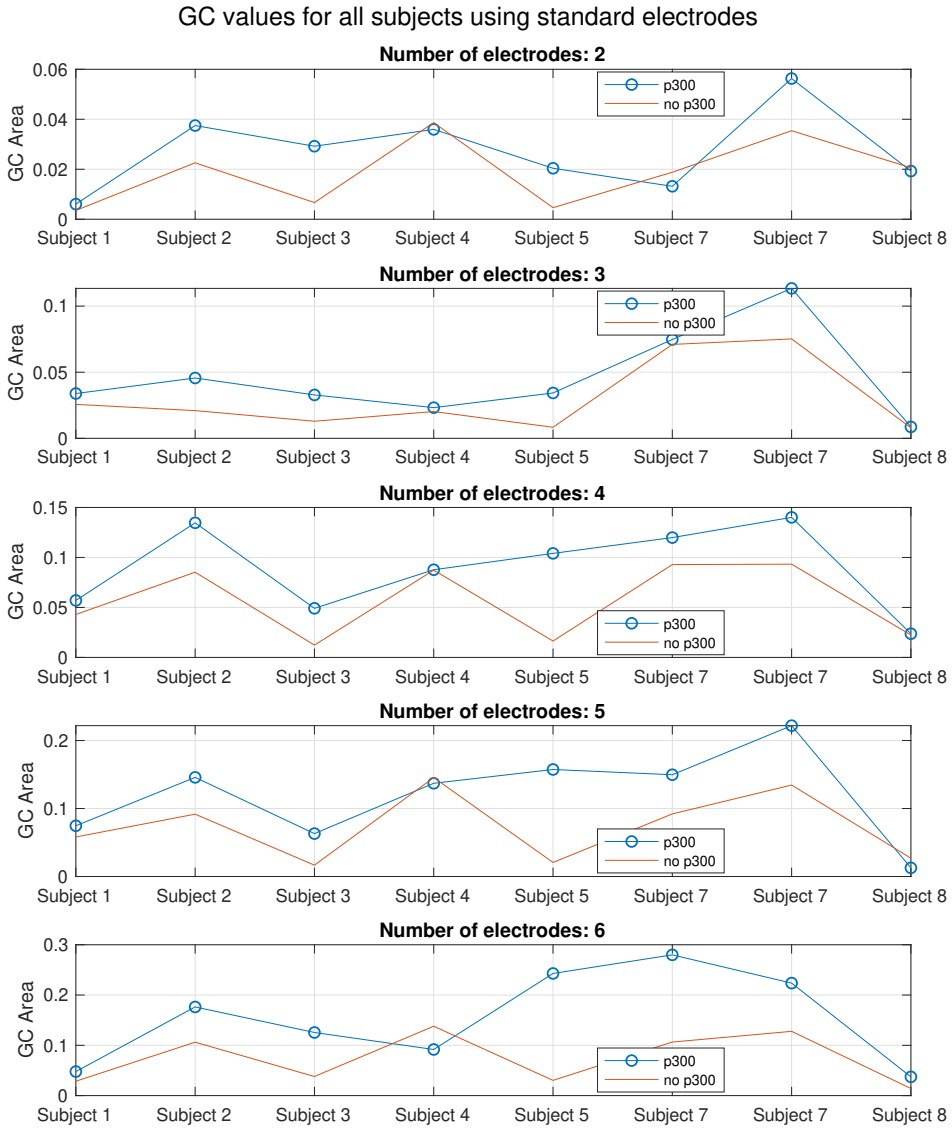

Figure 4.6: GC results for all subjects varying the number of electrodes using BLDA-FS electrodes.

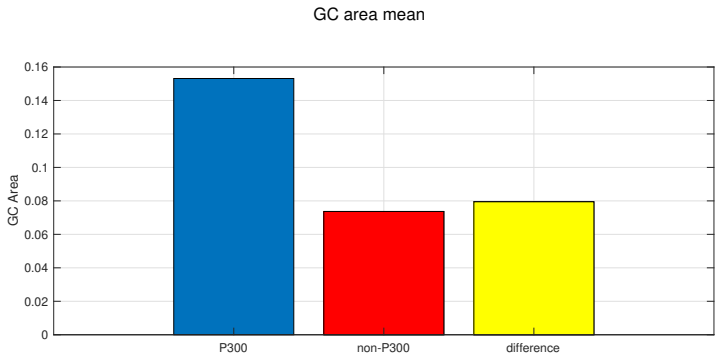

Figure 4.7: Mean value of GC area, considering all subjects and 8 selected electrodes with BLDA-FS.

4.3 R2 selection

The third proposed approach was to select electrodes from R2 as explained in Section 3.2.1.2 of Chapter 3, with the aim of contrasting the results obtained. For the selection of electrodes, as in the previous case, the rule of adjacent electrodes is applied, limiting the selected electrodes to those that are not spatially close to each other. The electrodes selected with this method are shown in Table 4.8.

Subject	Electrodes
1	Fp1, Fp2, Oz, F3, PO4, Fz, F4, PO3
2	Fp2, Fp1, F7, PO3, Pz, F3, P7, F4
3	PO3, Fz,Oz, Pz, P7, Fp2 , PO4, Cz
4	FC2, FC1, Fp1, Cp2, Fp2, CP1, P7, FC5
5	P8, O2, Cz, O1, C4, P4, F4, Pz
6	PO3, PO4, P8, Pz, Oz, FC1, FC6, P7
7	P7, O2, Fp1, Fp2, O1, P3, P8, P4
8	O1, O2, CP1, FC2, FC1, CP5, F8, P8

Table 4.8: Electrodes selected with r2 for subjects 1-8. The location of the selected electrodes is shown in Appendix B, Figure B.2.

As in the previous case, window selection is performed after defining the ideal values of overlap and overlapping windows for each subject. The window defined in this analysis was a window of 220 ms to 670 ms for all subjects except for subject 7, whose calculated window was 255 ms to 670 ms. The results of this calculation for all subjects are summarized in Table A.3. In turn, Figure 4.8 illustrates these results.

Subject	1	2	3	4	5	6	7	8
P300	0.0318	0.2017	0.0568	0.1304	0.1892	0.3425	0.0679	0.0632
no-P300	0.0169	0.2033	0.0343	0.1374	0.0090	0.1646	0.0379	0.0230

Table 4.9: Final area values for subjects 1-8 after window selection using r2 electrodes.

The t-test was performed on the data and yielded a p-value = 0.2352, indicating that the results were not significantly different. With this selection of electrodes, there are differences between the measured causality in the P300 and non-P300 signals, but these differences are not significant.

Figure 4.9, shows the differences between the calculated mean areas for the P300 area as well as for the non-P300 area and the difference between them. As expected, the area for the P300 causality is larger than for the non-P300 case. The difference maintains a value greater than zero.

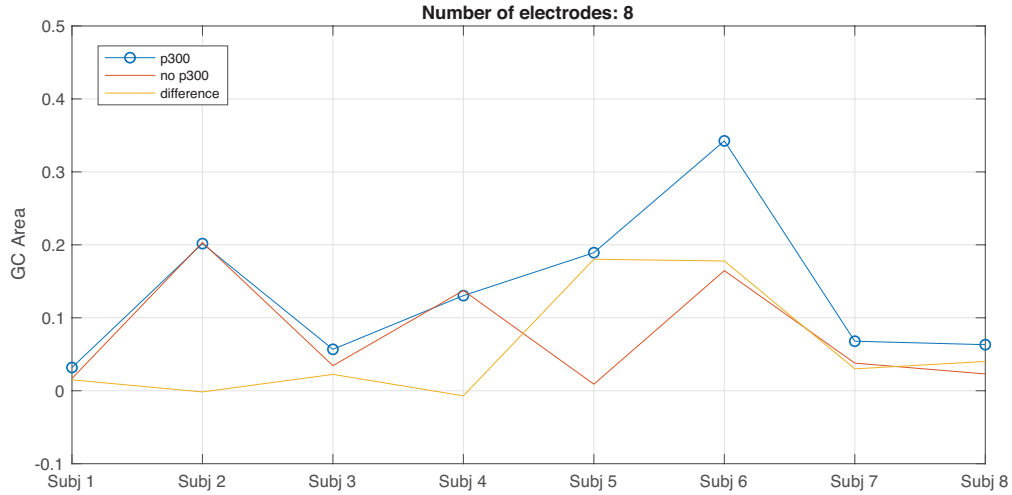

Figure 4.8: Final area results for subjects 1-8 after window selection using r2 electrodes.

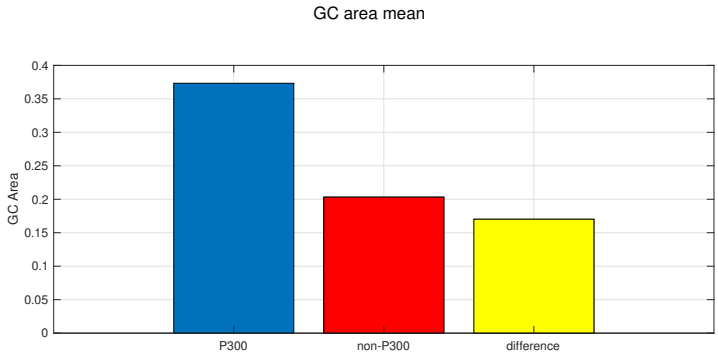

Figure 4.9: Mean value of GC area, considering all subjects and 8 selected electrodes with r2.

We wanted to analyze how the connectivity results change by varying the number of electrodes. The average connectivity results after this analysis are shown in Figure 4.10. On the other hand, Table 4.10 shows the p-values calculated for each case as well as the connectivity averages of both the P300 signal and the non-P300 signal.

N. Elec.	t-test p-value	P300 GC	non-P300 GC
8	0.2350	0.1354	0.0783
7	0.1841	0.1125	0.0617
6	0.2700	0.0983	0.0570
5	0.3730	0.0751	0.0493
4	0.3294	0.0604	0.0364
3	0.0491	0.0405	0.0170
2	0.0723	0.0124	0.0057

Table 4.10: Comparison of area results, considering a variable number of R2 electrodes.

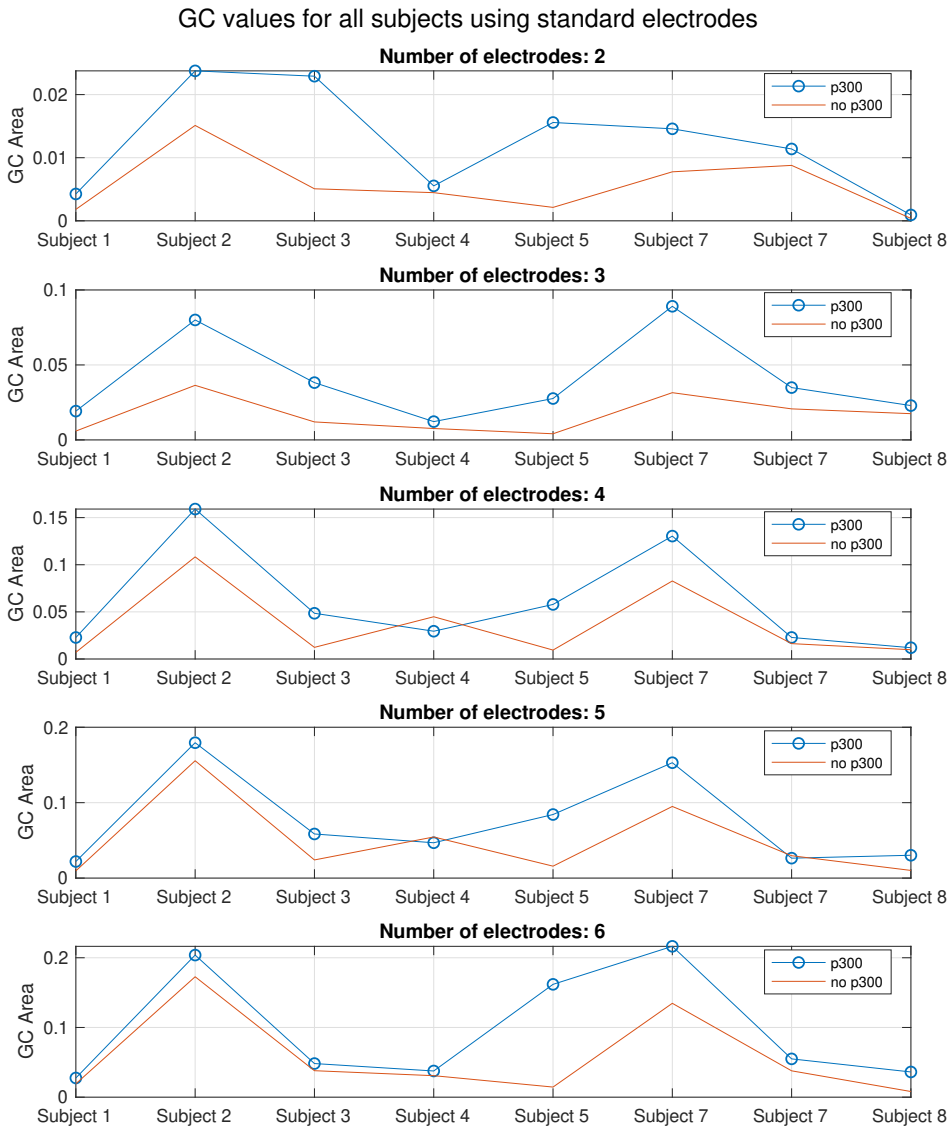

Figure 4.10: GC results for all subjects varying the number of electrodes using R2 electrodes.

As can be seen, we were able to obtain a p-value of less than 0.05 when 3 electrodes were used, indicating that in this case, the connectivity values between both signals have a significant difference. The average connectivity values in this case are shown in Figure 4.11.

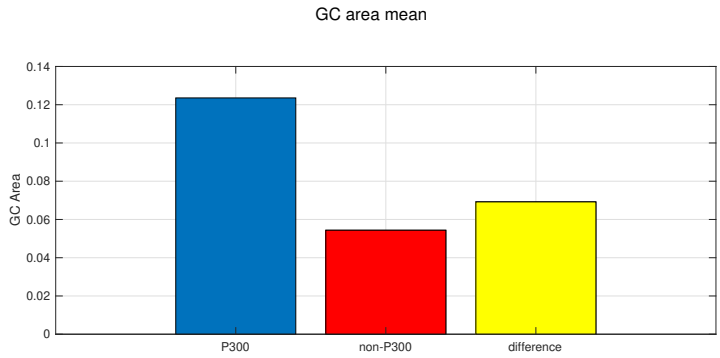

Figure 4.11: Mean value of GC area, considering all subjects and 3 selected electrodes with r2 shown in Table 4.8

Despite the condition established for the selection of the electrodes, which suggests not choosing two contiguous electrodes, it was observed that, especially when the electrodes were selected using r2, in most cases they were very close within the distribution of the scalp. Moreover, it is known from the literature analyzed at the beginning of this study that the distribution of the electrodes is crucial in the study of functional connectivity. Spatial separation of electrodes used in the analysis can potentially reduce erroneous values of causality.

Therefore, a second approach is proposed, which, as described in the methodology, essentially consists of dividing the scalp into four regions of interest, selecting a representative electrode for each region, and analyzing the existing behavior under these conditions. The following section shows the results obtained after this analysis.

4.4 Regions of Interest

As mentioned in the previous chapter, the distribution of electrodes on the scalp was divided into 4 clusters, which are detailed in Table 3.2. For the electrode selection within each ROI , the previously used selection approaches, BLDA-FS and r2, were also considered.

4.4.1 Electrode selection with BLDA and Forward Selection for ROIs

Window selection is performed after electrode selection. In the previous cases, it was observed that the selected window sizes were the same for several subjects, but in this analysis, the windows per subject are different. It was deemed necessary to show these results in Table 4.12.

After selecting the electrodes, as in the previous cases, the area values are calculated from the calculated window and overlap parameters. Figure 4.12, shows the area values calculated by each subject within the selected window, and in Figure 4.13, the differences in the mean of the Granger causality areas calculated for P300, non-P300 and the difference between these two signals can be observed.

Subject	RO1	RO2	RO3	RO4
1	AF3	T7	Fp2	C4
2	Fp2	CP2	Fp1	P7
3	F8	Oz	FC5	CP5
4	P3	CP6	Fz	F7
5	F4	Oz	F7	CP5
6	Cz	P7	FC6	FC5
7	C4	P3	Fz	AF3
8	P3	F3	Fp2	T8

Table 4.11: Electrodes selected with BLDA-FS using ROIs for subjects 1-8.The location of the selected electrodes is shown in Appendix B, Figure B.3.

Subject	1	2	3	4	5	6	7	8
θ_{min}	255	220	255	220	220	255	220	220
θ_{max}	670	670	630	670	670	670	630	670

Table 4.12: Selected window size for subjects 1-8. Description of the θ_{min} and θ_{max} values for window location using BLDA-FS with ROIs.

Subject	1	2	3	4	5	6	7	8
P300	0.0611	0.1458	0.0637	0.0961	0.2019	0.1582	0.0767	0.1107
no-P300	0.0419	0.1089	0.0247	0.1071	0.0718	0.0973	0.0510	0.0355

Table 4.13: Final area values for subjects 1-8 after window selection using BLDA-FS electrodes with ROIs.

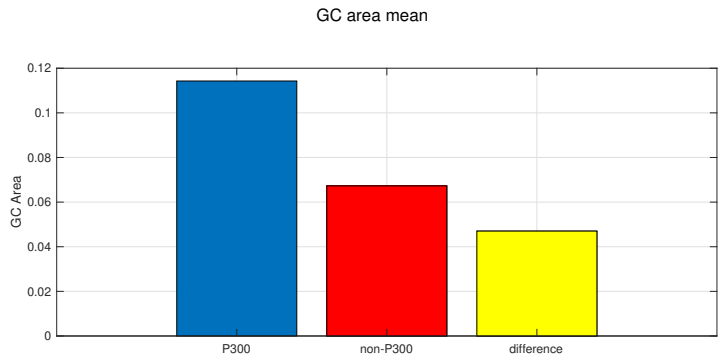

Figure 4.13: Mean value of GC area, considering all subjects and BLDA-FS electrodes with ROIs.

Statistical analysis by t-test was applied to the data generated after analysis for each case and obtained a resulting p-value of 0.0457, in this case the differences found in both samples are also considered significant.

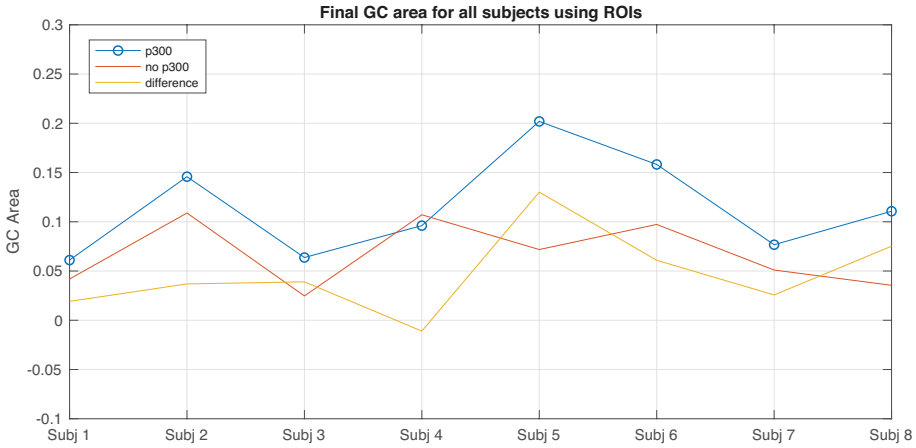

Figure 4.12: Final area results for subjects 1-8 after window selection using BLDA-FS electrodes with ROIs.

4.4.2 Electrode selection with r2 for ROIs

As in the BLDA selection for ROIs, one electrode per cluster was considered for the R2 analysis and the one giving the highest values in a given window was selected. The resulting electrodes are listed in Table 4.14.

Subject	RO1	RO2	RO3	RO4
1	Fp1	Fp2	O1	O2
2	Fp1	Fp2	O1	Pz
3	FC1	Fp2	PO3	Oz
4	FC1	FC2	CP1	CP2
5	Fp1	FC2	O1	P8
6	FC1	Fp2	PO3	PO4
7	Fp1	Fp2	P7	O2
8	FC1	FC2	CP1	O2

Table 4.14: Electrodes selected with r2 using ROIs for subjects 1-8. The location of the selected electrodes is shown in Appendix B, Figure B.4.

After the electrodes are selected by BLDA, the sliding windows and the overlap for which the GC values are calculated are determined. After generating the curve formed by the resulting points of each sliding window, we proceed to calculate the values of θ that bound the window at the beginning and end of the signal. The Table 4.15 shows the θ_{min} and θ_{max} values chosen for each subject, observing that the resulting windows are similar for all subjects.

After window selection, the area values are calculated for each subject, and the values are shown in both Figure 4.14 and the Table 4.16.

Figure 4.15, shows the calculated average area values for the P300 signal, the non-P300 signal, and the difference between the two. It can be seen that the average area calculated for the P300 signal is larger.

Subject	1	2	3	4	5	6	7	8
θ_{min}	220	220	220	220	255	220	255	220
θ_{max}	670	670	670	670	670	670	670	670

Table 4.15: Selected window size for subjects 1-8. Description of the θ_{min} and θ_{max} values for window location using r2 with ROIs.

Subject	1	2	3	4	5	6	7	8
P300	0.0442	0.1409	0.1144	0.0756	0.0922	0.00143	0.1298	0.0842
no-P300	0.0320	0.1147	0.0374	0.1074	0.0412	0	0.0688	0.0422

Table 4.16: Final area values for subjects 1-8 after window selection using r2 electrodes with ROIs.

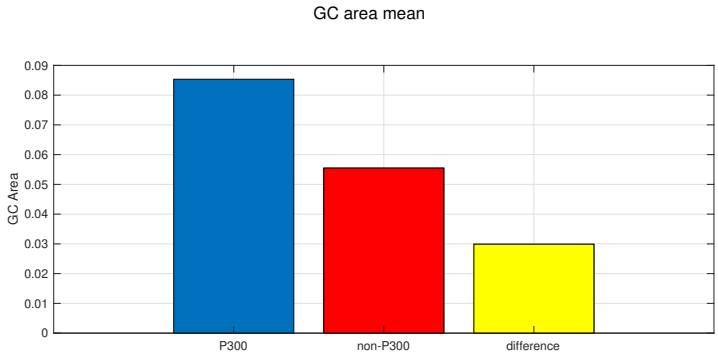

Figure 4.15: GC area considering all subjects and r2 selected electrodes with ROIs.

The t-test was applied to both samples and it was found that despite the difference that exists between the signals found, the differences are not considered significant, the p-value calculated by the test is equal to 0.183.

4.5 Granger Causality for abled and disabled subjects

Finally, according to the analyzes performed, it was found that there was a remarkable difference between the results of the able-bodied subjects and the subjects with disabilities. These differences in the area means for each case are shown in Figure 4.16.

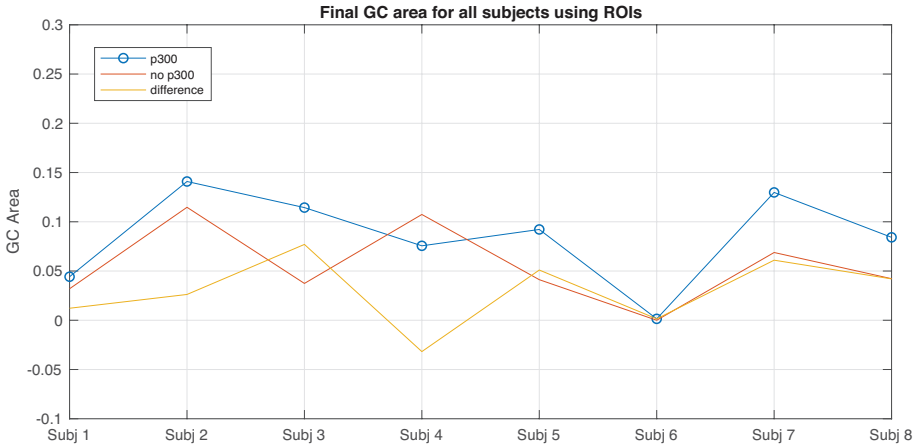

Figure 4.14: Final area results for subjects 1-8 after window selection using r2 electrodes with ROIs.

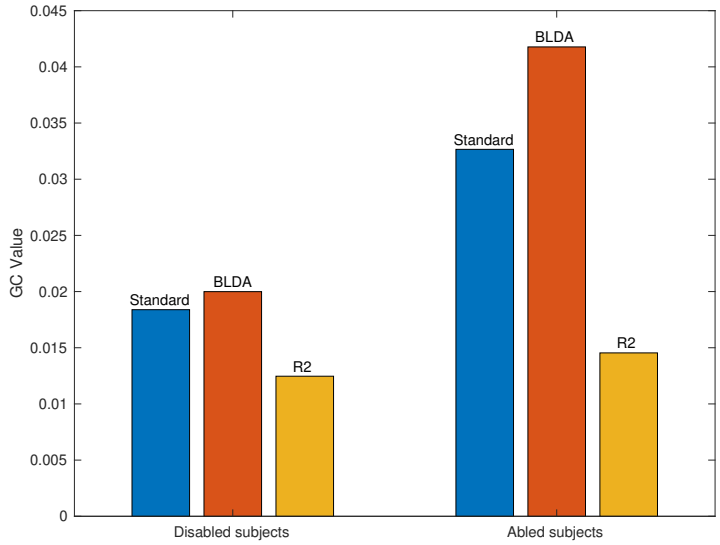

Figure 4.16: Comparison between abled and disabled subjects, data normalized as a function of the number of electrodes.

For Figure 4.16, the data were normalized as a function of the number of electrodes which are 4, 6, and 3 for standard, BLDA-FS (Table 4.5) and r2 (Table 3.7) electrodes respectively. These results were selected from the electrode combinations for which the alternative hypothesis was accepted according to the applied t-test.

From these results, we can first see that the difference in the connectivity values of the P300 and non-P300 signals calculated from the electrodes selected with BLDA-FS is the highest, followed by the standard electrodes and finally by r2, whose difference between the two analyzed groups is minimal.

Moreover, after dividing the subjects into two groups: abled (1-4) and disabled (5-8), we can see how the connectivity values are significantly lower in the case of the disabled subjects. These results

may suggest that functional connectivity occurs to a lesser extent in subjects with disabilities. The use of this metric can be used to quantify neuronal interactions, which may indicate some type of underlying neuronal pathology when low connectivity values are detected.

4.5.1 Summary of results

The following Table 4.17,summarizes the main features of the three general analyzes including the results of the hypothesis test, which are satisfactory in all cases, and ROIs analysis. It is worth noting how the area values of the causality generated from the P300 signal are slightly higher when using the electrodes selected by BLDA-FS in both analyses.

The electrodes selected for the general analysis with BLD - FS and r2 can be seen in the Tables 4.5 and 4.8. On the other hand, the electrodes selected for the analysis of ROI can be seen in the Tables 4.14 and . From these results, it can be seen that selection by r2 gives poor performance when using ROIs.

General Analysis				
N. Elec.	N. Electrodes	t-test p-value	P300 GC	no-P300 GC
Standard	4	0.01197	0.118	0.053
BLDA-FS	6	0.0497	0.153	0.073
R2	3	0.0491	0.0405	0.0170
ROIs Analysis				
N. Elec.	N. Electrodes	t-test p-value	P300 GC	no-P300 GC
BLDA	4	0.0457	0.1143	0.0673
R2	4	0.183	0.0853	0.0555

Table 4.17: Comparison of area results, between the analyzed approaches for electrode selection in general analysis and ROIs analysis.

5

Conclusions and Discussion

Several studies have shown that different brain areas are involved in the generation of a P300 signal (Polich, 2007, Tian et al., 2014, Y. Zhang et al., 2014), and as mentioned earlier, it has been found that it is networks within these areas that correlate with various cognitive processes such as attention, intelligence, working memory, etc. (Y. Li et al., 2009).

In this work, the levels of functional connectivity in P300 ERP-based EEG signals were evaluated. For this analysis, Granger Causality was used as a measure to quantify functional connectivity. As mentioned earlier, unlike several studies conducted in this case, this metric was used to try to distinguish neural networks when a target image is displayed and when it is not.

In this study, functional connectivity was evaluated by limiting the number of electrodes to eliminate the problem of noncollinearity, according to three selection methods: standard electrodes, electrodes selected by BLDA, electrodes selected by r2. In addition, the dataset was divided into independently selected windows to eliminate the problem of non-stationarity.

In a first approximation, the calculation of functional connectivity is analyzed, based on standard electrodes. From this analysis, it was found that after the presentation of a stimulus, i.e., when a target image is presented and a P300 signal is generated, there is a higher causality value, consequently, less activity was detected when the subject waits for the stimulus.

The second approach considered, using electrodes selected with BLDA-FS, shows similar results to the previous case, where higher causality values are detected when a target stimulus is presented, but causality values are higher for electrodes selected with BLDA-FS than when standard electrodes are used.

As a third approximation, the connectivity calculation considering r2 in the selection of electrodes is proposed. In this case, an increase in connectivity values is also observed when a P300 signal is generated, but this value is not much higher than the calculated one when no target stimulus is present. From this analysis, it is concluded that r2 selection is not a good selection approach because the connectivity results found between signals are less discriminative.

From the analysis carried out in this project, it could be establish that there is indeed a clear difference between the activity during a non-target trial, which tends to be lower, and the results of

brain activity during a target trial, in which the values of functional connectivity are higher in all cases, showing that the brain areas analyzed are closely connected and that during the development of cognitive functions there is a greater transmission of information.

The results obtained in this study using Granger Causality are consistent with those of (Kabbara et al., 2016), who demonstrates through the use of PLV that it is possible to clearly observe high synchronization between brain regions during a target trial, but no significant synchronization values were observed during a non-target trial.

It was also shown that a good electrode selection was crucial in measuring functional connectivity. The different selection of electrodes allowed various results to be found regarding the values of connectivity during the activity of P300. The results also suggest that the standard electrodes and electrodes selected from BLDA-FS are more discriminative. The r2 metric, on the other hand, was found to be not very discriminative. Furthermore, despite the small number of subjects examined, this study demonstrated that subjects with disabilities had lower connectivity values compared to non-disabled subjects.

The functional connectivity study performed in the present work could be extended in a future work by combining it with methods that achieve higher accuracy in visual stimulus classification (target vs. non-target) and P300 detection. In this way, connectivity measured by Granger causality can be used as a new feature for the classification of visually evoked responses, as it has been seen in other studies (Kabbara et al., 2016, H. Wang et al., 2016), since significant differences have been found in the characterization of target and non-target evoked responses.

The GC analysis performed focuses on the linear case, this type of approach, as pointed out in (Paluš and Vejmelka, 2007), generates some distrust in the correct detection of causality, since it can sometimes detect false causality. To address this limitation, as a next step we could use the method proposed in (Marinazzo et al., 2008b), which allows a non-linear computation of Granger Causality based on kernel functions. It is considered important to analyze the results that can be generated with this analysis and compare them with those obtained in this project. It is also suggested that an analysis be conducted with more subjects. More information would allow for more analysis and comparison parameters to validate the results obtained in this study.

Several connectivity studies have focused on going beyond connectivity to analyze the existing flow of information during cognitive processes using various directed metrics (F. Li et al., 2016, Astolfi et al., 2005, Astolfi et al., 2007, Baccalá and Sameshima, 2001, Kamiński et al., 2001). As a future study, the use of Granger Causality may be proposed to evaluate the information flow between different brain regions in the context of P300 ERPs. For this, it is necessary to improve the ROIs methodology used and adapt the proposed methodology to a directed connectivity analysis.

In Stam et al., 2007, the notion of the ”common sources problem” is introduced, referring to the influence that can exist between time series measured from the the scalp, and explaining how signals measured at nearby electrodes can register the same activity, leading to spurious correlations between these time series. One of the proposed strategies to deal with this problem is to try to determine the location of the sources. For this purpose, techniques such as (Low Resolution Electromagnetic Tomography) LORETA Winterer et al., 2001 have been used, managing to show that this technique allows the correct localization of cortical activity related to P300. This study attempted to limit electrode selection to non-adjacent electrodes; however, for a future study, the methodology proposed for this project can be directed towards using source localization methods to assess functional connectivity with Granger Causality between sources.

Bibliography

Aertsen, & Preißl. (1991). *Dynamics of activity and connectivity in physiological neuronal networks*. H. Schuster.

Akaike, H. (1974). A new look at the statistical model identification. *IEEE Transactions on Automatic Control*, *19*(6), 716–723. https://doi.org/10.1109/TAC.1974.1100705

Alexander, J. E., Porjesz, B., Bauer, L. O., Kuperman, S., Morzorati, S., O'connor, S. J., Rohrbaugh, J., Begleiter, H., & Polich, J. (1995). P300 hemispheric amplitude asymmetries from a visual oddball task. *Psychophysiology*, *32*(5), 467–475. https://doi.org/10.1111/j.1469-8986.1995.tb02098.x

Amin, H. U., Malik, A. S., Kamel, N., Chooi, W.-T., & Hussain, M. (2015). P300 correlates with learning & memory abilities and fluid intelligence. *Journal of NeuroEngineering and Rehabilitation*, *12*(1), 87. https://doi.org/10.1186/s12984-015-0077-6

Amor, F., Rudrauf, D., Navarro, V., N'diaye, K., Garnero, L., Martinerie, J., & Le Van Quyen, M. (2005). Imaging brain synchrony at high spatio-temporal resolution: Application to MEG signals during absence seizures. *Signal Processing*, *85*(11), 2101–2111. https://doi.org/10.1016/j.sigpro.2005.07.004

Ancona, N., Marinazzo, D., & Stramaglia, S. (2004). Radial basis function approach to nonlinear granger causality of time series. *Physical Review E*, *70*(5), 056221. https://doi.org/10.1103/PhysRevE.70.056221

Anderson. (1971). *The statistical analysis of time series* (1st ed.). John Wiley & Sons, Ltd. https://doi.org/10.1002/9781118186428

Anderson, C. W., Stolz, E. A., & Shamsunder, S. (1998). Multivariate autoregressive models for classification of spontaneous electroencephalographic signals during mental tasks. *IEEE transactions on bio-medical engineering*, *45*(3), 277–286. https://doi.org/10.1109/10.661153

Astolfi, L., Cincotti, F., Mattia, D., Babiloni, C., Carducci, F., Basilisco, A., Rossini, P. M., Salinari, S., Ding, L., Ni, Y., He, B., & Babiloni, F. (2005). Assessing cortical functional connectivity by linear inverse estimation and directed transfer function: Simulations and application to real data. *Clinical Neurophysiology*, *116*(4), 920–932. https://doi.org/10.1016/j.clinph.2004.10.012

Astolfi, L., Cincotti, F., Mattia, D., Marciani, M. G., Baccala, L. A., Fallani, F. d. V., Salinari, S., Ursino, M., Zavaglia, M., Ding, L., Edgar, J. C., Miller, G. A., He, B., & Babiloni, F. (2007). Comparison of different cortical connectivity estimators for high-resolution EEG recordings [_eprint: https://onlinelibrary.wiley.com/doi/pdf/10.1002/hbm.20263]. *Human Brain Mapping*, *28*(2), 143–157. https://doi.org/https://doi.org/10.1002/hbm.20263

Baccalá, L. A., & Sameshima, K. (2001). Partial directed coherence: A new concept in neural structure determination. *Biological Cybernetics*, *84*(6), 463–474. https://doi.org/10.1007/PL00007990

Barnett, L., & Seth, A. K. (2014). The MVGC multivariate granger causality toolbox: A new approach to granger-causal inference. *Journal of Neuroscience Methods*, *223*, 50–68. https://doi.org/10.1016/j.jneumeth.2013.10.018

Barrett, A. B., Murphy, M., Bruno, M.-A., Noirhomme, Q., Boly, M., Laureys, S., & Seth, A. K. (2012). Granger causality analysis of steady-state electroencephalographic signals during propofol-induced anaesthesia. *PLOS ONE*, *7*(1), e29072. https://doi.org/10.1371/journal.pone.0029072

Bashar, S. K., & Bhuiyan, M. I. H. (2016). Classification of motor imagery movements using multivariate empirical mode decomposition and short time fourier transform based hybrid method. *Engineering Science and Technology, an International Journal*, *19*(3), 1457–1464. https://doi.org/10.1016/j.jestch.2016.04.009

Bashashati, A., Fatourechi, M., Ward, R. K., & Birch, G. E. (2007). A survey of signal processing algorithms in brain-computer interfaces based on electrical brain signals. *Journal of Neural Engineering*, *4*(2), R32–57. https://doi.org/10.1088/1741-2560/4/2/R03

Bastos, A. M., & Schoffelen, J.-M. (2015). A tutorial review of functional connectivity analysis methods and their interpretational pitfalls. *Frontiers in Systems Neuroscience*, *9*, 175. https://doi.org/10.3389/fnsys.2015.00175

BCI2000 Wiki. (2013). *Coefficient of determination* [BCI2000 wiki]. Retrieved August 18, 2020, from https://www.bci2000.org/mediawiki/index.php/Glossary

Beckenbach, E. F. (2013, September 3). The theory of prediction. *Modern mathematics for the engineer: First series* (pp. 165–183). Courier Corporation.

Becker, D. E., & Shapiro, D. (1980). Directing attention toward stimuli affects the p300 but not the orienting response. *Psychophysiology*, *17*(4), 385–389. https://doi.org/10.1111/j.1469-8986.1980.tb00168.x

Birbaumer, N., Elbert, T., Canavan, A. G., & Rockstroh, B. (1990). Slow potentials of the cerebral cortex and behavior. *Physiological Reviews*, *70*(1), 1–41. https://doi.org/10.1152/physrev.1990.70.1.1

Bishop, C. (2006). *Pattern recognition and machine learning*. Springer-Verlag. Retrieved March 8, 2021, from https://www.springer.com/gp/book/9780387310732

Blankertz, B., Lemm, S., Treder, M., Haufe, S., & Müller, K.-R. (2011). Single-trial analysis and classification of ERP components — a tutorial. *NeuroImage*, *56*(2), 814–825. https://doi.org/10.1016/j.neuroimage.2010.06.048

Bola, M., & Sabel, B. A. (2015). Dynamic reorganization of brain functional networks during cognition. *NeuroImage*, *114*, 398–413. https://doi.org/10.1016/j.neuroimage.2015.03.057

Bostanov, V. (2004). BCI competition 2003-data sets ib and IIb: Feature extraction from event-related brain potentials with the continuous wavelet transform and the t-value scalogram. *IEEE Transactions on Biomedical Engineering*, *51*(6), 1057–1061. https://doi.org/10.1109/TBME.2004.826702

Brandeis, D., Banaschewski, T., Baving, L., Georgiewa, P., Blanz, B., Schmidt, M. H., Warnke, A., Steinhausen, H., Rothenberger, A., & Scheuerpflug, P. (2002). Multicenter p300 brain mapping of impaired attention to cues in hyperkinetic children. *Journal of the American Academy of Child & Adolescent Psychiatry*, *41*(8), 990–998. https://doi.org/10.1097/00004583-200208000-00018

Bressler, S. L., & Menon, V. (2010). Large-scale brain networks in cognition: Emerging methods and principles. *Trends in Cognitive Sciences*, *14*(6), 277–290. https://doi.org/10.1016/j.tics.2010.04.004

Bressler, S. L., & Seth, A. K. (2011). Wiener–granger causality: A well established methodology. *NeuroImage*, *58*(2), 323–329. https://doi.org/10.1016/j.neuroimage.2010.02.059

Brunner, P., Joshi, S., Briskin, S., Wolpaw, J., Bischof, H., & Schalk, G. (2010). Does the "p300" speller depend on eye gaze? *Journal of neural engineering*, *7*(5), 056013. https://doi.org/10.1088/1741-2560/7/5/056013

Burnham, K. P., & Anderson, D. R. (2003, December 4). *Model selection and multimodel inference: A practical information-theoretic approach*. Springer Science & Business Media.

Cecotti, H., Rivet, B., Congedo, M., Jutten, C., Bertrand, O., Maby, E., & Mattout, J. (2011). A robust sensor-selection method for p300 brain–computer interfaces. *Journal of Neural Engineering*, *8*(1), 016001. https://doi.org/10.1088/1741-2560/8/1/016001

Cecotti, H., & Ries, A. J. (2017). Best practice for single-trial detection of event-related potentials: Application to brain-computer interfaces. *International Journal of Psychophysiology*, *111*, 156–169. https://doi.org/10.1016/j.ijpsycho.2016.07.500

Chang, W., Wang, H., Lu, Z., & Liu, C. (2020). A concealed information test system based on functional brain connectivity and signal entropy of audio–visual ERP. *IEEE Transactions on Cognitive and Developmental Systems*, *12*(2), 361–370. https://doi.org/10.1109/TCDS.2020.2991359

Changoluisa, V., Varona, P., & De Borja Rodríguez, F. (2020). A low-cost computational method for characterizing event-related potentials for BCI applications and beyond. *IEEE Access*, *8*, 111089–111101. https://doi.org/10.1109/ACCESS.2020.3000187

Coben, R., & Mohammad-Rezazadeh, I. (2015). Neural connectivity in epilepsy as measured by granger causality. *Frontiers in Human Neuroscience*, *9*. https://doi.org/10.3389/fnhum.2015.00194

Comerchero, M. D., & Polich, J. (1999). P3a and p3b from typical auditory and visual stimuli. *Clinical Neurophysiology*, *110*(1), 24–30. https://doi.org/10.1016/S0168-5597(98)00033-1

Demiralp, T., Yordanova, J., Kolev, V., Ademoglu, A., Devrim, M., & Samar, V. J. (1999). Time-frequency analysis of single-sweep event-related potentials by means of fast wavelet transform. *Brain and Language*, *66*(1), 129–145. https://doi.org/10.1006/brln.1998.2028

Demiralp, T., Ademoglu, A., Schürmann, M., Basar-Eroglu, C., & Basar, E. (1999). Detection of p300 waves in single trials by the wavelet transform (WT). *Brain and Language*, *66*(1), 108–128. https://doi.org/10.1006/brln.1998.2027

Dien, J., Spencer, K. M., & Donchin, E. (2003). Localization of the event-related potential novelty response as defined by principal components analysis. *Brain Research. Cognitive Brain Research*, *17*(3), 637–650. https://doi.org/10.1016/s0926-6410(03)00188-5

Ding, M., Bressler, S. L., Yang, W., & Liang, H. (2000). Short-window spectral analysis of cortical event-related potentials by adaptive multivariate autoregressive modeling: Data preprocessing, model validation, and variability assessment. *Biological Cybernetics*, *83*(1), 35–45. https://doi.org/10.1007/s004229900137

Ding, M., Chen, Y., & Bressler, S. L. (2006). Granger causality: Basic theory and application to neuroscience. *arXiv:q-bio/0608035*. Retrieved January 4, 2020, from http://arxiv.org/abs/q-bio/0608035

Donchin, E., & Coles, M. G. H. (1988). Is the p300 component a manifestation of context updating? *Behavioral and Brain Sciences*, *11*(3), 357–374. https://doi.org/10.1017/S0140525X00058027

Durbin, J. (1960). The fitting of time-series models. *Revue de l'Institut International de Statistique / Review of the International Statistical Institute*, *28*(3), 233–244. https://doi.org/10.2307/1401322

Dux, P. E., & Marois, R. (2009). The attentional blink: A review of data and theory. *Attention, Perception, & Psychophysics*, *71*(8), 1683–1700. https://doi.org/10.3758/APP.71.8.1683

Efron, B. (1979). Bootstrap methods: Another look at the jackknife. *Annals of Statistics*, *7*(1), 1–26. https://doi.org/10.1214/aos/1176344552

Fabiani, M., Karis, D., & Donchin, E. (1986). P300 and recall in an incidental memory paradigm. *Psychophysiology*, *23*(3), 298–308. https://doi.org/10.1111/j.1469-8986.1986.tb00636.x

Fahimi Hnazaee, M., Khachatryan, E., Chehrazad, S., Kotarcic, A., De Letter, M., & Van Hulle, M. M. (2020). Overlapping connectivity patterns during semantic processing of abstract and concrete words revealed with multivariate granger causality analysis. *Scientific Reports*, *10*(1), 2803. https://doi.org/10.1038/s41598-020-59473-7

Farwell, L. A., & Donchin, E. (1988). Talking off the top of your head: Toward a mental prosthesis utilizing event-related brain potentials. *Electroencephalography and Clinical Neurophysiology*, *70*(6), 510–523. https://doi.org/10.1016/0013-4694(88)90149-6

Friedman, D. (1984). P300 and slow wave: The effects of reaction time quartile. *Biological Psychology*, *18*(1), 49–71. https://doi.org/10.1016/0301-0511(84)90028-0

Friston, K. J. (1994). Functional and effective connectivity in neuroimaging: A synthesis. *Human Brain Mapping*, *2*(1), 56–78. https://doi.org/10.1002/hbm.460020107

Friston, K. J. (2011). Functional and effective connectivity: A review. *Brain Connectivity*, *1*(1), 13–36. https://doi.org/10.1089/brain.2011.0008

Furdea, A., Halder, S., Krusienski, D. J., Bross, D., Nijboer, F., Birbaumer, N., & Kübler, A. (2009). An auditory oddball (p300) spelling system for brain-computer interfaces. *Psychophysiology*, *46*(3), 617–625. https://doi.org/10.1111/j.1469-8986.2008.00783.x

Fusar-Poli, P., Crossley, N., Woolley, J., Carletti, F., Perez-Iglesias, R., Broome, M., Johns, L., Tabraham, P., Bramon, E., & McGuire, P. (2011). White matter alterations related to p300 abnormalities in individuals at high risk for psychosis: An MRI–EEG study. *Journal of Psychiatry & Neuroscience : JPN*, *36*(4), 239–248. https://doi.org/10.1503/jpn.100083

Gao, J.-F., Yang, Y., Huang, W.-T., Lin, P., Ge, S., Zheng, H.-M., Gu, L.-Y., Zhou, H., Li, C.-H., & Rao, N.-N. (2016). Exploring time- and frequency- dependent functional connectivity and brain networks during deception with single-trial event-related potentials. *Scientific Reports*, *6*, 37065. https://doi.org/10.1038/srep37065

Gao, Z.-K., Cai, Q., Dong, N., Zhang, S.-S., Bo, Y., & Zhang, J. (2016). Complex network inference from p300 signals: Decoding brain state under visual stimulus for able-bodied and disabled subjects. *Physica A: Statistical Mechanics and its Applications*, *460*, 294–303. https://doi.org/10.1016/j.physa.2016.05.035

Ghaderi, F., Kim, S. K., & Kirchner, E. A. (2014). Effects of eye artifact removal methods on single trial p300 detection, a comparative study. *Journal of Neuroscience Methods*, *221*, 41–47. https://doi.org/10.1016/j.jneumeth.2013.08.025

Graimann, B., Allison, B., & Pfurtscheller, G. (Eds.). (2010). *Brain-computer interfaces: Revolutionizing human-computer interaction*. Springer.

Granger, C. W. J. (1969). Investigating causal relations by econometric models and cross-spectral methods. *Econometrica*, *37*(3), 424–438. https://doi.org/10.2307/1912791

Gray, H. M., Ambady, N., Lowenthal, W. T., & Deldin, P. (2004). P300 as an index of attention to self-relevant stimuli. *Journal of Experimental Social Psychology*, *40*(2), 216–224. https://doi.org/10.1016/S0022-1031(03)00092-1

Guevara, R., Velazquez, J. L. P., Nenadovic, V., Wennberg, R., Senjanović, G., & Dominguez, L. G. (2005). Phase synchronization measurements using electroencephalographic recordings. *Neuroinformatics*, *3*(4), 301–313. https://doi.org/10.1385/NI:3:4:301

Guo, M., Xu, G., Wang, L., & Fu, L. (2016). Functional brain network analysis during auditory oddball task. *2016 Asia-Pacific International Symposium on Electromagnetic Compatibility (APEMC)*, *01*, 1098–1100. https://doi.org/10.1109/APEMC.2016.7522955

Hämäläinen, M., Hari, R., Ilmoniemi, R. J., Knuutila, J., & Lounasmaa, O. V. (1993). Magnetoencephalography-theory, instrumentation, and applications to noninvasive studies of the working human brain. *Reviews of Modern Physics*, *65*(2), 413–497. https://doi.org/10.1103/RevModPhys.65.413

Hamilton, J. D. (1994). *Time series analysis*. Princeton University Press.

Hassanien, A. E. (Ed.). (2015). *Brain-computer interfaces: Current trends and applications*. Springer.

Herrera, L., Rubio, G., Pomares, H., Paechter, B., Guillén, A., & Rojas, I. (2009). Strengthening the forward variable selection stopping criterion. *5769*, 215–224. https://doi.org/10.1007/978-3-642-04277-5_22

Hoffmann, U., Vesin, J.-M., Ebrahimi, T., & Diserens, K. (2008). An efficient p300-based brain–computer interface for disabled subjects. *Journal of Neuroscience Methods*, *167*(1), 115–125. https://doi.org/10.1016/j.jneumeth.2007.03.005

Homan, R. W., Herman, J., & Purdy, P. (1987). Cerebral location of international 10–20 system electrode placement. *Electroencephalography and Clinical Neurophysiology*, *66*(4), 376–382. https://doi.org/10.1016/0013-4694(87)90206-9

Honig, L. S., Ramsay, R. E., & Sheremata, W. A. (1992). Event-related potential p300 in multiple sclerosis. relation to magnetic resonance imaging and cognitive impairment. *Archives of Neurology*, *49*(1), 44–50. https://doi.org/10.1001/archneur.1992.00530250048015

Horwitz, B. (2003). The elusive concept of brain connectivity. *NeuroImage*, *19*(2), 466–470. https://doi.org/10.1016/S1053-8119(03)00112-5

Hosseinifard, B., Moradi, M., & Rostami, R. (2013). Classifying depression patients and normal subjects using machine learning techniques and nonlinear features from EEG signal. *Computer Methods and Programs in Biomedicine*, *109*(3), 339–345. https://doi.org/10.1016/j.cmpb.2012.10.008

Hwang, H.-J., Kim, S., Choi, S., & Im, C.-H. (2013). EEG-Based Brain-Computer Interfaces: A Thorough Literature Survey. *International Journal of Human–Computer Interaction*, *29*(12), 814–826. https://doi.org/10.1080/10447318.2013.780869

Irani, F. (2011). Functional Near-Infrared Spectroscopy. In R. A. Cohen & L. H. Sweet (Eds.), *Brain Imaging in Behavioral Medicine and Clinical Neuroscience* (pp. 93–101). Springer. https://doi.org/10.1007/978-1-4419-6373-4_7

Jian, W., Chen, M., & McFarland, D. J. (2017). EEG based zero-phase phase-locking value (PLV) and effects of spatial filtering during actual movement. *Brain Research Bulletin*, *130*, 156–164. https://doi.org/10.1016/j.brainresbull.2017.01.023

Jiang, X., Bian, G.-B., & Tian, Z. (2019). Removal of artifacts from EEG signals: A review. *Sensors (Basel, Switzerland)*, *19*(5). https://doi.org/10.3390/s19050987

Johnson, R., Pfefferbaum, A., & Kopell, B. S. (1985). P300 and long-term memory: Latency predicts recognition performance. *Psychophysiology*, *22*(5), 497–507. https://doi.org/10.1111/j.1469-8986.1985.tb01639.x

Kabbara, A., Khalil, M., El-Falou, W., Eid, H., & Hassan, M. (2016). Functional brain connectivity as a new feature for p300 speller. *PloS One*, *11*(1), e0146282. https://doi.org/10.1371/journal.pone.0146282

Kamiński, M., Ding, M., Truccolo, W. A., & Bressler, S. L. (2001). Evaluating causal relations in neural systems: Granger causality, directed transfer function and statistical assessment of significance. *Biological Cybernetics*, *85*(2), 145–157. https://doi.org/10.1007/s004220000235

Kaper, M., Meinicke, P., Grossekathoefer, U., Lingner, T., & Ritter, H. (2004). BCI competition 2003-data set IIb: Support vector machines for the p300 speller paradigm. *IEEE Transactions on Biomedical Engineering*, *51*(6), 1073–1076. https://doi.org/10.1109/TBME.2004.826698

Karis, D., Fabiani, M., & Donchin, E. (1984). p300" and memory: Individual differences in the von restorff effect. *Cognitive Psychology*, *16*(2), 177–216. https://doi.org/10.1016/0010-0285(84)90007-0

Kayser, C., & Logothetis, N. K. (2013). The Electrophysiological Background of the fMRI Signal. In S. Ulmer & O. Jansen (Eds.), *fMRI: Basics and Clinical Applications* (pp. 25–36). Springer. https://doi.org/10.1007/978-3-642-34342-1_4

Kim, D.-W., Hwang, H.-J., Lim, J.-H., Lee, Y.-H., Jung, K.-Y., & Im, C.-H. (2011). Classification of selective attention to auditory stimuli: Toward vision-free brain-computer interfacing. *Journal of Neuroscience Methods*, *197*(1), 180–185. https://doi.org/10.1016/j.jneumeth.2011.02.007

Kirchgässner, G., & Wolters, J. (2008, August 27). *Introduction to modern time series analysis*. Springer Science & Business Media.

Klem, G. H., Lüders, H. O., Jasper, H. H., & Elger, C. (1999). The ten-twenty electrode system of the international federation. the international federation of clinical neurophysiology. *Electroencephalography and Clinical Neurophysiology. Supplement*, *52*, 3–6.

Krusienski, D. J., Sellers, E. W., Cabestaing, F., Bayoudh, S., McFarland, D. J., Vaughan, T. M., & Wolpaw, J. R. (2006). A comparison of classification techniques for the p300 speller. *Journal of Neural Engineering*, *3*(4), 299–305. https://doi.org/10.1088/1741-2560/3/4/007

Kuś, R., Kamiński, M., & Blinowska, K. J. (2004). Determination of EEG activity propagation: Pair-wise versus multichannel estimate. *IEEE transactions on bio-medical engineering*, *51*(9), 1501–1510. https://doi.org/10.1109/TBME.2004.827929

Lachaux, J.-P., Rodriguez, E., Martinerie, J., & Varela, F. J. (1999). Measuring phase synchrony in brain signals. *Human Brain Mapping*, *8*(4), 194–208. https://doi.org/10.1002/(SICI)1097-0193(1999)8:4⟨194::AID-HBM4⟩3.0.CO;2-C

Lehnertz, K. (1999). Non-linear time series analysis of intracranial EEG recordings in patients with epilepsy–an overview. *International Journal of Psychophysiology: Official Journal of the International Organization of Psychophysiology*, *34*(1), 45–52. https://doi.org/10.1016/s0167-8760(99)00043-4

Levinson, N. (1946). The wiener (root mean square) error criterion in filter design and prediction. *Journal of Mathematics and Physics*, *25*(1), 261–278. https://doi.org/10.1002/sapm1946251261

Li, F., Chen, B., Li, H., Zhang, T., Wang, F., Jiang, Y., Li, P., Ma, T., Zhang, R., Tian, Y., Liu, T., Guo, D., Yao, D., & Xu, P. (2016). The time-varying networks in p300: A task-evoked EEG study. *IEEE transactions on neural systems and rehabilitation engineering: a publication of the IEEE Engineering in Medicine and Biology Society*, *24*(7), 725–733. https://doi.org/10.1109/TNSRE.2016.2523678

Li, F., Tao, Q., Peng, W., Zhang, T., Si, Y., Zhang, Y., Yi, C., Biswal, B., Yao, D., & Xu, P. (2020). Inter-subject p300 variability relates to the efficiency of brain networks reconfigured from resting- to task-state: Evidence from a simultaneous event-related EEG-fMRI study. *NeuroImage*, *205*, 116285. https://doi.org/10.1016/j.neuroimage.2019.116285

Li, F., Yi, C., Jiang, Y., Liao, Y., Si, Y., Dai, J., Yao, D., Zhang, Y., & Xu, P. (2019). Different contexts in the oddball paradigm induce distinct brain networks in generating the p300. *Frontiers in Human Neuroscience*, *12*. https://doi.org/10.3389/fnhum.2018.00520

Li, M., Li, W., Zhao, J., Meng, Q., Sun, F., & Chen, G. (2013). An adaptive p300 model for controlling a humanoid robot with mind. *2013 IEEE International Conference on Robotics and Biomimetics (ROBIO)*, 1390–1395. https://doi.org/10.1109/ROBIO.2013.6739660

Li, Y., Liu, Y., Li, J., Qin, W., Li, K., Yu, C., & Jiang, T. (2009). Brain anatomical network and intelligence. *PLoS Computational Biology*, *5*(5). https://doi.org/10.1371/journal.pcbi.1000395

Liu, M., Wu, W., Gu, Z., Yu, Z., Qi, F., & Li, Y. (2018). Deep learning based on batch normalization for p300 signal detection. *Neurocomputing*, *275*, 288–297. https://doi.org/10.1016/j.neucom.2017.08.039

Lotte, F., Bougrain, L., Cichocki, A., Clerc, M., Congedo, M., Rakotomamonjy, A., & Yger, F. (2018). A review of classification algorithms for EEG-based brain–computer interfaces: A 10 year update. *Journal of Neural Engineering*, *15*(3), 031005. https://doi.org/10.1088/1741-2552/aab2f2

Lu, J., McFarland, D. J., & Wolpaw, J. R. (2012). Adaptive Laplacian filtering for sensorimotor rhythm-based brain–computer interfaces. *Journal of Neural Engineering*, *10*(1), 016002. https://doi.org/10.1088/1741-2560/10/1/016002

Luck, S. J. (2012). Event-related potentials. *APA handbook of research methods in psychology, vol 1: Foundations, planning, measures, and psychometrics* (pp. 523–546). American Psychological Association. https://doi.org/10.1037/13619-028

Ludwig, S. A., & Kong, J. (2017). Investigation of different classifiers and channel configurations of a mobile p300-based brain–computer interface. *Medical & Biological Engineering & Computing*, *55*(12), 2143–2154. https://doi.org/10.1007/s11517-017-1658-2

Manyakov, N. V., Chumerin, N., Combaz, A., & Van Hulle, M. M. (2010). On the selection of time interval and frequency range of EEG signal preprocessing for p300 brain-computer interfacing. In P. D. Bamidis & N. Pallikarakis (Eds.), *XII mediterranean conference on medical and biological engineering and computing 2010* (pp. 57–60). Springer. https://doi.org/10.1007/978-3-642-13039-7_15

Marinazzo, D., Pellicoro, M., & Stramaglia, S. (2008a). Kernel granger causality and the analysis of dynamical networks. *Physical Review E*, *77*(5), 056215. https://doi.org/10.1103/PhysRevE.77.056215

Marinazzo, D., Pellicoro, M., & Stramaglia, S. (2008b). Kernel method for nonlinear granger causality. *Physical Review Letters*, *100*(14), 144103. https://doi.org/10.1103/PhysRevLett.100.144103

Markazi, S. A., Qazi, S., Stergioulas, L. S., Ramchurn, A., & Bunce, D. (2006). Wavelet filtering of the p300 component in event-related potentials. *2006 International Conference of the IEEE Engineering in Medicine and Biology Society*, 1719–1722. https://doi.org/10.1109/IEMBS.2006.260691

McCarthy, G., & Donchin, E. (1981). A metric for thought: A comparison of p300 latency and reaction time. *Science*, *211*(4477), 77–80. https://doi.org/10.1126/science.7444452

McQuarrie, A. D. R., & Tsai, C.-L. (1998). *Regression and time series model selection*. World Scientific.

Mohammed, E. A., Naugler, C., & Far, B. H. (2015, January 1). Chapter 32 - emerging business intelligence framework for a clinical laboratory through big data analytics. In Q. N. Tran & H. Arabnia (Eds.), *Emerging trends in computational biology, bioinformatics, and systems biology* (pp. 577–602). Morgan Kaufmann. https://doi.org/10.1016/B978-0-12-802508-6.00032-6

Momennezhad, A., Shamsi, M., Ebrahimnezhad, H., & Saberkari, H. (2014). Classification of EEG-p300 signals extracted from brain activities in BCI systems using -SVM and BLDA algorithms. *Applied Medical Informatics.*, *34*(2), 23–35. Retrieved August 31, 2020, from https://ami.info.umfcluj.ro/index.php/AMI/article/view/474

Morf, M., Vieira, A., L. Lee, D. T., & Kailath, T. (1978). Recursive multichannel maximum entropy spectral estimation. *IEEE Transactions on Geoscience Electronics*, *16*(2), 85–94. https://doi.org/10.1109/TGE.1978.294569

Müller-Putz, G. R., Scherer, R., Brauneis, C., & Pfurtscheller, G. (2005). Steady-state visual evoked potential (SSVEP)-based communication: Impact of harmonic frequency components. *Journal of Neural Engineering*, *2*(4), 123–130. https://doi.org/10.1088/1741-2560/2/4/008

Müller-Putz, G. R., Scherer, R., Neuper, C., & Pfurtscheller, G. (2006). Steady-state somatosensory evoked potentials: Suitable brain signals for brain-computer interfaces? *IEEE transactions on neural systems and rehabilitation engineering: a publication of the IEEE Engineering in Medicine and Biology Society*, *14*(1), 30–37. https://doi.org/10.1109/TNSRE.2005.863842

Nam, C. S., Nijholt, A., & Lotte, F. (2018). *Brain-computer interfaces handbook: Technological and theoretical advances*. CRC Press. Retrieved March 8, 2020, from https://research.utwente.nl/en/publications/brain-computer-interfaces-handbook-technological-and-theoretical-

Naumann, E., Huber, C., Maier, S., Plihal, W., Wustmans, A., Diedrich, O., & Bartussek, D. (1992). The scalp topography of p300 in the visual and auditory modalities: A comparison of three normalization methods and the control of statistical type II error. *Electroencephalography and Clinical Neurophysiology*, *83*(4), 254–264. https://doi.org/10.1016/0013-4694(92)90119-3

Navarro. (2014). Electroencefalografía. *Instrumentación biomédica*. Universidad de Alcalá.

Niedermeyer, E., & Silva, F. H. L. d. (2005). *Electroencephalography: Basic principles, clinical applications, and related fields*. Lippincott Williams & Wilkins.

Nisar, H., Thee, K. W., Lim, S. H., Yap, V. V., Teh, P. C., Nor, N. M., & Chow, C. M. (2018). Brain functional connectivity analysis using single trial EEG for understanding individual mechanisms. *2018 IEEE 14th International Colloquium on Signal Processing Its Applications (CSPA)*, 209–214. https://doi.org/10.1109/CSPA.2018.8368714

Nunez, P. L., Nunez, E. P. o. B. E. P. L., Srinivasan, R., & Srinivasan, A. P. o. C. S. R. (2006). *Electric fields of the brain: The neurophysics of EEG*. Oxford University Press.

Nunez, P. L., Srinivasan, R., Westdorp, A. F., Wijesinghe, R. S., Tucker, D. M., Silberstein, R. B., & Cadusch, P. J. (1997). EEG coherency: I: Statistics, reference electrode, volume conduction, laplacians, cortical imaging, and interpretation at multiple scales. *Electroencephalography and Clinical Neurophysiology*, *103*(5), 499–515. https://doi.org/10.1016/S0013-4694(97)00066-7

Padilla-Buritica, J. I., Ferrandez-Vicente, J. M., Castaño, G. A., & Acosta-Medina, C. D. (2020). Non-stationary group-level connectivity analysis for enhanced interpretability of oddball tasks. *Frontiers in Neuroscience*, *14*. https://doi.org/10.3389/fnins.2020.00446

Paluš, M., & Vejmelka, M. (2007). Directionality of coupling from bivariate time series: How to avoid false causalities and missed connections. *Physical Review E*, *75*(5), 056211. https://doi.org/10.1103/PhysRevE.75.056211

Peng, H.-L., Liu, J.-Q., Tian, H.-C., Xu, B., Dong, Y.-Z., Yang, B., Chen, X., & Yang, C.-S. (2015). Flexible dry electrode based on carbon nanotube/polymer hybrid micropillars for biopotential recording. *Sensors and Actuators A: Physical*, *235*, 48–56. https://doi.org/10.1016/j.sna.2015.09.024

Peters, J. F., Billinger, T. W., & Knott, J. R. (1977). Event related potentials of brain (CNV and p300) in a paired associate learning paradigm. *Psychophysiology*, *14*(6), 579–585. https://doi.org/10.1111/j.1469-8986.1977.tb01203.x

Pfueller, U., Oelkers-Ax, R., Gmehlin, D., Parzer, P., Roesch-Ely, D., Weisbrod, M., & Bender, S. (2011). Maturation of p300 amplitude and short-term learning as reflected by p300 habituation between trial blocks in children. *International Journal of Psychophysiology*, *79*(2), 184–194. https://doi.org/10.1016/j.ijpsycho.2010.10.005

Piccione, F., Giorgi, F., Tonin, P., Priftis, K., Giove, S., Silvoni, S., Palmas, G., & Beverina, F. (2006). P300-based brain computer interface: Reliability and performance in healthy and paralysed participants. *Clinical Neurophysiology*, *117*(3), 531–537. https://doi.org/10.1016/j.clinph.2005.07.024

Picton, T. (1992). The P300 Wave of the Human Event-Related Potential. *Journal of Clinical Neurophysiology*, *9*(4), 456–479. Retrieved February 24, 2020, from insights.ovid.com

Polich, J. (2007). Updating p300: An integrative theory of p3a and p3b. *Clinical Neurophysiology: Official Journal of the International Federation of Clinical Neurophysiology*, *118*(10), 2128–2148. https://doi.org/10.1016/j.clinph.2007.04.019

Polich, J., & Margala, C. (1997). P300 and probability: Comparison of oddball and single-stimulus paradigms. *International Journal of Psychophysiology*, *25*(2), 169–176. https://doi.org/10.1016/S0167-8760(96)00742-8

Polikoff, J. B., Bunnell, H. T., & Jr, W. J. B. (1995). *Toward a p300-based computer interface*.

Protopapa, F., Siettos, C. I., Evdokimidis, I., & Smyrnis, N. (2014). Granger causality analysis reveals distinct spatio-temporal connectivity patterns in motor and perceptual visuo-spatial working memory. *Frontiers in Computational Neuroscience*, *8*. https://doi.org/10.3389/fncom.2014.00146

Qin, Y., Zhan, Y., Wang, C., Zhang, J., Yao, L., Guo, X., Wu, X., & Hu, B. (2016). Classifying four-category visual objects using multiple ERP components in single-trial ERP. *Cognitive Neurodynamics*, *10*(4), 275–285. https://doi.org/10.1007/s11571-016-9378-0

Quian Quiroga, R., Kraskov, A., Kreuz, T., & Grassberger, P. (2002). Performance of different synchronization measures in real data: A case study on electroencephalographic signals. *Physical Review E*, *65*(4), 041903. https://doi.org/10.1103/PhysRevE.65.041903

Ramadan, R. A., & Vasilakos, A. V. (2017). Brain computer interface: Control signals review. *Neurocomputing*, *223*, 26–44. https://doi.org/10.1016/j.neucom.2016.10.024

Riccio, A., Schettini, F., Simione, L., Pizzimenti, A., Inghilleri, M., Olivetti-Belardinelli, M., Mattia, D., & Cincotti, F. (2018). On the relationship between attention processing and p300-based brain computer interface control in amyotrophic lateral sclerosis. *Frontiers in Human Neuroscience*, *12*. https://doi.org/10.3389/fnhum.2018.00165

Riccio, A., Simione, L., Schettini, F., Pizzimenti, A., Inghilleri, M., Olivetti Belardinelli, M., Mattia, D., & Cincotti, F. (2013). Attention and p300-based BCI performance in people with amyotrophic lateral sclerosis. *Frontiers in Human Neuroscience*, *7*. https://doi.org/10.3389/fnhum.2013.00732

Rivet, B., Cecotti, H., Maby, E., & Mattout, J. (2012). Impact of spatial filters during sensor selection in a visual p300 brain-computer interface. *Brain Topography*, *25*(1), 55–63. https://doi.org/10.1007/s10548-011-0193-y

Rivet, B., Souloumiac, A., Gibert, G., & Attina, V. (2008). P300 speller brain-computer interface: Enhancement of p300 evoked potential by spatial filters p300, 6.

Rubinov, M., & Sporns, O. (2010). Complex network measures of brain connectivity: Uses and interpretations. *NeuroImage*, *52*(3), 1059–1069. https://doi.org/10.1016/j.neuroimage.2009.10.003

Ryan, D. B., Townsend, G., Gates, N. A., Colwell, K., & Sellers, E. W. (2017). Evaluating brain-computer interface performance using color in the p300 checkerboard speller. *Clinical Neurophysiology*, *128*(10), 2050–2057. https://doi.org/10.1016/j.clinph.2017.07.397

Saavedra, C., & Bougrain, L. (2010). Wavelet denoising for p300 single-trial detection, 227–231. Retrieved September 3, 2020, from https://hal.inria.fr/inria-00549218

Salazar, V. (2020). *Theoretical and experimental study of p300 ERP in the context of brain-computer interfaces. part II: An experimental study of inter-and intra-subject variability based on EEG*

recordings. (Master Thesis). Universidad Autónoma de Madrid. Escuela Politécnica Superior.

Schreiber, T. (2000). Measuring information transfer. *Physical Review Letters*, *85*(2), 461–464. https://doi.org/10.1103/PhysRevLett.85.461

Sellers, E. W., & Donchin, E. (2006). A p300-based brain–computer interface: Initial tests by ALS patients. *Clinical Neurophysiology*, *117*(3), 538–548. https://doi.org/10.1016/j.clinph.2005.06.027

Semlitsch, H. V., Anderer, P., Schuster, P., & Presslich, O. (1986). A solution for reliable and valid reduction of ocular artifacts, applied to the p300 ERP. *Psychophysiology*, *23*(6), 695–703. https://doi.org/10.1111/j.1469-8986.1986.tb00696.x

Serby, H., Yom-Tov, E., & Inbar, G. (2005). An improved p300-based brain-computer interface. *IEEE Transactions on Neural Systems and Rehabilitation Engineering*, *13*(1), 89–98. https://doi.org/10.1109/TNSRE.2004.841878

Sheng, Y., Liu, S., Wang, W., He, Y., Liu, X., Ke, Y., An, X., & Ming, D. (2018). A study on RSVP paradigm based on brain computer interface across subjects. *2018 9th International Conference on Awareness Science and Technology (iCAST)*, 42–46. https://doi.org/10.1109/ICAwST.2018.8517249

Speier, W., Deshpande, A., & Pouratian, N. (2015). A method for optimizing EEG electrode number and configuration for signal acquisition in p300 speller systems. *Clinical Neurophysiology*, *126*(6), 1171–1177. https://doi.org/10.1016/j.clinph.2014.09.021

Sporns, O., Tononi, G., & Kötter, R. (2005). The human connectome: A structural description of the human brain. *PLoS Computational Biology*, *1*(4). https://doi.org/10.1371/journal.pcbi.0010042

Stam, C. J., Nolte, G., & Daffertshofer, A. (2007). Phase lag index: Assessment of functional connectivity from multi channel EEG and MEG with diminished bias from common sources. *Human Brain Mapping*, *28*(11), 1178–1193. https://doi.org/10.1002/hbm.20346

Stephan, K. E., & Friston, K. J. (2009, January 1). Functional connectivity. In L. R. Squire (Ed.), *Encyclopedia of neuroscience* (pp. 391–397). Academic Press. https://doi.org/10.1016/B978-008045046-9.00308-9

Stone, M. (1979). Comments on model selection criteria of akaike and schwarz. *Journal of the Royal Statistical Society: Series B (Methodological)*, *41*(2), 276–278. https://doi.org/10.1111/j.2517-6161.1979.tb01084.x

Sutton, S., Braren, M., Zubin, J., & John, E. R. (1965). Evoked-potential correlates of stimulus uncertainty. *Science*, *150*(3700), 1187–1188. https://doi.org/10.1126/science.150.3700.1187

Tahirovic, A., Matteucci, M., & Mainardi, L. (2015). An averaging technique for the p300 spatial distribution. *Methods of Information in Medicine*, *54*(3), 215–220. https://doi.org/10.3414/me13-02-0037

Takahashi, D. (2019, October 5). *Fast fourier transform algorithms for parallel computers*. Springer Nature.

Terrell, C. (2019, September 2). *Predictions in time series using regression models*. Scientific e-Resources.

Thee, K. W., Nisar, H., & Soh, C. S. (2018). Graph theoretical analysis of functional brain networks in healthy subjects: Visual oddball paradigm. *IEEE Access*, *6*, 64708–64727. https://doi.org/10.1109/ACCESS.2018.2877035

Thee, K. W., Nisar, H., Yeap, K. H., & Soh, C. S. (2018). Evaluation of oddball cases: Single trial EEG connectivity study based on p300 and motor response. *2018 12th International Conference on Signal Processing and Communication Systems (ICSPCS)*, 1–6. https://doi.org/10.1109/ICSPCS.2018.8631728

Thomas M. Cover, & Joy A. Thomas. (2006). *Elements of information theory* (Second Edition). Wiley Interscience. Retrieved August 24, 2020, from https://onlinelibrary.wiley.com/doi/book/10.1002/047174882X

Tian, Y., Liang, S., & Yao, D. (2014). Attentional orienting and response inhibition: Insights from spatial-temporal neuroimaging. *Neuroscience Bulletin*, *30*(1), 141–152. https://doi.org/10.1007/s12264-013-1372-5

Tiwari, N., Edla, D. R., Dodia, S., & Bablani, A. (2018). Brain computer interface: A comprehensive survey. *Biologically Inspired Cognitive Architectures*, *26*, 118–129. https://doi.org/10.1016/j.bica.2018.10.005

Townsend, D. W. (2008). Dual-modality imaging: Combining anatomy and function. *Journal of Nuclear Medicine: Official Publication, Society of Nuclear Medicine*, *49*(6), 938–955. https://doi.org/10.2967/jnumed.108.051276

van Dinteren, R., Arns, M., Jongsma, M. L. A., & Kessels, R. P. C. (2014). P300 development across the lifespan: A systematic review and meta-analysis. *PLoS ONE*, *9*(2). https://doi.org/10.1371/journal.pone.0087347

Varela, F., Lachaux, J. P., Rodriguez, E., & Martinerie, J. (2001). The brainweb: Phase synchronization and large-scale integration. *Nature Reviews. Neuroscience*, *2*(4), 229–239. https://doi.org/10.1038/35067550

Verschuere, B., Rosenfeld, J. P., Winograd, M. R., Labkovsky, E., & Wiersema, R. (2009). The role of deception in p300 memory detection. *Legal and Criminological Psychology*, *14*(2), 253–262. https://doi.org/10.1348/135532508X384184

Vidal, J. (1977). Real-time detection of brain events in EEG. *Proceedings of the IEEE*, *65*(5), 633–641. https://doi.org/10.1109/PROC.1977.10542

Wang, H., Chang, W., & Zhang, C. (2016). Functional brain network and multichannel analysis for the p300-based brain computer interface system of lying detection. *Expert Systems with Applications*, *53*, 117–128. https://doi.org/10.1016/j.eswa.2016.01.024

Wang, H. E., Bénar, C. G., Quilichini, P. P., Friston, K. J., Jirsa, V. K., & Bernard, C. (2014). A systematic framework for functional connectivity measures. *Frontiers in Neuroscience*, *8*. https://doi.org/10.3389/fnins.2014.00405

Winterer, G., Mulert, C., Mientus, S., Gallinat, J., Schlattmann, P., Dorn, H., & Herrmann, W. M. (2001). P300 and LORETA: Comparison of normal subjects and schizophrenic patients. *Brain Topography*, *13*(4), 299–313. https://doi.org/10.1023/a:1011184814194

Wolpaw, J., & Wolpaw, E. W. (2012). *Brain-Computer Interfaces: Principles and Practice*. Oxford University Press.

Wolpaw, J. R., Birbaumer, N., McFarland, D. J., Pfurtscheller, G., & Vaughan, T. M. (2002). Brain–computer interfaces for communication and control. *Clinical Neurophysiology*, *113*(6), 767–791. https://doi.org/10.1016/S1388-2457(02)00057-3

Wu, D., King, J.-T., Chuang, C.-H., Lin, C.-T., & Jung, T.-P. (2018). Spatial filtering for EEG-based regression problems in brain–computer interface (BCI). *IEEE Transactions on Fuzzy Systems*, *26*(2), 771–781. https://doi.org/10.1109/TFUZZ.2017.2688423

Yuyi1, Z. (2017). Motor imagery EEG discrimination using hilbert-huang entropy. Retrieved September 3, 2020, from https://www.biomedres.info/abstract/motor-imagery-eeg-discrimination-using-hilberthuang-entropy-6359.html

Zetterberg, L. H. (1969). Estimation of parameters for a linear difference equation with application to EEG analysis. *Mathematical Biosciences*, *5*(3), 227–275. https://doi.org/10.1016/0025-5564(69)90044-3

Zhang, Y., Tang, A. C., & Zhou, X. (2014). Synchronized network activity as the origin of a p300 component in a facial attractiveness judgment task. *Psychophysiology*, *51*(3), 285–289. https://doi.org/10.1111/psyp.12153

Zhang, Y.-T. (2013, November 20). *The international conference on health informatics: ICHI 2013, vilamoura, portugal on 7-9 november, 2013*. Springer Science & Business Media.

Appendices

A

Appendix: Results

This appendix shows the causality results per subject, calculated with the three proposed considerations, with each electrode combination.

A.1 Standard Electrodes

This section of the Appendix presents the results of causality for each subject, taking into account all the variants of standard electrodes considered in the Table 4.4.

A.1.1 Comparison of results after varying the number of standard electrodes.

Subject	1	2	3	4	5	6	7	8
P300 - e:7	0.2235	0.3645	0.1864	0.4728	0.3221	0.6835	0.3644	0.2038
no-P300 - e:7	0.1230	0.3525	0.0686	0.4799	0.1014	0.1008	0.1605	0.2060
P300 - e:6	0.1090	0.2517	0.1224	0.2971	0.3040	0.4530	0.2633	0.1882
no-P300 - e:6	0.0747	0.1687	0.0873	0.3200	0.1158	0.0218	0.1151	0.1344
P300 - e:5	0.0537	0.2162	0.1250	0.1587	0.2729	0.4293	0.1837	0.1471
no-P300 - e:5	0.0148	0.1018	0.0781	0.1640	0.1002	0.0260	0.1024	0.1166
P300 - e:4	0.0615	0.0864	0.0896	0.0824	0.1997	0.3061	0.0989	0.0637
no-P300 - e:4	0.0438	0.0332	0.0692	0.1062	0.0817	0.0119	0.0414	0.0475
P300 - e:3	0.0377	0.0443	0.0643	0.0421	0.1208	0.1596	0.0446	0.0421
no-P300 - e:3	0.0353	0.0068	0.0578	0.0596	0.0444	0.0139	0.0083	0.0391
P300 - e:2	0.0104	0.0046	0.0382	0.0260	0.0068	0.0651	0.0183	0.0069
no-P300 - e:2	0	0	0.0473	0.0128	0	0.0105	0.0075	0.0116

Table A.1: Final area values for subjects 1-8 after window selection varying the number of standard electrodes shown in Table 4.4. e represents electrodes.

A.2 BLDA-FS Electrodes

A.2.1 Comparison of results after varying the number of BLDA-FS electrodes.

This section of the Appendix presents the results of causality for each subject, taking into account all the variants of electrodes selected with BLDA-FS considered in the Table 4.5.

Subject	1	2	3	4	5	6	7	8
P300 - e:6	0.0565	0.1876	0.1241	0.0981	0.2433	0.2872	0.2141	0.4824
no-P300 - e:6	0.0497	0.1051	0.0561	0.124	0.0467	0.1042	0.1273	0.0231
P300 - e:5	0.0865	0.1422	0.0774	0.1332	0.1643	0.1578	0.2112	0.012
no-P300 - e:5	.0.0765	0.093	0.021	0.1412	0.0281	0.0912	0.1281	0.016
P300 - e:4	0.0521	0.1365	0.0501	0.0876	0.1022	0.1292	0.1422	0.0251
no-P300 - e:4	0.0286	0.1062	0.0380	0.1379	0.0303	0.1065	0.1278	0.0141
P300 - e:3	0.0412	0.0485	0.0398	0.0256	0.0387	0.0745	0.1182	0.0135
no-P300 - e:3	0.0282	0.0261	0.0189	0.0253	0.0104	0.0702	0.0714	0.0141
P300 - e:2	0.0083	0.0375	0.0311	0.0365	0.0201	0.0151	0.0582	0.0211
no-P300 - e:2	0.0061	0.0211	0.0060	0.0372	0.0201	0.0178	0.0381	0.0198

Table A.2: Final area values for subjects 1-8 after window selection varying the number of BLDA-FS electrodes shown in Table 4.5. e represents electrodes.

A.3 R2 Electrodes

This section of the Appendix presents the results of causality for each subject, taking into account all the variants of electrodes selected with r2 considered in the Table 4.8

A.3.1 Comparison of results after varying the number of R2 electrodes.

Subject	1	2	3	4	5	6	7	8
P300 - e:7	0.0330	0.2193	0.0505	0.0639	0.1749	0.2385	0.0783	0.0414
no-P300 - e:7	0.0207	0.1670	0.0375	0.0644	0.0084	0.1349	0.0458	0.0149
P300 - e:6	0.0275	0.2038	0.0482	0.0376	0.1618	0.2164	0.0549	0.0362
no-P300 - e:6	0.0192	0.1728	0.0380	0.0308	0.0145	0.1347	0.0378	0.0081
P300 - e:5	0.0220	0.1795	0.0585	0.0468	0.0843	0.1530	0.0264	0.0303
no-P300 - e:5	0.0096	0.1556	0.0241	0.0545	0.0158	0.0950	0.0297	0.0102
P300 - e:4	0.0228	0.1591	0.0485	0.0295	0.0579	0.1304	0.0229	0.0120
no-P300 - e:4	0.0071	0.1083	0.0123	0.0448	0.0095	0.0828	0.0163	0.0099
P300 - e:3	0.0192	0.0800	0.0382	0.0122	0.0276	0.0891	0.0349	0.0229
no-P300 - e:3	0.0059	0.0364	0.0120	0.0076	0.0041	0.0315	0.0207	0.0175
P300 - e:2	0.0043	0.0238	0.0229	0.0055	0.0156	0.0146	0.0114	0.0009
no-P300 - e:2	0.0018	0.0151	0.0051	0.0045	0.0021	0.0078	0.0088	0.0004

Table A.3: Final area values for subjects 1-8 after window selection varying the number of r2 electrodes shown in Table 4.8. e represents electrodes.

B

Appendix: Electrode selection

B.1 Electrodes locations: BLDA-FS and R2 selection for all subjects and ROIs

This section of the Appendix shows, first, the location of the electrodes selected by BLDA-FS from the Table 4.5 and r2 from the Table 4.8 considering all electrodes. Second, it shows the location of the electrodes selected by BLDA-FS from the Table 4.11 and r2 from the Table 4.14 when analysed by ROIs.

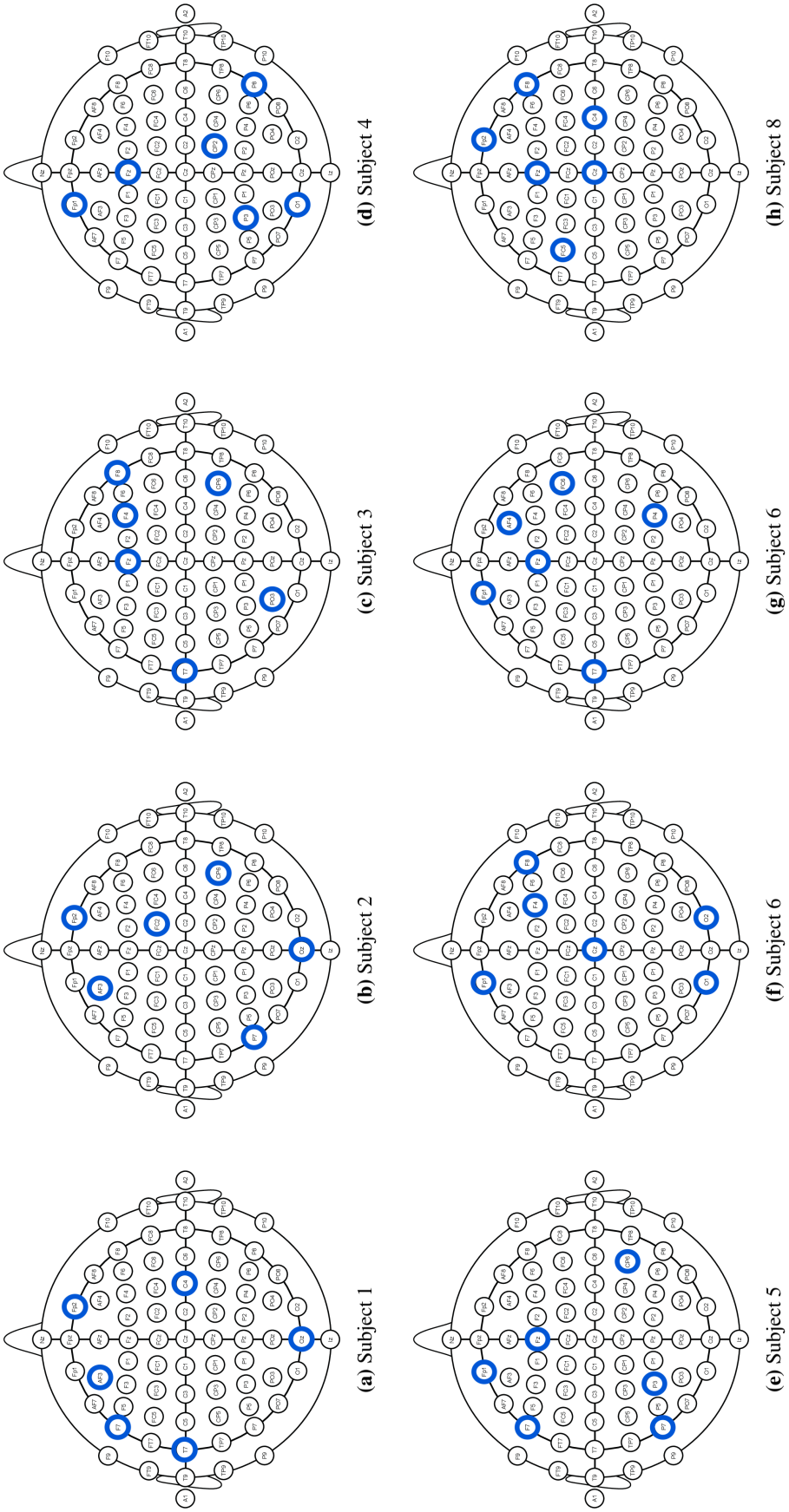

(a) Subject 1 **(b)** Subject 2 **(c)** Subject 3 **(d)** Subject 4

(e) Subject 5 **(f)** Subject 6 **(g)** Subject 6 **(h)** Subject 8

Figure B.1: Electrode location using BLDA-FS for subjects 1-8 from Table 4.5.

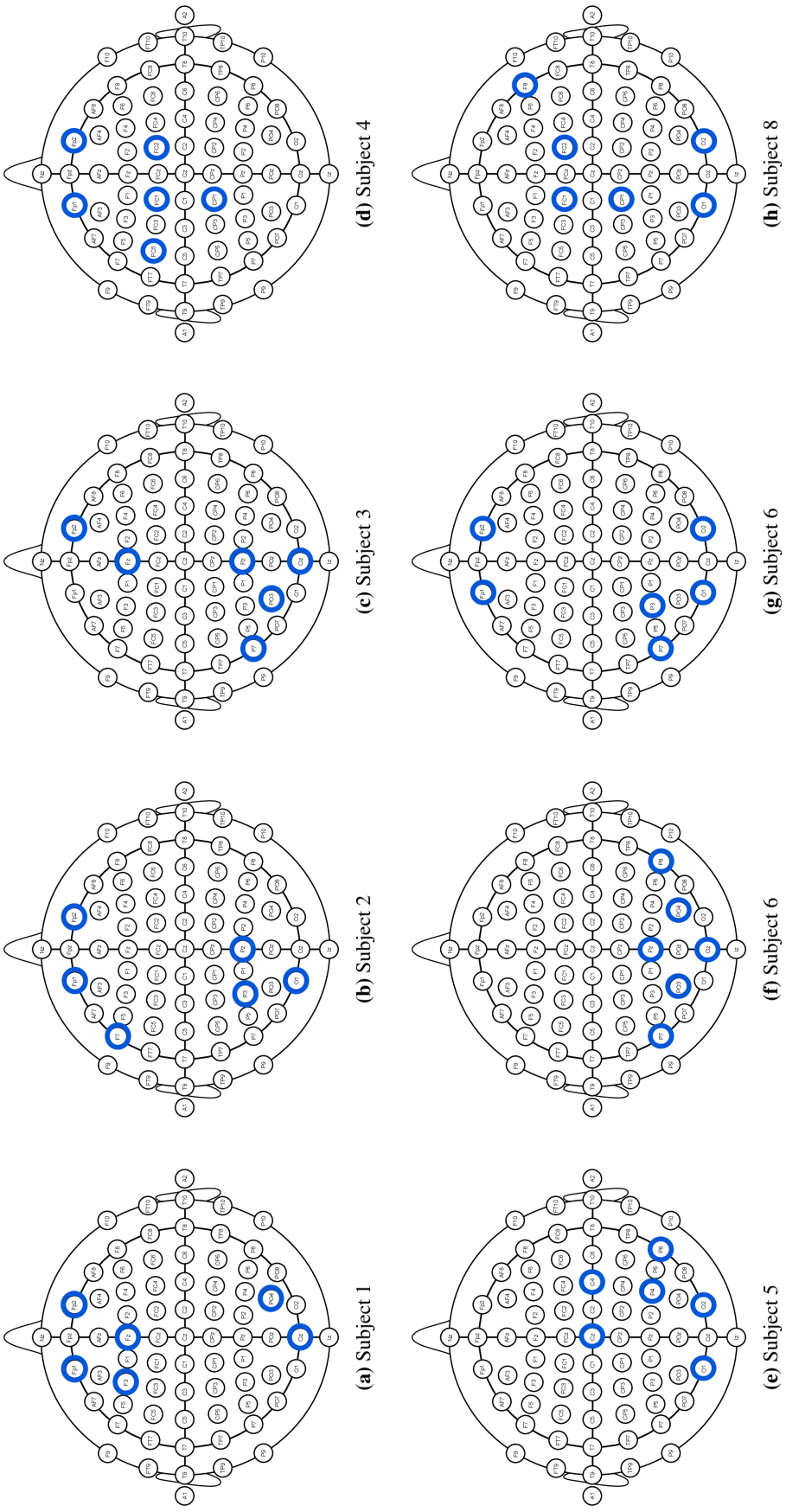

(a) Subject 1 **(b)** Subject 2 **(c)** Subject 3 **(d)** Subject 4 **(e)** Subject 5 **(f)** Subject 6 **(g)** Subject 6 **(h)** Subject 8

Figure B.2: Electrode location using r2 selection for subjects 1-8 from Table 4.8.

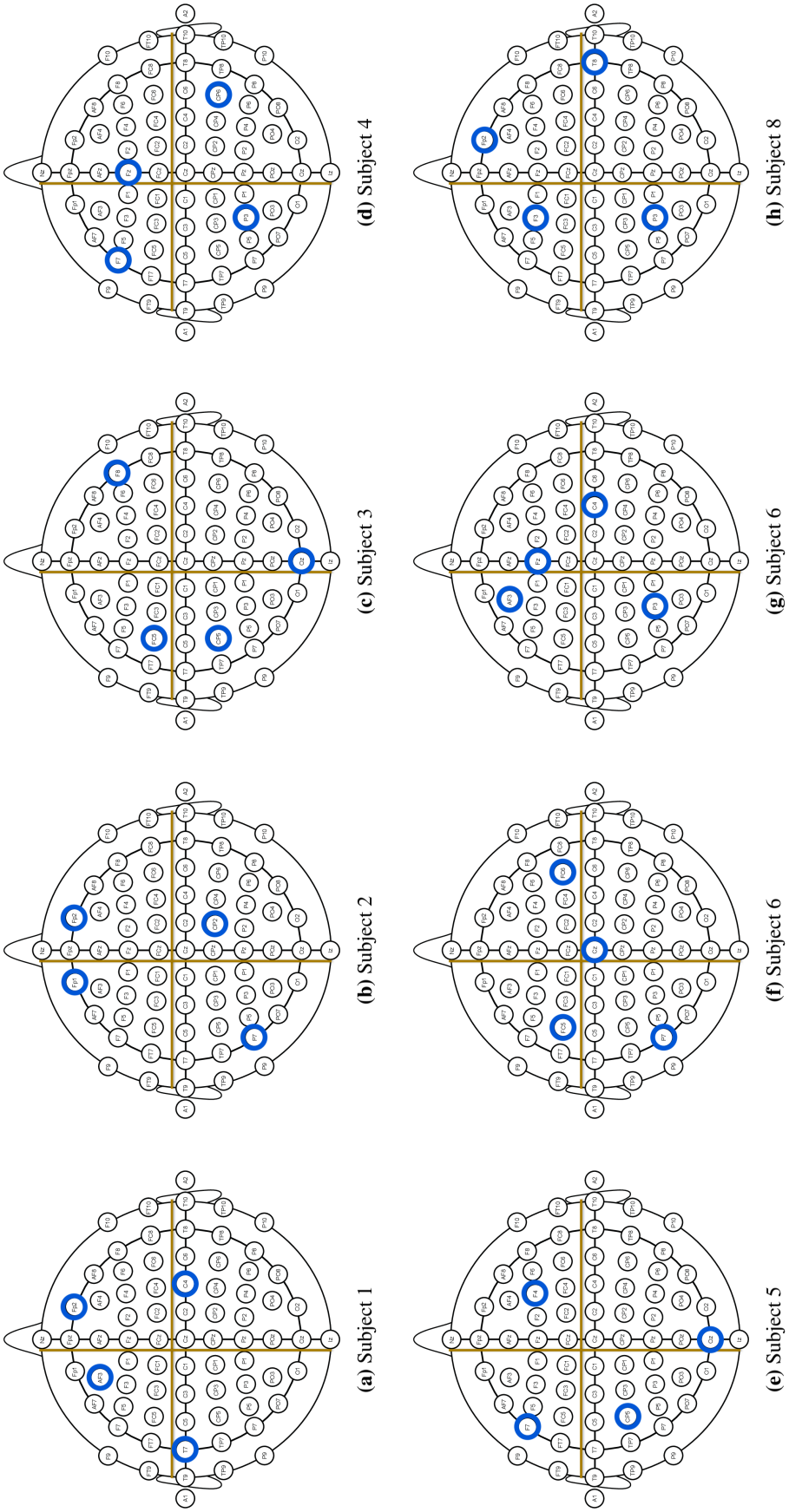

(a) Subject 1 **(b)** Subject 2 **(c)** Subject 3 **(d)** Subject 4

(e) Subject 5 **(f)** Subject 6 **(g)** Subject 6 **(h)** Subject 8

Figure B.3: Electrode location using BLDA-FS for ROIs in subjects 1-8 from Table 4.11.

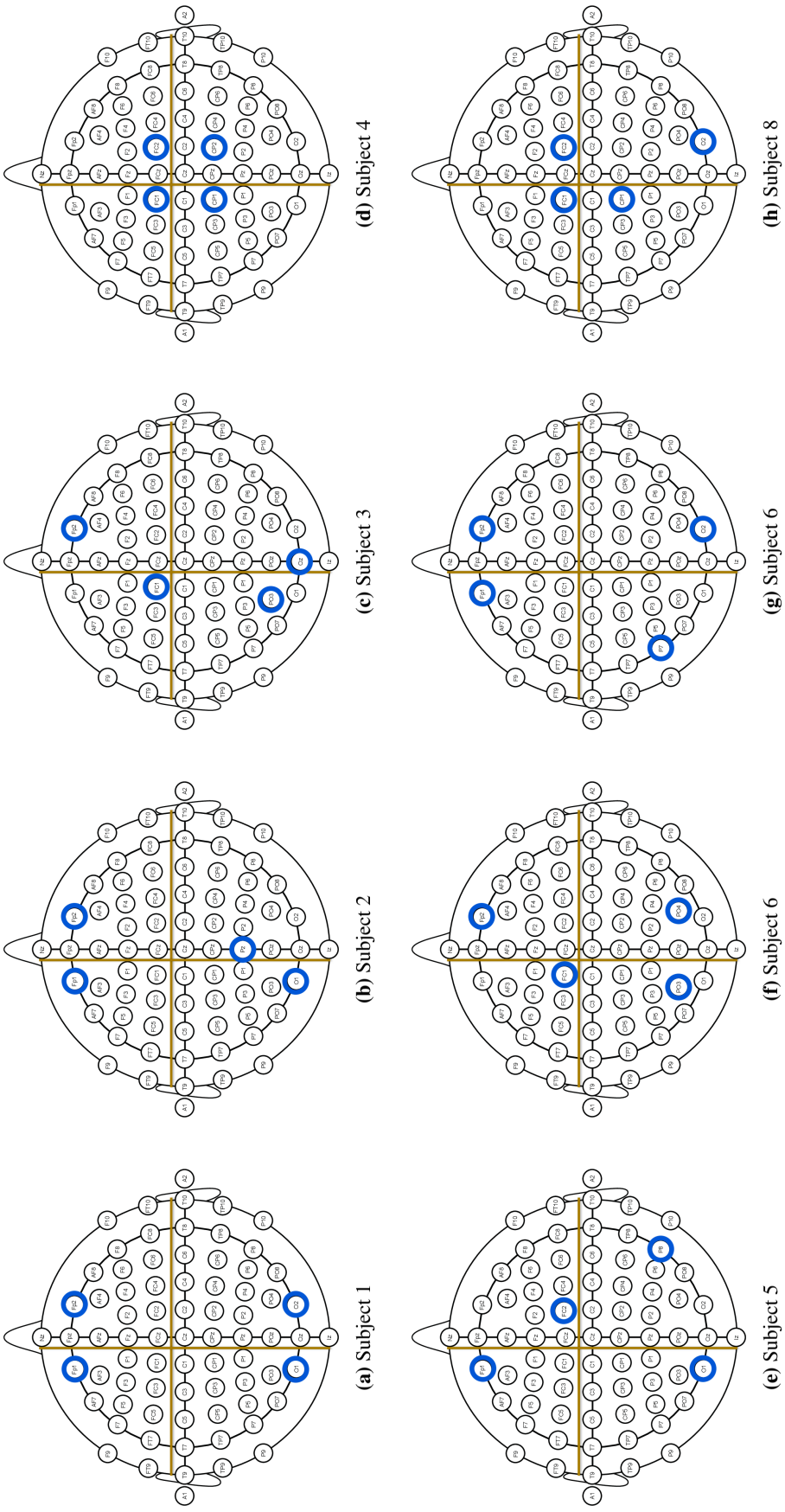

(a) Subject 1 **(b)** Subject 2 **(c)** Subject 3 **(d)** Subject 4

(e) Subject 5 **(f)** Subject 6 **(g)** Subject 6 **(h)** Subject 8

Figure B.4: Electrode location using r2 selection for ROIs in subjects 1-8 from Table 4.14 .